EQUILIBRIA AND HADRON MULTIPLICITIES

IN HEAVY-ION COLLISIONS

Thesis by

A. C. P. Maso

In Partial Fulfillment of the Requirements for

the Degree of Doctor of Philosophy

McGill University,

Montreal, Canada.

(submitted December, 1984)

ACKNOWLEDGEMENTS

I am very happy to mention in the first place my deep debt to my Wife, my Parents and my Brothers. This Thesis is wholeheartedly dedicated to all of them. Without their generous support, encouragement, cooperation, and understanding this whole enterprise could never have reached a successful conclusion. My wife Danielle in particular has put up with me during this very difficult period in our lives with great courage and cheerful determination.

Thanks to Professor Subal Das Gupta for his support and guidance throughout the preparation of this work. Thanks also to Dr. Pierre Valin and Nader Mobed for some discussions. Professor Dave Ryan and Dr. Pierre Valin made available useful sources of experimental nucleon-nucleon cross-sections. Dr. Byron Jennings has helped in the early stages particularly in debugging computer programs. The Consulting Service of the McGill Computer Department provided valuable help many times. And to all those people at McGill University who helped indirectly with their friendliness and goodwill my sincere gratitude.

ABSTRACT

The intranuclear cascade is an approximate microscopic model of heavy-ion collisions in which the space-time evolution of the nucleons is followed as they collide with one another. This model is used: (a) to test the validity of simpler models as the two-fireball model; (b) to estimate the validity of the assumption of chemical equilibrium and to calculate the total pion production cross-sections; (c) to investigate the average primordial charge multiplicity and the number of participants as a function of the beam energy.

La cascade intranucléaire est un modèle microscopique approximatif des collisions des ions lourds dans lequel l'évolution des nucléons dans l'espace et le temps est suivie au fil des collisions. Ce modèle est utilisé pour: (a) faire des études comparatives avec d'autres modèles plus simples comme le modèle des deux boules de feu; (b) étudier la validité de l'hypothèse de l'équilibre chimique et calculer la section efficace totale pour la production de pions; (c) calculer la multiplicité moyenne des particules chargées primordiales et aussi le nombre de participants en fonction de l'énergie de collision.

A cascata intranuclear é um modêlo aproximado microscópico da colisão de ions pesados no qual a evolução dos nucleons no espaço e no tempo é acompanhada a medida que sofrem colisões entre si. Esse modêlo é utilizado para: (a) estudar a validade de outros modêlos mais simples como o modêlo das duas bolas de fogo; (b) estudar a validade da hipótese do equilíbrio químico e calcular o coeficiente de difusão total para a produção de pions; (c) calcular a multiplicidade média das partículas carregadas primordiais, e também o número de participantes em função da energia de colisão.

1 - INTRODUCTION

1.I Heavy-ion physics.

The original motivation for the study of heavy ion collisions
was the possibility of observing unusual states of nuclear
matter, which could possibly lead to the detection of some
novel phenomena. There were speculations a decade ago about
the possible existence of exotic phenomena, such as density
isomers, pion condensates (Migdal-78), the quark-gluon plasma
(Shuryak-80), and also about the equation of state for nuclear
matter (Boguta-82). Although the original expectations have
not yet been met, the last few years saw rapid progress both in
the experimental and theoretical domains.

Machines that had already become obsolete in the field of
elementary particle physics gained a new lease on life when
they were converted to heavy ion research. The centers of
neutron stars and supernovas are thought to contain nuclear
matter greatly compressed at high densities. Laboratory data,
however, only became available when the Bevalac (Berkeley, USA)
and the Syncrophasotron (Dubna, USSR) went on stream in their

new roles to accelerate heavy ions. Since then other machines were adapted to heavy ion research (CERN SC, Saclay), new ones have been built (Saturne II and GANIL in France, the Michigan State Superconducting Cyclotron, USA), and others are planned or under construction (SIS in Darmstadt, Germany, the Numatron in Nagoya, Japan, TIS in Moskow, USSR, the VENUS proposal in Berkeley, USA) (Nagamiya-82). The study of heavy ions has been transformed from a curiosity ten years ago into a major field of nuclear science today.

The field of heavy ions is normally divided into different energy regimes, where different phenomena become dominant changing the underlying physics. The following regions are recognized (Faessler-83):

(a) Heavy ion atomic physics (E < 10 A.Mev).

It is concerned with such topics as the formation of short-lived superheavy nuclear quasi-molecules in a uranium-uranium collision which results in the emission of one or more positrons of atomic origin (Backe-83). Fusion-evaporation reactions (Roeckl-83) are used to produce nuclei far from the region of beta stability; the production of elements 107 and 109 through compound-nuclear reactions followed by one neutron evaporation has been particularly successful. One may hope soon to reach the expected region of long-lived heavy elements with 112 to 114 protons (Faessler-83).

(b) Nuclear physics near the Coulomb barrier (4 - 20 A.Mev).

High spin states present a great deal of interest for nuclear structure physics (Henning-83) as the shell and Coulomb energies become comparable with the rotational energies. The nuclear shape changes as a function of the spin states and one can measure its relaxation times (Norenberg-83). Under certain conditions (Ngo-83) the collision can lead to fusion of the two nuclei with the subsequent formation of a compound nucleus or fast fission.

(c) Nuclear physics near the sound barrier (30 - 200 A.Mev).

Before the completion of the Superconducting Cyclotron at M.S.U. the study of the intermediate region was only possible at the CERN Synchrocyclotron (Faessler-83). This is a transition region from low energy phenomena to the relativistic high energy reactions and where one expects to see nuclear matter off its ground state density at moderate temperatures and entropy (Stocker-83). The possible coexistence of nuclear liquid and gas phases has been considered (Gelbke-83); one can also distinguish between central fusion-like reactions and the peripheral ones. Lynen's data may indicate the existence of hot spots in this energy region (Faessler-83). Experimental data are available on pion production below the free nucleon-nucleon scattering threshold (Jakobsson-83). The low and intermediate energy regions are being actively studied by a large number of physicists (Faessler-83).

(d) The participant-spectator region (0.2 - 4.0 A.Gev).

This is the Bevalac physics region, and the one most thouroughly studied resulting in a great abundance of data and theoretical models. The reaction mechanism in this region is often thought to be divided into two stages (Warwick-82); first a fast energy deposition accompanied by the emission of fast light particles, which is normally associated with the participants; it is followed by a second slow stage characterized by the disassembly of the excited spectator residues. The participants consist of the overlapping portions of the projectile and target nucleons that are mutually swept during the collision. One can also distinguish between high multiplicity central events and peripheral ones; in the case of the central events where one ion is small and the other one large the accuracy of the clean-cut participant-spectator picture has been questioned (Warwick-82). This Thesis is concerned exclusively with this energy region.

(e) The quark-gluon plasma region (E > 5.0 A.Gev).

Little experimental data are available in this last region, mostly from the analysis of cosmic rays (Gyulassy-83). It is supposed that as more energy is brought into the interaction region hadronic matter will finally begin to boil off; QCD predicts the deconfinement of hadronic matter into a plasma of quarks and gluons at high energy densities (Specht-83).- Obviously the study of this region is of interest both to nuclear and particle physics, thus

bringing these two fields together again.

1.2 The participant-spectator region.

A great amount of data, mostly from the Bevalac at the Lawrence
Berkeley Laboratory, has already been accumulated with
projectiles from protons to argon nuclei and. energies ranging
from 50 to 2100 A.Mev. The projectiles used are being extended
to include the whole periodic table, and while most of the data
obtained up to now consist of inclusive measurements
(Warwick-83), the results of more sophisticated 4π exclusive
experiments are already available and collision energies are
expected to reach 20 A.Gev (Nagamiya-82).

The experimental procedures begin by completely stripping the
projectile atoms from their atomic electrons. The resulting
ions are then accelerated and made to collide with a stationary
target. The reaction products can be detected in a streamer
chamber or alternatively in counter experiments.

Streamer chamber photographs provide a very vivid view of the
results of the collision. There one can easily identify
peripheral collisions characterized by a forward jet in the
direction of the beam arising from the fragmentation of the
projectile. Less peripheral collisions show a large number of

jets at wide angles but still present the forward jet as in the first case. Finally there are central collisions where the number of jets is much larger and the forward jet may disappear entirely (Nagamiya-82).

Counter experiments reveal a similar picture: in the rapidity and transverse momenta plane $(y, p_\perp/mc)$ target-like fragments are clustered around the target rapidity $(y_t, 0)$ whereas projectile-like fragments appear around the point $(y_p, 0)$. These are regarded respectively as the target and projectile spectators. In violent collisions a large number of fragments are spread in the region between these two points. Such fragments are associated with the participants. Experimentally the projectile spectators are confined to a very narrow angle around the direction of the beam; the target spectators can be distinguished from the participants by their small momenta. The Fermi momentum (270 Mev/c) sets the scale, in a somewhat arbitrary manner, between large and small momentum transfers thus differentiating the participants from the spectators.

Most data are presented in the form of inclusive cross-sections, in which one chosen reaction product is measured to the exclusion of all others that may be present. Inclusive cross-section for particles (protons, pions, etc.) and composites (deuterons, tritons, He-3, He-4, etc.) are found throughout the literature. These are assumed to come from the participants (Gosset-77, Sandoval-80, Nagamiya-81, Manko-82, Sandoval-80a).

Theoretical developments are keeping the pace with the avalanche of data. One would expect that a comprehensive theory of nuclear collisions should be based on Quantum Chromodynamics, which is generally believed to be the correct theory of strong interactions. But until the mathematical difficulties of this theory are overcome, if ever, we must content ourselves with phenomenological models. The great complexity of the problems precludes their direct solution in fundamental terms. As a result many different models have been proposed which succeed to explain certain aspects of the data, but not others. Sometimes they complement each other in their ranges of application or compete while incorporating mutually contradictory assumptions.

Various models are available to explain the data in the Bevalac region: thermodynamic models, intranuclear cascades, hydrodynamic models, classical equations of motion, rows-on-rows model, and others. Of all these models, the thermodynamic model can claim to be the most widely used (Das Gupta-81). Most existing models in this region are formulated in semi-classical terms. The partial wave sums are replaced by integrations over impact parameters; the amplitudes for two partial waves or impact parameters do not interfere. At the nucleon-nucleon level, however, a quantum mechanical description is essential. The semi-classical description may find some support from the very high relative momenta of the heavy-ions and their constituents, and the short wavelengths compared with the characteristic distances of the system.

(Fraenkel-82).

There are also final state interactions. These interactions involve the coalescence of nucleons to form composites such as deuterons, alpha-particles, etc., and also the Coulomb interactions that can change the shape of the spectra quite noticeably for charged pions and to a lesser extent for protons (Libbrecht-79, Cugnon-81).

At low energies one can as a first approximation ignore the production of pions and relativistic effects and attempt the integration of Newton's classical equations of motion (Bodmer-81). The method, originally developed for the problems of molecular dynamics, is restricted to non-relativistic energies (Fraenkel-82). The number of degrees of freedom is fixed so that pion production cannot be included in the method (Fraenkel-82).

For high energy collisions the nuclear mean field is unimportant and collisions between nuclei can be regarded as hard scattering between nucleons. This approximation is the basis for the intranuclear cascade model, the direct knock-out model, and the rows-on-rows model (Fraenkel-82). The direct knock-out model is the long mean free path limit of the intranuclear cascade model; the rows-on-rows model is a linear cascade using the Glauber theory to take advantage of the forward peaked nucleon-nucleon cross-sections at high energies (Fraenkel-82).

In the limit of very small mean free paths one has the hydrodynamical model; ideal fluids are described by the Euler equations, and viscosity and thermal conductivity are included in the Navier-Stokes equation; potential effects can be accounted for through the nuclear equation of state. The hydrodynamical model is possibly valid only for central collisions of large nuclei where high densities and local equilibrium are attained (Fraenkel-82).

The thermodynamic model incorporates geometrical concepts leading to the participant-spectator picture. The participants from the target and the projectile are assumed to fuse together and form a fireball. All points of the available phase space are equally probable for the participants (Das Gupta-81). When there is a large number of particles the grand-canonical ensemble provides a suitable approximation (Jennings-82).

The present situation is remindful of the famous parable about the elephant and the seven blind men. Comparing the assumptions and the results of the various models among each other and the data, one can gain a deeper insight into their limitations and strengths, and thus reach a better understanding of the underlying Physics.

1.3 Scope of original work in this Thesis.

In chapter 2 we continue with a more detailed review of the theoretical models and other items that are directly relevant for this Thesis. The original work in this Thesis is found in chapters 3, 4, and 5, Appendices 7.2.3, 7.3, 7.4, 7.5, and 7.6, with the summary and the final conclusions in chapter 6. Chapter 3 is concerned with the question of thermal equilibration in the fireball type models. Chapter 4 deals with the validity of the assumption of chemical equilibrium in heavy ion collisions in connection with the total cross-section for the production of pions. In chapter 5 we study the average primordial charge multiplicities and the validity of the participant-spectator picture as a function of the beam energy.

(a) Fireball type models.

Cugnon et al, using a cascade code, compute the final nucleon transverse momentum and rapidity distributions for the central collision of two calcium-like nuclei, where complete isospin degeneracy is assumed (Cugnon-81). Relativistic Maxwell-Boltzmann fits to these distributions yield different transverse and rapidity temperatures. The existence of these two different temperatures raises doubts about thermal equilibration in the collision.

We demonstrate, using the two-fireball model, that two temperatures are obtained quite naturally if there are two sources moving with respect to their center of mass. The

additional assumption of a radial collective flow (Siemens-79) to the two-fireball model (Gale-83) leads to transverse and rapidity temperatures in very close agreement with those obtained by Cugnon et al.

(b) Pion production and chemical equilibrium.

We study the total inclusive pion cross-section in the cascade model and the attainment of chemical equilibrium. A detailed description of the intranuclear cascade is given later; suffice it to mention here that it includes, among others, the following channels for hard collisions: $N + N \rightarrow N + \Delta$, and $N + \Delta \rightarrow N + N$.

If the rate of production of deltas is equal to its rate of absorption, we have chemical equilibrium. In the thermodynamic model (described later) the production of the deltas is calculated assuming chemical equilibrium. There has been much debate whether chemical equilibrium is reached in heavy ion collisions.

The cascade model calculations begin as the two nuclei are given opposite initial momenta and touch each other. In subsequent times the nucleons and the deltas produced undergo hard collisions. There is an initial diving phase followed by the stage of compression; the number of deltas is initially zero and then begins to increase. For medium mass nuclei at about 800 A.Mev the collisions are over in about 25 fm/c. In the model, the number of deltas will not

change after the collisions cease.

One question is whether the number of deltas approaches its chemical equilibrium value. We investigate this by artificially confining the baryons within a spherical cavity at the point of maximum compression and letting the system evolve for a long time. The number of deltas fluctuate about a final steady value; this value agrees with the thermodynamic prescription. This number, however, is not far from the number of deltas obtained from an usual cascade calculation (without the artificial reflecting wall) where the system disassembles in about 30 fm/c.

Thus for medium mass nuclei and for central collisions (for which this test was done) the cascade model prediction should not be very different from the thermodynamic prediction. For non-zero impact parameters, however, the number of participants is smaller and chemical equilibration is unlikely. Thus it is useful to compute the inclusive pion production cross-sections (this involves integrating over all impact parameters) using the cascade model. Usual cascade model codes employ simple parametrized versions of the nucleon-nucleon cross-sections and are valid only for $N = Z$ systems. An extended version devised for this work is applicable to non symmetric systems. This is described in a later chapter. This is essential because much more data are available for $N \neq Z$ systems. We use also more accurate nucleon-nucleon

cross-section data taken from experiments. We examine the sensitivity of the final results on the nucleon-nucleon input data. There are other tests for chemical equilibrium that can be devised. These are discussed in chapter 4.

(c) Average multiplicities and geometry.

The participant-spectator model is commonly used in relativistic heavy-ion collisions. In this model the overlapping parts of the two nuclei for a given impact parameter form the participants. The non-overlapping parts form the target and projectile spectators. The participants undergo violent collisions and all of the nucleons are liberated, although some still come out in small clusters such as deuterons, tritons, etc. The spectators are only slightly excited and therefore do not produce many charged tracks. All the pions must invariably come from the participants.

The average multiplicity is the average number of charged particles produced in the heavy-ion reaction. The calculation of this number in the participant-spectator model requires an integration over all impact parameters. Another commonly used concept is the associated multiplicity. Sandoval et al, for example, measured the multiplicity in coincidence with the detection of a proton in a telescope placed at ninety degrees with respect to the beam direction. These experiments measured the associated multiplicities for a variety of projectiles and targets at

many energies. For a fixed projectile and target combination the associated multiplicity increases with the beam energy and the claim was made that this result is inconsistent with the participant-spectator model.

We show that the associated multiplicity experiments do not obviously rule out the validity of the clean cut geometry. Some other dynamic model for pion and composite production has to be invoked along with the clean cut geometry in order to compare with the experimental data. The lack of agreement could be due to the dynamical assumptions and not to the geometrical assumptions. We show that the simplest fireball model, which uses the clean cut geometry, fits the experimental data quite well although fancier models do not fare that well.

One has therefore to look for other experimental data to check the validity of the geometrical asssumptions. Some experiments by Nagamiya et al can be used for this purpose. These experiments (to be described later) do show some evidence of a beam energy dependence which is obviously absent in a geometrical model. Some more sophisticated model is needed.

We use a Glauber type model to calculate the average number of participants as a function of the beam energy. The input for this model is the nucleon-nucleon cross-section which is energy dependent. The experimental trends are

reproduced although the calculated value of the dependence on the beam energy is less than the experimental value. Lastly, we use the cascade model to define the participants and this model gives an adequate explanation of the experimental data.

2 - THEORETICAL MODELS

2.1 The thermodynamic fireball model.

2.1.1 Introduction.

The application of thermodynamics to sub-atomic phenomena dates back to 1950 when E. Fermi (Fermi-50) developed a statistical model for the multiple production of pions in high energy nucleon-nucleon collisions. He assumed that in such a collision the energy in their center of mass is released into a small volume surrounding the two nucleons and distributed among the various degrees of freedom available in this volume according to statistical laws until upon expansion the system is converted into particles that fly out in all directions. More recently the fireball model for relativistic collisions of heavy ions (Westfall-76) was proposed along somewhat similar lines and with the addition of geometrical concepts.

Geometry leads to the participant-spectator picture. Those nucleons which lie in the overlapping regions of the two colliding nuclei interact strongly with one another and are

therefore called the participants; the non-overlapping regions do not interact with each other and proceed along their original trajectories to form the spectators. The participants will concern us most as they are the seat of the most violent hadronic collisions and where high nuclear densities and high temperatures are expected. The projectile and target participants are assumed to fuse completely forming a fireball. All the energy in the center of mass frame of the participants is available for thermalization. High number of collisions make all points of the available phase space equally probable. There is experimental evidence for multiple nucleon-nucleon collisions (Nagamiya-82) and also for the importance of single nucleon-nucleon collision processes. After passing through the point of maximum compression and high density the fireball expands until the density becomes so low that all interactions cease. Beyond this freeze out point it continues to expand as a non-interacting gas. The freeze out density f_c is usually assumed to be lower than the normal nuclear density and usually in the range between 0.04 and 0.08 nucleons/fm^3.

The number of participants can be calculated by numerical integration (Gosset-77) under the assumption of straight line geometrical cuts or alternatively one can use Glauber theory to the same effect (Glauber-70). The clean cut separation between participants and spectators is obviously an idealization. Some nucleons are likely to scatter at large angles so that it is reasonable to expect some degree of communication across the boundary surface. In the case of central collisions of light

projectiles with heavy targets the valididy of the straight geometrical cut is questioned (Gutbrod-82). We shall return to this problem later in chapter 5.

Protons, composites (deuterons, tritons, alpha-particles, etc.) and other particles originating from the fireball reach the detectors. If we limit ourselves to collision energies up to about 2.0 A.Gev then the only other particles important enough to be included in the model are the pions. It is generally assumed that the pions are formed in the fireball mostly through the creation and the decay of the delta resonances (Kapusta-77, Cugnon-80). The production of lambda hyperons and K-mesons is negligible below 2.0 A.Gev. At the critical density when all interactions cease, the surviving deltas finally decay into pions and nucleons. Pions, deltas and composites are included into the fireball model through the further assumption of chemical equilibrium (Mekjian-77). The fireball then, is assumed to be a hot gas in thermal and chemical equilibrium (Das Gupta-78).

2.1.2 The Maxwell-Boltzmann limit.

When the fireball reaches the critical density ρ_c we can apply the thermodynamics of a non-interacting gas. A phase space calculation is usually considered very difficult. The canonical or the grand canonical ensembles provide suitable aproximations in most cases (Jennings-81) for systems with a large number of particles and for detected particle momenta

below 1.0 Gev/c.

For a given impact parameter b, the baryon number B(b) and the charge Q(b) of the fireball are determined by geometry and its energy E(b) and velocity v(b) are obtained by kinematics (Kapusta-77). Relativistic mechanics is used throughout. Each hadronic species in the fireball is distributed according to the laws of quantum statistics; in momentum space we have:

$$\frac{d^3 n_i}{dp^3} = \frac{g_i \cdot V(b)}{(2\pi)^3} \left[e^{(\sqrt{m_i^2 + p^2} - \mu_i)/T} \pm 1 \right]^{-1} \qquad (2.1.1)$$

where m_i is the mass, μ_i the chemical potential, V(b) is the fireball volume corresponding to the critical density ρ_c, T is the temperature, and the particle multiplicity factor is $g_i = (2I_i + 1)(2S_i + 1)$. Here S_i is the spin and I_i is the isospin. Natural units $\hbar = c = k = 1$ are used. This expression reduces in the limit of high temperatures to a relativistic Maxwell-Boltzmann distribution:

$$\frac{d^3 n_i}{dp^3} = \frac{g_i \cdot V(b)}{(2\pi)^3} \cdot e^{\mu_i/T} \cdot e^{-\frac{1}{T}\sqrt{m_i^2 + p^2}} \qquad (2.1.2)$$

Upon integration (Appendix 7.1) one obtains the total number of particles $n_i(b)$:

$$n_i(b) = \frac{g_i V(b)}{2\pi^2} e^{\mu_i/T} m_i^2 T \, K_2\left(m_i/T\right) \qquad (2.1.3)$$

and the total energy $E_i(b)$:

$$E_i(b) = \frac{g_i V(b)}{2\pi^2} e^{\mu_i/T} m_i^3 T \left[K_1\left(\frac{m_i}{T}\right) + \frac{3T}{m_i} K_2\left(\frac{m_i}{T}\right) \right] \qquad (2.1.4)$$

Here K_1 and K_2 are modified Bessel functions sometimes called the McDonald functions (Abramowitz-68).

The assumption of chemical equilibrium provides the means to calculate the chemical potentials for all other species present in the fireball (Reif-65) as a function of the proton and neutron potentials, e.g., for a given reaction $a_1 A_1 + a_2 A_2 = a_3 A_3$ then, one has the relation $a_1 \mu_1 + a_2 \mu_2 = a_3 \mu_3$. The unknown quantities (the fireball temperature T, the critical volume V, the proton chemical potential μ_p and the neutron chemical potential μ_n) are found by solving the system of equations (Kapusta-77):

$$E(b) = \sum_i n_i(b) E_i(b) \qquad (2.1.5)$$

$$Q(b) = \sum_i n_i(b) \, Q_i(b) \qquad (2.1.6)$$

$$B(b) = \sum_i n_i(b) \, B_i(b) \qquad (2.1.7)$$

$$\rho_c \, V(b) = \sum_i n_i(b) \qquad (2.1.8)$$

The cross-sections in the laboratory frame are obtained by making use of the Lorentz invariance of $Ed^3 n_i / dp^3$, where $E^2 = m_i^2 + p^2$, and integrating over all the impact parameters (Das Gupta-81):

$$E_L \frac{d^3 n_i}{dp^3} = \int E \frac{d^3 n_i(b)}{dp^3} 2\pi b \, db \qquad (2.1.9)$$

The contributions to the pion and nucleon cross-sections from the decay of the deltas (Kapusta-77) are obtained by evaluating the integral (Appendix 7.2):

$$E \frac{d^3 n_i(b)}{dp^3} = \frac{m_\Delta}{2 p_0 p} \int_{E_\Delta^-}^{E_\Delta^+} \frac{d^3 n_\Delta(b)}{dp_\Delta^3} E_\Delta \, dE_\Delta \qquad (2.1.10)$$

were i refers to pion or nucleon, E_{0i} and $\vec{p}_0$ are its energy and

momentum in the rest frame of the delta, and

$E_\Delta^\pm = m_\Delta (E_{oi}E \pm p_o p)/m_i^2.$

2.1.3 The phase space approximation.

Sometimes it is necessary to do a full phase space calculation (Das Gupta-81). The inclusive cross-sections are then given by the ratio of two phase space integrals (Forest-80):

$$\frac{d^3 n_i(b)}{d p^3} = \frac{n}{D} \tag{2.1.11}$$

where D and n are given by:

$$D = \sum_{n_a} \left[\frac{V}{(2\pi)^3}\right]^N \cdot \prod_a \frac{(2S_a+1)^{n_a}}{n_a!} \cdot \int \delta\left(E - \sum_{J=1}^N E_J(p_J)\right) \cdot$$

$$\cdot \delta\left(\vec{P} - \sum_{J=1}^N \vec{p}_J\right) \cdot \delta_{Q,\sum n_i Q_i} \cdot \delta_{B,\sum n_i B_i} \cdot \prod_{J=1}^N d^3 p_J \tag{2.1.12}$$

and

$$n = \sum_{n_a} n_i \left[\frac{V}{(2\pi)^3}\right]^N \cdot \prod_a \frac{(2S_a+1)^{n_a}}{n_a!} \int \delta\left(E - E_i(p_i) - \sum_{J=1}^{N-1} E_J(p_J)\right) \cdot$$

$$\cdot \delta\left(\vec{p} - \vec{p}_i - \sum_{J=1}^{N-1} \vec{p}_J\right) \cdot \delta_{Q,\sum n_i Q_i} \cdot \delta_{B,\sum n_i B_i} \cdot \prod_{J=1}^{N-1} d^3 p_J \tag{2.1.13}$$

A good approximation method (Jennings-81) is available, which is based on the saddle point inversion of the Laplace

transform. The Laplace transform of the phase space integral is formally identical to the grand canonical partition function. It is very easily obtained. The results are more general, but one recovers the grand canonical results with the additional assumption that the saddle points of the numerator and the denominator are approximately the same.

2.1.4 Extensions of the fireball model.

The fireball model reproduces the main features of proton spectra rather well for the collisions of heavy ions. Proton spectra for the collisions of carbon on carbon show signs of anisotropy in the center of mass frame, while the fireball model predicts spherically symmetric distributions (Das Gupta-78a). The fireball model also overestimates the pion cross-sections by at least a factor of 2. These discrepancies with the experimental data motivated further studies and new elaborations of the basic model, such as, the firestreak model, the two-fireball model, the implosion-explosion model and the two-fireball/blast-wave model.

(a) The firestreak model.

In this model the participants are divided into a number of tubes that thermalize independently of one another (Myers-78). It is mainly a further elaboration of the geometrical concepts. This model conserves angular momentum explicitly whereas the fireball models do not (Gosset-78). This feature only becomes important for collisions with

energies above 1.0 A.Gev in the laboratory. It predicts with success the nucleon and the composite spectra (Gosset-78), but the triton cross-sections are grossly incorrect, while the pion cross-sections are not improved over the simple fireball predictions (Das Gupta-81). The firestreak model will not interest us any further in this thesis.

(b) The two-fireball model.

The two-fireball model (Das Gupta-78) introduces collective motions to account for the strong anisotropy shown by the proton cross-sections in the collisions of light ions. The fundamental idea of this model is that the participants are not stopped completely in their center of mass frame during the collision. Instead they are only slowed down by some transparency factor. This means that a fraction of their energies is not available for thermalization and remain in the form of collective translational motions. The one-fireball model is recovered as the masses of the ions increase and the transparency factor approaches zero. The parameters in this model are determined by solving equations 2.1.5 to 2.1.8 in the rest frames of each fireball (Appendix 7.1.2).

(c) The implosion-explosion model.

This model introduces fireball explosions that create a blast wave of nucleons and pions in the form of collective outward radial flows (Siemens-79). The particles near the surface of a hot and dense fireball face an anisotropic environment. The randomness of their kinetic energies is thus reduced and eventually the whole mass acquires an average outward radial velocity V_r. Thermal energy is converted to work. More energy for the explosion comes from the elastic forces between nucleons (compressional forces), from the reabsorption of pions, and the de-excitation of resonances (Siemens-79).

The distributions for each hadronic species in the frame of the fireball are calculated from the basic assumption that in a spherically expanding fireball there is a local Maxwell-Boltzmann distribution for each frame moving radially outward with the average velocity V_r. Using again the Lorentz invariance of the product $E\, d^3 n_i / dp^3$, we obtain the momentum distributions in the fireball frame:

$$\frac{d^3 n_i(b)}{dp^3} = \frac{A \gamma_r e^{-x_2}}{2 x_1 x_2}\left[(x_2 - x_1 + 1)e^{x_1} - (x_2 + x_1 + 1)e^{-x_1}\right] \quad (2.1.14)$$

where A is a normalization constant, $\gamma_r = 1/\sqrt{1 - V_r^2}$, $x_1 = \gamma_r V_r p/T$, and $x_2 = \gamma_r E/T$ (Appendix 7.1.3).

The parameters are obtained as before from the equations

2.1.5 to 2.1.8 for the conserved quantities. Siemens and Rasmussen find that about one half of the available energy appears as translational kinetic energy of expansion in the collisions of neon on sodium fluoride at 800 A.Mev. This model leads to lower apparent pion temperatures, as suggested by the experimental data (Siemens-79).

(d) The two-fireball/blast-wave model.

In this model the cross-sections for pions, protons and deuterons are constrained from the beginning to their correct values. This amounts to fixing two ratios: σ_p/σ_d and σ_p/σ_π. These are obtained by varying the two parameters of the fireball model: the critical density ρ_c and the temperature T (Gale-83).

The temperature T is adjusted by reducing the amount of energy that is available for thermalization. This, of course, requires the introduction of collective motions. Accordingly, translational collective motion is simulated by using two fireballs. But this is not enough, so that it is also necessary to introduce radial collective flows of the type used in the implosion-explosion model.

A relatively large portion of the energy goes into the radial expansion making this effect far more important than the translational collective flows. The latter, however, are still necessary to account for the anisotropy of the spectra in the center of mass frame of the participants. In

chapter 3 we compare the predictions of this model with the results of the cascade calculations.

2.2 The intranuclear cascade model.

2.2.1 Introduction.

The cascade model has been used in recent years with great success. One might say that it is neither a model nor a theory, but a simulation. One important characteristic of the cascade model is the absence of adjustable parameters. It is a microscopic model, and the only input data needed are the nucleon-nucleon cross-sections. Thus each collision is treated according to the experimental nucleon-nucleon cross-sections, but between collisions all the hadronic species present follow classical free paths.

There are many different cascade models, almost as many as there are researchers in this field, and they do not form a single approach. All cascade models, however, can be grouped into two categories: in the first one the collision is described as a series of binary nucleon-nucleon collisions; the other describes the interaction of a colliding nucleus with a medium characterized by a mean free path, the procedure is repeated with the other nucleus, and the results are

symmetrized in the end (Cugnon-82). In this thesis we will be exclusively concerned with first type.

The cascade model has been used in the range of 200 A.Mev to 2.0 A.Gev. A colliding nucleon must be able to resolve individually the nucleons in the other nucleus for a classical description to be valid. This means that the De Broglie wavelengths must be small compared with the nuclear dimensions, and that sets the lower limit of applicability. Above 2.0 A.Gev one has to consider the production of other hadronic species besides the pions and the deltas, but ultimately it is the need to include the quark degrees of freedom at higher energies that may set the upper limits. The conditions of validity are still debatable (Cugnon-82).

Other approaches closely related to the cascade are the rows on rows and the clear knock-out models. The rows on rows model, based on Glauber theory, is essentially a one dimensional cascade, but it disregards the space evolution of the system; nucleons interact within tubes of cross-sections σ_{NN}, and the tubes do not interact with each other (Hufner-77). The clear knock-out model puts in evidence the importance of the first hard scattering as opposed to multiple scatterings. The hydrodynamical model requires high densities and small mean free paths (Stocker-83), and the fireball model does not include the time factor at all.

The distinct advantage of the cascade model, despite its great

computational effort, lies in the possibility of calculating
non-observable quantities, such as the maximum densities
reached in the collisions, or, in the calculations of
off-equilibrium situations, fluctuations, and finite particle
number effects (Cugnon-82).

2.2.2 General description.

In the simplest cascade model each nucleus is represented by a
collection of hard spheres of radius $R = \left(\sigma_{H+}/\pi\right)^{1/2}$ and the time
evolution of the system follows a classical deterministic path,
which amounts to the solution of the Classical Equations of
Motion (Nagamiya-82). This approach reproduces the qualitative
trends of the data, the largest discrepancies being at forward
angles and low energies of the detected particles. Such a
simple model is restricted to low collision energies where pion
production is not a significant factor.

We present a general description based mainly on the Cugnon
Monte Carlo models (Cugnon-80, Cugnon-81). The calculation
follows the collision of two identical nuclei in their center
of mass system. Relativistic mechanics is used. Complete
isospin degeneracy is assumed so that only one chargeless type
of nucleon, of pion, and of delta are considered. This
simplifying assumption restricts some results to charge
symmetric systems. Appendix 7.7 presents the mathematical
details of a simple version of the Cugnon code that we have
used in this work. In chapter 4 we describe an extended version

of this code where we introduce the isospin formalism that allows the study of non-symmetric systems, and also new revised nucleon-nucleon cross-sections. Much of the experimental data available is for the collisions of unequal nuclei with $N \neq Z$.

Each nucleus is represented by a sphere of radius $1.12\ A^{1/3}$, where A is the mass number. Point-like nucleons are assigned positions according to a random uniform distribution in the target and the projectile rest frames. The nucleons are also assigned random initial Fermi motion (Cugnon-81). If field effects are not included at the same time there is the inconvenience that the nuclei disassemble spontaneously even in the absence of any collision. For this reason the simple version used in this work does not include the initial Fermi motion, since we also do not introduce field effects. Although Fermi motion and field effects are important physical characteristics of nuclei they do not affect significantly the results we are interested in this Thesis. Binding energy is neglected in some models (Cugnon-80, Cugnon-81). Cahay et al (Cahay-82) introduce field effects using both scalar and vector potentials. Mean field and Pauli blocking effects have also been introduced in the context of the Boltzmann equation (Bertsch-84). Pauli principle effects are mocked approximately by forbidding soft collisions when the total center of mass energy of two colliding nucleons is below 1895 Mev (Cugnon-81).

Single pion production in nucleon-nucleon collisions is introduced via the formation and decay of the delta resonances.

The deltas are usually assumed to have a mass distribution (Cugnon-81). The behavior of the deltas in compressed nuclear matter and their cross-sections are uncertain. The elastic $\Delta + \Delta \rightarrow \Delta + \Delta$ and $N + \Delta \rightarrow N + \Delta$ cross-sections are assumed to be the same as for the nucleons in free space. The inelastic $N + \Delta \rightarrow N + N$ cross-sections are obtained by detailed balance from the corresponding $N + N \rightarrow N + \Delta$ cross-sections. Cugnon et al (Cugnon-81) assumes a delta lifetime much larger than the collision time: the surviving deltas at the end of the collision determine the number of pions. This model of the delta behavior is retained in the version of the code used here. Other cascade codes, such as the Berkeley one, include further channels: once formed the delta can decay into a nucleon and a pion, which can subsequently be absorbed by another nucleon to form another delta. The final pion multiplicities are not affected strongly by the addition of these other channels.

The nuclei are Lorentz boosted to the desired collision energy. The calculations begin by allowing all the nucleons to move freely with their initial momenta. Their positions and momenta are updated at regular time intervals. When two nucleons pass each other at their closest distance of approach, and this distance is below a minimum value, the pair is allowed to scatter. The different channels available are chosen by Monte Carlo sampling of the ratios of the corresponding cross-sections. The calculations continue until the number of collisions falls below a predetermined value or until a time

limit is reached (Cugnon-80). Each cascade run is repeated with different random numbers from thirty to forty times in order to obtain sufficient statistics to calculate the average values of the quantities of interest. We introduced into the simple version of the code the calculation of the standard deviations of the means.

2.2.3 Some results of the cascade.

Inclusive proton cross-sections are well reproduced in the carbon on carbon, neon on neon, and argon on argon systems at 800 A.Mev, but there is a discrepancy in the pion cross-sections (Cugnon-80). For the system calcium on calcium at 800 A.Mev the average number of collisions is 3 and that for neon on uranium at 250 A.Mev is about 5 (Cugnon-82).

The calculations have also been analysed in terms of interacting clusters: members of different clusters interact only weakly with one another, the cut off being the Fermi momentum (Cugnon-81a). The separation between participants and spectators appears to follow closely the clean-cut geometrical picture, implying small transverse momentum transfers probably due to the forward-peaked nucleon-nucleon cross-sections (Cugnon-82).

The participants, usually divided into 2 or 3 clusters, are subject to strong compression and high temperatures for a very short time and expand rapidly indicating a possible blast wave

(Cugnon-82). The existence of a sidesplash and of a strong shock wave are predicted for the collisions of neon on nickel at 250 A.Mev (Cugnon-81).

2.3 Thermal and chemical equilibria.

The cascade model offers the opportunity to study the evolution of a relativistic heavy-ion collision (Cugnon-81). Cugnon et al studied the central collisions of two calcium-like nuclei in the energy range 0.4 - 3.0 A.Gev to investigate if the system reaches thermal equilibrium at some time during the collision:

(a) The matter density evolution is plotted both in the beam direction and in the transversal plane. The matter density here is defined as the baryon number density. The cascade calculation shows that at 1.0 A.Gev the nuclear matter is compressed in the beam direction, gradually passing through a maximum at about 8 fm/c, when the shape of the system is quite oblate, then decompresses very fast becoming explosive in all directions. This picture is qualitatively the same at 2.0 A.Gev, but all phases are shortened as the energy increases. At the point of maximum compression the system is significantly slowed down, but the nucleons have large random velocities.

(b) Rapidity and transverse momentum distributions of the

baryons show clear changes from the initial ones. The final spectra appear not to be fully thermalized showing remnants of the initial opposite flows. The spectra are fit with relativistic Maxwell-Boltzmann distributions to extract transverse and longitudinal temperatures. The latter are found to be systematically higher than the former, indicating the possible lack of thermal equilibration of the system. The asymmetry parameter defined as

$$\gamma = \frac{\langle P_\perp^2 \rangle}{\langle P_\parallel^2 \rangle} \qquad (2.3.1)$$

i.e., the ratio of the expected values of the squares of the transverse and the parallel momenta in the center of mass frame of the system, is equal to 2 for complete thermal equilibration. The calculated values in the cascade model are much lower and closer to 1, indicating again the possible lack of thermal equilibration of the system.

(c) Pion multiplicities are overestimated. The pion spectra yield different transverse and longitudinal temperatures, both lower than the corresponding ones for the baryons, indicating again the possible lack of thermal equilibration.

We return to this problem in chapter 3, where were compare the results obtained by Cugnon et al with the two-fireball/blast wave model and show that these results can be reproduced very

closely by the thermodynamic model with collective flows.

One of the basic assumptions of the thermodynamic model is that
the participants reach chemical equilibrium at some point
during the collision (Mekjian-77). This simplifying assumption
has been the subject of much investigation by various authors.
One study (Cugnon-81) investigates the time evolution of the
number of deltas and the pion multiplicities within the
framework of the intranuclear cascade. They find that the
number of deltas increase almost linearly during the diving
phase, remains almost constant during the phase of maximum
compression, and then decrease slowly as the system expands.
At the stage of maximum compression the equilibrium number of
deltas (Appendix 7.8.1) is given roughly by

$$\frac{N_\Delta}{N_?} \approx 4\, e^{-(m_\Delta - m_?)/T} \tag{2.3.2}$$

They conclude that the final pion multiplicities contain
information from this stage of quasi-equilibrium before the
system decompresses.

Another study of the chemical evolution in an expanding
fireball (Cugnon-83) shows that the chemical abundances may be
very far from their equilibrium values. The model used assumes
a spherical fireball, characterized by a single temperature,
where the abundances are determined from the equation for
chemical evolution:

$$\frac{d\rho_i}{dt} = -\frac{\rho_i}{V}\frac{dV}{dt} - L_i + G_i \qquad\qquad (2.3.3)$$

as the fireball is allowed to expand with a rate consistent with the cascade calculations. V is the fireball volume, ρ_i is the particle density for species i, L_i and G_i are the loss and gain terms respectively. In a fast expansion the reaction rates can be quite different from their equilibrium values.

Equilibrium rate calculations (Harris-84) show that thermal and chemical equilibrium are closely approached during the stage of maximum compression and that the pion plus delta abundances at this stage become the final observed pion multiplicity.

In chapter 4 we define carefully the equilibrium situation within the intranuclear cascade code and show that the participants can approach chemical equilibration very closely at the stage of maximum compression.

2.4 Average multiplicities and geometry.

Multiplicity means the number of charged particles emerging from an event (collision). The analysis of individual events can be performed either by using a streamer chamber, photographic emulsions, or other 4π detectors.

It is necessary to distinguish between the primordial charges

and the measured charges. Suppose that the projectile contributes Q_1 protons and N_1 neutrons, and the target contributes Q_2 protons and N_2 neutrons, to the participants. In other words, the participants have $Q = Q_1 + Q_2$ primordial protons, and $N = N_1 + N_2$ primordial neutrons. As a result of the collision one would see a number of proton tracks, of deuteron tracks, etc., as well as pions. From the principle of charge conservation we have:

$$Q = n_p + n_d + n_t + 2\left(n_{3_{He}} + n_{4_{He}}\right) + \ldots + n_{\pi^+} - n_{\pi^-} \quad (2.4.1)$$

In a multiplicity experiment one measures typically instead n_p + n_d + n_t + $n_{3_{He}}$ + $n_{4_{He}}$ + ... + n_{π^+} + n_{π^-}. It is then clear that the measured multiplicity is a function both of the geometry and the dynamical assumptions regarding the production of composites and also of pions. The average charge multiplicity is given by (Gosset-77):

$$\langle M \rangle = \frac{\int n_c(b)\, 2\pi b\, db}{\int 2\pi b\, db} \quad (2.4.2)$$

where $n_c(b)$ = $n_p(b) + n_d(b) + n_t(b) + n_{3_{He}}(b) + \ldots + n_{\pi^+}(b)$ + $n_{\pi^-}(b)$. Gutbrod et al (Gutbrod-78) measured the associated charged particle multiplicity, which is defined as the number of charged particles measured only when there is at the same time the detection of a charged particle at 90 degree to the beam direction in the laboratory frame. The trigger particle

can be a proton or any other charged light fragment. This puts an extra bias towards central collisions since in such collisions more charged particles are produced and hence there is a greater probability of having a charged particle at 90 degrees. The associated charged particle multiplicity thus measures (Cecil-79):

$$\langle M_a \rangle = \frac{\int [n_c(b) - 1] \frac{dn}{d\Omega}(\frac{\pi}{2}, b) \, 2\pi b \, db}{\int \frac{dn}{d\Omega}(\frac{\pi}{2}, b) \, 2\pi b \, db} \qquad (2.4.3)$$

The rise of the associated multiplicity with the beam energy for the same projectile-target combination has been advanced as a proof that the simple geometrical clean-cut participant-spectator model fails (Gutbrod-78, Sandoval-80).

It is now clear that the associated multiplicity tests a combination of geometrical and dynamical assumptions, since the number of charged particles depends not only upon the primordial charges but also upon the model employed for composite and pion productions. In order to test the geometry alone we have to compare primordial charge cross-sections. It is calculated following equation 2.4.1 (Nagamiya-81):

$$\sigma_Q = \sum_i z_i \sigma_i \qquad (2.4.4)$$

Assuming the colliding ions to be spheres of constant density the simple geometrical model gives a very simple answer for the

primordial charge cross-section:

$$\sigma_Q = \pi r_0^2 \left(z_p A_t^{2/3} + z_t A_p^{2/3} \right) \qquad (2.4.5)$$

The data of Nagamiya et al (Nagamiya-81) can be used to test the constancy of this figure. This data, however, is not always sufficient because the cross-sections for positive pions are not measured in some cases. Nonetheless it is obvious that $\sum_i z_i \sigma_i$ has some dependence on the incident beam energy, and hence the participant-spectator model has to be examined more carefully. This model may still be valid, but the independence of the straight line geometry on the incident energy assumed previously may have to be given up.

The cascade model supports the participant-spectator picture of high energy collisions. This is clearly seen in the collision of two calcium-like nuclei at 1.0 A.Gev (Cugnon-81) from the contour plots of the matter density in the reaction plane. However, there is no clean-cut separation between the participants and the spectators as the former continue to expand.

The equidensity curves can be fitted well by the sum of a central Gaussian and two Lorentz-contracted Gaussians (Cugnon-81):

$$\rho(r) = \frac{A_P}{(r_0\sqrt{\pi})^3}e^{-r^2/r_0^2} + \frac{1}{2}\frac{A-A_P}{(a\sqrt{\pi})^3} \cdot$$
$$\cdot \left[e^{-\frac{1}{a^2}\left[(x-x_1)^2+y_1^2+\gamma^2(z-z_1)^2\right]} + e^{-\frac{1}{a^2}\left[(x+x_1)^2+y_1^2+\gamma^2(z+z_1)^2\right]}\right] \quad (2.4.6)$$

where A_P, r_0, x_1, z_1, a are adjustable parameters, γ is the Lorentz factor for the center of mass of the nuclei, and A is the total nucleon number. A_P is fairly constant, r_0, z_1, a are linear functions of the time, and x_1 increases slowly. The spectator velocity $\dot{z}_1$ is close to the velocity of the nuclei before the collision. The increase of x_1 indicates a small sidesplash (Cugnon-81). The number of participants A_P is always smaller than its clean-cut geometrical counterpart. .

A similar equation holds for the nuclear charge density, (Cugnon-80a) showing expansion velocities of about 0.4c for the participants. Again the participant charge is less than that calculated from the clean-cut geometry. This time-dependent nuclear charge distribution is used to calculate the final state Coulomb distortion of the pion and the nucleon spectra (Cugnon-80a).

The participants are further analysed in terms of clusters (Cugnon-81a). Members of the same cluster are linked by violent interactions, whereas the connection between members of different clusters is very weak. An interaction is classified as violent if the four-momentum transfer is larger than a cut off value, which is typically taken as the Fermi momentum. Central events contain on the average about 3 clusters,

suggesting some scaling with the total nucleon number.

3 - THERMAL EQUILIBRIUM

3.1 Introduction.

We address the problem of thermal equilibration in heavy-ion collisions by comparing two models with fundamentally different basic assumptions: the thermodynamic fireball model, and the intranuclear cascade model. The first one represents a macroscopic approach while the later is a microscopic model. The thermodynamic models contain as a basic postulate the assumption that the participants can be described at the freeze-out point as a non-interacting relativistic gas in thermal and chemical equilibrium; they may also include longitudinal and radial collective flows. The cascade models on the other hand contain no assumption or constraint regarding conditions for equilibrium of any kind, limiting itself to follow the individual interactions of its constituents to the final stage of the collision. This feature of the cascade models make them particularly suitable for the description of off-equilibrium situations.

The results of the cascade calculations resemble the

experimental data in the sense that they present the same complexity and require extensive treatment before one can extract some physical results from them; it is also difficult to trace a calculated result to a particular physics input. It is useful therefore to compare this model with simpler more transparent models, such as the thermodynamic fireball models.

Cugnon et al (Cugnon-81) examine the collisions of two calcium-like nuclei, where complete charge degeneracy is assumed, at zero impact parameter (b = 0) for various collision energies. Only chargeless nucleons and chargeless delta resonances are included in the calculations. The chargeless pions are produced from the subsequent decay of the deltas at the freeze out stage of the collision. The cascade code (Cugnon-81) already described in Chapter 2 includes the initial Fermi motion of the nucleons, but does not take into account any field effects at the same time. This way the nuclei tend to dissipate even in the absence of any collision, but this expansion is slow enough to have only a minor influence on the results.

Cugnon et al, using their cascade code, calculated the final rapidity and perpendicular momentum distributions, dN/dy and $dN/dp_\perp$, both for baryons (nucleons plus deltas) and for pions in the center of mass frame of the two nuclei. The rapidity of a particle has a very simple transformation property between different Lorentz frames, which makes it a popular variable to replace the parallel momentum $p_\parallel$. In relativistic mechanics the

rapidity y along an axis is defined as

$$y = \frac{1}{2} \log \frac{E + p_n}{E - p_n} \qquad (3.1.1)$$

for a particle of energy E and momentum p with projection p_n along the axis and $p_\perp$ in the perpendicular plane. It can be shown immediately, using the Lorentz transformation for the energy-momentum of a particle, that the rapidities in two different frames are connected by the relation:

$$y^* = y + \frac{1}{2} \log \frac{1 + V_F}{1 - V_F} \qquad (3.1.2)$$

where V_F is the relative velocity of the two frames.

They fit these distributions with appropriate relativistic Maxwell-Boltzmann curves and extract rapidity and perpendicular momentum temperatures. Different temperatures result in each case (Table 3.4.1). The uncertainties in the rapidity temperatures are between 20 and 30 Mev, and in the perpendicular momentum temperatures are about 10 Mev. These results are clearly conflicting with the predictions of the one-fireball model. This model predicts a single temperature $(T_\perp = T_y)$.

3.2 Fireball type models.

We study the collisions of two calcium-like nuclei at zero impact parameter (b = 0) for the projectile energy of 1.0 A.Gev, using fireball type models. Likewise, we include only chargeless nucleons and chargeless deltas in the models; in the freeze out stage of the collisions the deltas are allowed to decay into nucleons and pions. The formation of composites is also not taken into account so that the results may be comparable with the cascade model calculations of Cugnon et al.

In the simple one-fireball model each hadronic species is distributed according to a relativistic Maxwell-Boltzmann distribution:

$$\frac{d^3 n_i}{dp^3} = \frac{g_i V}{(2\pi)^3} e^{\mu_i/T} e^{-\frac{1}{T}\sqrt{m_i^2 + p^2}} \tag{3.2.1}$$

where m_i is the particle mass, μ_i is the chemical potential, V is the fireball volume corresponding to the freeze out density ρ_c, T is the fireball temperature, and the multiplicity factor $g_i = (2I_i + 1)(2S_i + 1)$ takes into account the particle spin S_i and the isospin I_i. There are three unknown parameters: the nucleon chemical potential μ_N, the fireball temperature T, and

the fireball volume V. The chemical potential of the deltas is obtained from the nucleon chemical potential by the law of chemical equilibrium, as for example, the reaction $N + N \rightarrow N + \Delta$ leads to the relation $\mu_\Delta = \mu_N$ for the delta chemical potential. The unknown parameters are determined by solving the system of equations 2.1.5 to 2.1.8 for the conserved quantities (the energy E of the fireball, its charge Q, and its baryon number B), and the freeze out density ρ_c.

The rapidity distribution is obtained from the relativistic Maxwell-Boltzmann distribution in momentum space by transforming the variables $(p_\perp, p_\parallel)$ to (E, y), and integrating over the particle energy (Appendix 7.3):

$$\frac{dn_i}{dy} = \frac{n_i T^2}{2 m_i^2 K_2(m_i/T)} \left[\left(1 + \frac{m_i}{T} \cosh y \right)^2 + 1 \right] \frac{e^{-\frac{m_i}{T} \cosh y}}{\cosh^2 y} \tag{3.2.2}$$

The perpendicular momentum distribution is obtained likewise from the Maxwell-Boltzmann distribution in momentum space by direct integration over the parallel momentum $p_\parallel$ (Appendix 7.4):

$$\frac{dn_i}{dp_\perp} = \frac{n_i}{m_i^2 T K_2\left(\frac{m_i}{T}\right)} \sqrt{m_i^2 + p_\perp^2} \cdot p_\perp \cdot K_1 \left(\frac{1}{T} \sqrt{m_i^2 + p_\perp^2} \right) \tag{3.2.3}$$

Here K_1 and K_2 are modified Bessel functions known as the MacDonald functions.

These two forms can be used to extract the rapidity and the perpendicular momentum temperatures by a least squares fit to the corresponding distributions obtained from other models such as the cascade, the two-fireball, and the two-fireball/blast-wave models.

3.3 The two-fireball model.

The simple one-fireball model predicts spherically symmetric distributions. However, the spectra from the collisions of light nuclei, such as carbon on carbon, show signs of anisotropy in their center of mass frame. This means that the target and the projectile participants are slowed down significantly during the collision but still present remnants of their initial collective flows along the collision axis. Such a situation can be suitably represented by assuming that two fireballs are formed instead of only one, such that they retain some of their initial momenta before the collision. The momenta after the collision is related to the momenta before the collision by the so called transparency factor (Appendix 7.1.2):

$$P_f = e \cdot P_i \qquad (3.3.1)$$

where P_i is the initial momentum of the nuclei before the

collision and $P_{\vec{f}}$ is the fireball momentum, both in their center of mass frame. The transparency factor e is a function of the average number of nucleon-nucleon collisions during the reaction (Appendix 7.1.2):

$$e = 0.55^{0.47 + 0.61\bar{\nu}} \qquad (3.3.2)$$

Here $\bar{\nu}$ is the average number of nucleon-nucleon collisions that a nucleon suffers during the reaction.

The introduction of collective translational flows into the fireball model reduces the degree of symmetry of the momentum distributions. In particular, we can expect different properties along the collision axis and its transverse plane. Thus the two-fireball model can lead to different apparent longitudinal (rapidity) and transverse temperatures as we shall see below. The basic features of the cascade calculations are already apparent in the two-fireball model.

We produce a two-fireball calculation at 1.0 A.Gev and zero impact parameter, including only nucleons and deltas. The pions are obtained from the decay of the deltas in the freeze-out stage as in the Cugnon code. The two-fireball model assumes that each fireball is in thermal and chemical equilibrium with a relativistic Maxwell-Boltzmann distribution holding for each one of the hadronic species present. Here the parameters (chemical potentials, temperature, volume, freeze out density)

are defined in the rest frames of each fireball. There is a single temperature for both fireballs and it does not matter if the two fireballs are separated from each other physically in space or not. Equations 2.1.5 to 2.1.8 for the conserved quantities are written in the frames of each fireball for simplicity. The thermodynamical calculation is essentially identical to the case of the one-fireball model, but now the energy available for thermalization is reduced by the amount that remains as collective translational motion along the collision axis.

The Lorentz invariance of Ed^3n_i/dp^3 allows us to calculate the rapidity distribution in the center of mass of the two fireballs. A change from the cylindrical coordinates $(p_\perp, p_\parallel)$ to (E,y) leads to the integral (Appendix 7.3.2):

$$\frac{dn_i}{dy*} = \frac{2\pi}{\cosh^2 y*} \int_{m_i \cosh y*}^{\infty} E \frac{dn_i}{dp^3} E* dE* \qquad (3.3.1)$$

The starred variables refer to quantities in the center of mass frame, and the others to the fireball frame. Each hadronic species in the fireball is distributed according to the Maxwell-Boltzmann law. Transform the variables in the fireball frame to the center of mass frame, introduce the notation

$$\phi^{\pm} = \cosh y^* \pm V_F \sinh y^* \qquad (3.3.2)$$

integrate and add together the distributions for each fireball. We get finally (Appendix 7.3.2):

$$\frac{dn_i}{dy^*} = \frac{g_i V e^{\mu_i/T}}{(2\pi \gamma_F)^2} T^3 \left[\left\{ \left(\frac{m_i \gamma_F \phi^+}{T} + 1 \right)^2 + 1 \right\} \cdot \right.$$

$$\left. \cdot \frac{e^{-\frac{m_i}{T} \gamma_F \phi^+}}{\phi^+} + \left(\frac{m_i \gamma_F \phi^-}{T} + 1 \right)^2 \frac{e^{-\frac{m_i}{T} \gamma_F \phi^-}}{\phi^-} \right] \qquad (3.3.3)$$

The surviving deltas at the freeze-out stage decay into nucleons and pions. The pion rapidity distribution is obtained from equation 3.3.1, where now the integrand contains the pion distribution Ed^3n_i/dp^3 in the fireball (Appendix 7.2):

$$\frac{dn_i^{\pm}}{dy^*} = \frac{g_i V e^{\mu_\Delta/T}}{4\tau^2 \cosh^2 y^*} \int_{m_i \cosh y^*}^{\infty} \left[\left(\frac{m_\Delta E_{0i} \phi^{\pm} E^*}{m_i^2} + T \right) \frac{m_\Delta T}{P_0 \chi^{\pm}} \cdot \right.$$

$$\left. \cdot \left(\alpha^{\pm} - \omega^{\pm} \right) + \frac{m_\Delta^2 T}{m_i^2} \left(\alpha^{\pm} + \omega^{\pm} \right) \right] E^* dE^* \qquad (3.3.4)$$

where we use the notation

$$\chi^{\pm} = \left[(\phi^{\pm} E^*)^2 - m_i^2 \right]^{1/2} \qquad (3.3.5)$$

$$\psi^{\pm} = exp\left[\frac{m_\Delta p_o}{m_i^2 T} \chi^{\pm} - \frac{m_\Delta E_{oi}}{m_i^2 T} \phi^{\pm} E^* \right] \qquad (3.3.6)$$

$$\omega^{\pm} = exp\left[-\frac{m_\Delta p_o}{m_i^2 T} \chi^{\pm} - \frac{m_\Delta E_{oi}}{m_i^2 T} \phi^{\pm} E^* \right] \qquad (3.3.7)$$

The integral above is evaluated numerically for each fireball and the results are added together to produce the final distribution.

The perpendicular momentum distribution is calculated by projecting the Maxwell-Boltzmann distribution into the perpendicular plane. This is achieved by integrating over the parallel momentum. Since the perpendicular momentum is not affected by the Lorentz transformation we can write (Appendix 7.4):

$$\frac{dn_i}{dp_\perp^*} = 2\pi p_\perp^* \int_{-\infty}^{\infty} \frac{d^3 n_i}{dp^3} dp_{\parallel} \qquad (3.3.8)$$

The joint distribution for the two fireballs is:

$$\frac{dn_i}{dp_\perp^*} = \frac{g_i V e^{\mu_i/T}}{\pi^2} \sqrt{m_i^2 + p_\perp^{*2}} \cdot p_\perp^* \cdot K_1\left(\frac{1}{T}\sqrt{m_i^2 + p_\perp^{*2}}\right) \qquad (3.3.9)$$

The same reasoning goes also for the decay products of the deltas, but here again the integration must be evaluated numerically. The perpendicular momentum distribution for the pions is (Appendix 7.4.2):

$$\frac{dn_i}{dp_\perp^*} = \frac{g_\Delta V}{\pi^2} e^{\mu_\Delta/T} p_\perp^* \int_0^\infty \frac{dp_\parallel}{E} e^{-\frac{m_\Delta E_{0i}}{m_i^2 T} E} \cdot$$

$$\cdot \left[\frac{m_\Delta T}{p_0 p}\left(\frac{m_\Delta E_{0i} E}{m_i^2} + T\right)\sinh\frac{m_\Delta p_0 p}{m_i^2 T} - \frac{m_\Delta^2 T}{m_i^2}\cosh\frac{m_\Delta p_0 p}{m_i^2 T}\right] \qquad (3.3.10)$$

where we substitute $p = (p_\perp^2 + p_\parallel^2)^{1/2}$ and $E^2 = m_i^2 + p^2$.

We calculate the rapidity and perpendicular momentum distributions for the baryons adding together the distributions for the nucleons and the deltas. We compare them with the corresponding Maxwell–Boltzmann forms (equations 3.2.1 and 3.2.2) and determine the temperature parameters in these curves by the least squares method. We do the corresponding calculations for the pion distributions. Different rapidity and perpendicular momentum temperatures result in each case, both for the baryons and for the pions (Table 3.4.1). This prediction of different temperatures indicates only that some

longitudinal collective flow remained after the collision; the lower pion temperatures, however, are due to a kinematic effect reflecting the smaller pion mass.

3.4 The two-fireball/blast-wave model.

The two-fireball model above reproduces the main features of the Cugnon cascade yielding different transverse and longitudinal temperatures both for the baryons and for the pions. The Cugnon cascade predicts a transverse temperature of 100 Mev (93 Mev for the two-fireball model) and a rapidity temperature of 130 Mev (117 Mev for the two-fireball model). For the pions we have 82 Mev (84 Mev) and 100 Mev (116 Mev) in the same order respectively.

The two-fireball model (like the one-fireball model) has the deficiency that the number of pions predicted is too high. The number of deuterons and protons are given quite adequately by the model. Now the number of pions and deuterons depend (in the thermodynamic model) upon two parameters: the freeze out density ρ_c and the temperature T. In earlier calculations (Das Gupta-79) in the two-fireball model the value of ρ_c was taken equal to 0.12 fm^{-3}. The value of T was not an adjustable parameter; it depended upon the beam energy. Not all of the beam energy in the center of mass was converted into thermal energy; some longitudinal velocity remained and the energy

associated with this longitudinal velocity was not available for thermalization. The final longitudinal velocities are not really free parameters of the model; they can be deduced from high energy pp data and in any case, the experimental data on proton anisotropy put severe limits on the amount of longitudinal velocity that remains.

To resolve the problem of overestimation of pion production one can take the following point of view: the two determining quantities ρ_c and T in the two-fireball model can be fixed from the known experimental ratios σ_p/σ_α and σ_p/σ_π. Since there was never any difficulty in obtaining the correct σ_p this would mean that one has the correct total cross-sections for protons, deuterons and pions, the three most copious species produced in the Bevalac energy regime.

The temperature so deduced is less than the temperature obtained in the original two-fireball model. This means that some of the beam energy is transformed into collective energy which is other than longitudinal velocity. Following Siemens and Rasmussen, this is taken to be an outward constant radial velocity in each of the two fireballs.

The particles near the surface of a hot and dense fireball face an anisotropic environment and consequently the randomness of their kinetic energies is reduced resulting in a net collective outward radial flow with an average radial velocity V_r. The basic assumption here is that there is a Maxwell-Boltzmann

distribution for each hadronic species in the fireball in all frames moving radially outwards with the expansion velocity V_r. The Lorentz invariance of the product $E d^3 n_i/dp^3$ allows us to obtain the momentum distributions in the rest frames of the fireballs (Appendix 7.1.3):

$$\frac{d^3 n_i}{dp^3} = \frac{g_i V \gamma_r e^{\mu_i/T}}{16\pi} \left[(x_2 - x_1 + 1)e^{x_1} - (x_2 + x_1 + 1)e^{-x_1} \right] \frac{e^{-x_2}}{x_1 x_2} \qquad (3.4.1)$$

Here the gamma factor $\gamma_r = 1/\sqrt{1 - V_r^2}$, $x_1 = \gamma_r V_r p/T$, and $x_2 = \gamma_r E/T$.

The introduction of both translational and radial flows into the fireball model allows for the reduction of the amount of energy that is available for thermalization, thus permitting the variation of the temperature parameter of the model. As it turns out, the radial explosion consumes far more energy than the translational flows. The latter, though less important, is still necessary to account for the center of mass anisotropy of the spectra in the collisions of lighter ions.

The calculational procedures here are entirely analogous to the case of the two-fireball model, but now each hadronic species follows the Maxwell-Boltzmann distribution in each radial frame moving with the radial velocity V_r or equivalently the calculated distribution of equation 3.4.1 above in the fireball frames. Equations 2.1.5 to 2.1.8 for the conserved quantities can be written in the radial frames for simplicity. The

parameters of the model are then defined in any of the infinite number of these entirely equivalent frames. The energy available for thermalization in the radial frames is connected to the energy of the collision in the center of mass frame of the two fireballs by the sequence of two Lorentz transformations:

$$E_r = \frac{1}{\gamma_r} \cdot \frac{r}{\gamma} \cdot E \qquad (3.4.2)$$

where γ is the gamma factor between the center of mass frame and the frame of each fireball, and γ_r connects the frame of one fireball and any of its radial frames. The fraction of kinetic energy committed to the radial expansion is taken from calculations with this model for the case of Ar + KCl at 800 A.Mev (Gale-83). It amounts to 41% of the energy of the collision, which produces a value of 94% for the radial gamma factor γ_r.

The rapidity distribution in the frame of one fireball is obtained by changing the variables $(p_\perp, p_\parallel)$ to (E, y) and integrating over the energy:

$$\frac{dn_i}{dy} = 2\pi \int_{m_i \cosh y}^{\infty} \frac{d^3 n_i}{dp^3} \frac{E^2}{\cosh^2 y} dE \qquad (3.4.3)$$

The distribution of each hadronic species is given by equation 3.4.1 instead of the Maxwell-Boltzmann (Appendix 7.3.3):

$$\frac{dn_i'}{dy} = \frac{g_i V e^{\mu_i/T}}{16\cosh^2 y} \int_{m_i\cosh y}^{\infty} \left[(x_2 - x_1 + 1)e^{x_1} - (x_2 + x_1 + 1)e^{-x_1}\right] \frac{e^{-x_2} E^2 dE}{x_1 x_2} \quad (3.4.4)$$

with $x_1 = \gamma_r V_r \sqrt{E^2 - m_i^2}/T$, and $x_2 = \gamma_r E/T$. The distribution in the center of mass frame is obtained by noting that $dy^* = dy$ and evaluating numerically the integral above for each fireball using the appropriate value of the rapidity in each case:

$$\frac{dn_i'}{dy^*} = \frac{dn_i'}{dy}\left(y = y^* + \frac{1}{2}\log\frac{1+v_F}{1-v_F}\right) + \frac{dn_i'}{dy}\left(y = y^* - \frac{1}{2}\log\frac{1+v_F}{1-v_F}\right) \quad (3.4.5)$$

The rapidity distribution for the pions is evaluated numerically for each fireball with the appropriate value of the rapidity as above and added together (Appendix 7.3.3):

$$\frac{dn_i'}{dy} = \frac{\pi m_\Delta}{p_0 \cosh^2 y} \int_{m_i\cosh y}^{\infty} \frac{E\, dE}{\sqrt{E^2 - m_i^2}} \int_{E_\Delta^-}^{E_\Delta^+} \frac{dn_\Delta^3}{dp_\Delta^3} E_\Delta\, dE_\Delta \quad (3.4.6)$$

where the distribution of the deltas in the fireball frames is given again by the same equation 3.4.1 above.

The calculation of the perpendicular momentum distribution is entirely analogous to the case of the two-fireball model above, except that one has to use the appropriate distributions for this model in the integrands. Using equation 3.4.1 into equation 3.3.8 we get:

$$\frac{d n_i}{d y} = \frac{g_i V \gamma_r e^{\mu_i/T}}{4} \cdot P_\perp^* \int_0^\infty \left[(x_2 - x_1 + 1) e^{x_1} - (x_2 + x_1 + 1) e^{-x_1} \right] \frac{e^{-x_2} d p_{||}}{x_1 x_2} \qquad (3.4.7)$$

with $\quad x_1 = \gamma_T V_r \sqrt{p_\perp^{*2} + p_{||}^2}/T, \quad x_2 = \gamma_r \sqrt{m_i^2 + p_\perp^{*2} + p_{||}^2}/T$. The integral is evaluated numerically.

The pion distribution is obtained by from equation 3.3.8 using 3.4.1 into 2.1.10:

$$\frac{d n_i}{d p_\perp^*} = \frac{g_\Delta m_\Delta P_\perp^*}{16 p_0} e^{\mu_\Delta/T} \int_{-\infty}^{+\infty} \frac{d p_{||}}{\sqrt{P_\perp^{*2} + p_{||}^2} \sqrt{m_i^2 + P_\perp^2 + p_{||}^2}} \cdot$$

$$\cdot \int_{E_\Delta^-}^{E_\Delta^+} \left[(x_2 - x_1 + 1) e^{x_1} - (x_2 + x_1 + 1) e^{-x_1} \right] \frac{e^{-x_2}}{x_1 x_2} E_\Delta d E_\Delta \qquad (3.4.8)$$

The double integral is evaluated numerically.

We calculate the rapidity and perpendicular momentum distributions in this model and extract the temperature parameters by fitting the corresponding curves in the one-fireball model by a least squares method. The apparent temperatures in the center of mass rise and the difference between pions and nucleons is accentuated. The predictions of this model for the transverse temperature is 112 Mev (100 Mev for the cascade) and for the rapidity temperature is 132 Mev (130 Mev for the cascade) in the case of the baryons. For the

pions we get 88 Mev (82 Mev) and 117 Mev (100 Mev) in the same order respectively. The quantitative agreement between the cascade and the fireball models is greatly improved in the case of the baryons, with the addition of the outward radial collective flows to each fireball. The apparent. pion temperatures do not improve over the two-fireball model predictions (Table 3.4.1).

Cugnon et al calculate the asymmetry parameter Y to further test the degree of thermalization of the participants. The asymmetry parameter is defined as the ratio of the expected values of the squares of the perpendicular and of the parallel momenta in the center of mass frame of the participants:

$$Y = \frac{\langle P_\perp^{*2} \rangle}{\langle P_\parallel^{*2} \rangle} \qquad (3.4.9)$$

For a system of particles with entirely random momenta the value of the asymmetry parameter should be very close to its theoretical value, which is equal to 2.0.

It is obvious that $\langle P_\perp^{*2} \rangle = \langle P_\perp^2 \rangle$ so we can do the evaluation in the rest frame of the fireball:

$$\langle P_\perp^{*2} \rangle = \frac{g \cdot V}{8 \pi_i} e^{\mu/T} \int_0^\infty P_\perp^2 dP_\perp \int_{-\infty}^\infty \left[(x_2 - x_1 + 1) e^{x_1} - (x_2 + x_1 + 1) e^{-x_1} \right] \frac{e^{-x_2} dP_\parallel}{x_1 x_2} \quad (3.4.10)$$

We also need to evaluate $\langle P_\parallel^{*2} \rangle$ in order to calculate the

asymmetry ratio Y. We have (Appendix 7.5.3):

$$\langle p_{\shortparallel}^{*2} \rangle = \gamma^2 \left[\langle p_{\shortparallel}^2 \rangle + V_F \langle E^2 \rangle \right] \tag{3.4.11}$$

Noting that $E^2 = m_i^2 + p_{\perp}^2 + p_{\shortparallel}^2$, we obtain finally:

$$Y = \frac{\langle p_{\perp}^2 \rangle}{\gamma^2 \left[(1 + V_F) \langle p_{\shortparallel}^2 \rangle + V_F^2 (m_i^2 + \langle p_{\perp}^2 \rangle) \right]} \tag{3.4.12}$$

The only quantity left to calculate in this expression is $\langle p_{\shortparallel}^2 \rangle$ in the fireball frame. We have:

$$\frac{dn_i}{dp_{\shortparallel}} = 2\pi \int_0^\infty \frac{d^3 n_i}{dp^3} \, p_{\perp} \, dp_{\perp} \tag{3.4.13}$$

from which we get:

$$\langle p_{\shortparallel}^2 \rangle = \frac{2\pi}{n_i} \int_{-\infty}^\infty p_{\shortparallel}^2 \, dp_{\shortparallel} \int_0^\infty \frac{d^3 n_i}{dp^3} \, p_{\perp} \, dp_{\perp} \tag{3.4.14}$$

so that with the appropriate distribution for this model

$$\langle p_{\shortparallel}^2 \rangle = \frac{g_i \, V \, \gamma_r \, e^{\mu_i/T}}{8 n_i} \int_{-\infty}^\infty p_{\shortparallel}^2 \, dp_{\shortparallel} \int_0^\infty p_{\perp} \, dp_{\perp} \cdot$$

$$\cdot \left[\left(x_2 - x_1 + 1 \right) e^{x_1} - \left(x_2 + x_1 + 1 \right) e^{-x_1} \right] \frac{e^{-x_2}}{x_1 x_2} \qquad (3.4.15)$$

This double integral is evaluated numerically.

The Cugnon cascade predicts a value of 1.2 for the asymmetry parameter for the baryons, while our own calculation produces a value of 1.7 using this version of the fireball model. The reason for this discrepancy may be that our rapidity and perpendicular momentum distributions are fit extremely well (Figure 9.2) by the Boltzmann curves; on the other hand the distributions obtained from the cascade code show deviations from a perfect Boltzmann distribution.

TABLE 3.4.1 Rapidity and transverse temperatures.

Comparison of the rapidity and transverse temperatures for the system calcium on calcium at 1.0 A.Gev.

	$T_\perp(N)$	$T_y(N)$	$T_\perp(\pi)$	$T_y(\pi)$
Cascade (Cugnon-81)	100	130	82	100
Two-fireball	93	117	84	116
Two-fireball/blast-wave	112	132	88	117

In conclusion we may say that the two-fireball/blast-wave model reproduces the different longitudinal and transverse temperatures obtained from the cascade model calculations. These different temperatures result from residual longitudinal motions left after the collision and are futher enhanced by the

collective radial flows resulting from the blast in each of the two fireballs. These collective flows coexist with thermal equilibrium in the fireballs. It shows that the results of the cascade calculations do not necessarily imply the lack of thermal equilibration in the collision, but only that the existence of collective motions must be properly taken into account.

4 - PION PRODUCTION AND CHEMICAL EQUILIBRIUM

4.1 Introduction.

In chapter 3 we saw that thermal equilibration of the participants is not in conflict with the results of the cascade calculations of Cugnon et al. Now we investigate the attainment of chemical equilibration for the number of deltas within the framework of the intranuclear cascade. A description of the cascade code is presented in section 4.2 and also in the Appendix 7.7. We modify this code by introducing the isospin formalism so that it can be applied to the study of charge-asymmetric systems. This extended version of the code is important because most of the data available now are for $N \neq Z$ systems. We also introduce new revised average total nucleon-nucleon cross-sections from experimental data.

4.2 The cascade code.

4.2.1 The simple version.

The basic cascade code used in this work is a simple version of the Bertsch-Cugnon code. The calculation follows the collision of two identical nuclei in their center of mass system. Relativistic mechanics is used throughout. The mathematical details of the calculations in the code are relegated to Appendix 7.7. The original version of this code assumes complete isospin degeneracy so that only one chargeless type of nucleon, of pion, and of delta are considered. This simplifying assumption restricts some results to charge symmetric systems. Much of the experimental data available, however, is concerned with the collisions of unequal and non-symmetric nuclei with $N \neq Z$. We expanded the original version to allow for the collisions of unequal nuclei, and also introduced the isospin formalism into the code to permit the study of the collisions of charge-asymmetric systems.

Each nucleus is represented by a sphere of radius $1.12 \ A^{1/3}$, where A is the mass number. Point-like nucleons are assigned random positions inside the spheres representing the colliding nuclei in their rest frames. This simple version does not include the initial Fermi motion, since we also do not introduce field effects. Although Fermi motion and field effects are important physical characteristics of nuclei they do not affect significantly the results we are interested in

this Thesis. Pauli principle effects are mocked approximately by forbidding soft collisions when the total center of mass energy of two colliding nucleons is below 1895 Mev (Cugnon-81).

Single pion production in nucleon-nucleon collisions is introduced via the formation and decay of the delta resonances. The deltas are assumed to have a mass distribution (Cugnon-81). The behavior of the deltas in compressed nuclear matter and their cross-sections are uncertain. The elastic $\Delta + \Delta \rightarrow \Delta + \Delta$ and $N + \Delta \rightarrow N + \Delta$ cross-sections are assumed to be the same as for the nucleons in free space. The inelastic $N + \Delta \rightarrow N + N$ cross-sections are obtained by detailed balance from the corresponding $N + N \rightarrow N + \Delta$ cross-sections. Cugnon (Cugnon-81) assumes a delta lifetime much larger than the collision time: the surviving deltas at the end of the collision determine the number of pions. This model of the delta behavior is retained in the version of the code used here.

The nuclei are Lorentz boosted to the desired collision energy. The calculations begin by allowing all the nucleons to move freely with their initial momenta. Their positions and momenta are updated at regular time intervals. When two nucleons pass each other at their closest distance of approach, and this distance is below a minimum value, the pair is allowed to scatter. The different channels available are chosen by Monte Carlo sampling of the ratios of the corresponding cross-sections. The calculations continue until a time limit

is reached. By this time the number of collisions has essentially dropped to zero. Each cascade run is repeated with different random numbers from thirty to forty times in order to obtain sufficient statistics to calculate the average values of the quantities of interest. We introduced into the simple version of the code the calculation of the standard deviations of the means.

4.2.2 The isospin formalism.

We use the isospin formalism to calculate the branching ratios and cross-sections when the charge states of the nucleons and the deltas are introduced into the cascade code.

The nucleon has spin $J = 1/2$ and isospin $I = 1/2$; the delta resonance has $J = 3/2$ and $I = 3/2$. A pair of nucleons can be in the state $I = 1$ or $I = 0$, while the pair delta-nucleon can have $I = 2$ or $I = 1$. Isospin conservation then, allows only the coupling of the $I = 1$ states. The branching ratios are obtained in the usual way from the Clebsch-Gordan coefficients:

$$\sigma\left(pp \to \Delta^+ p\right) = \frac{1}{4}\,\sigma\left(I = 1\right) \tag{4.2.1}$$

$$\sigma\left(pp \to \Delta^{++}n\right) = \frac{3}{4} \sigma\left(I=1\right) \tag{4.2.2}$$

$$\sigma\left(pn \to \Delta^{+}n\right) = \frac{1}{4} \sigma\left(I=1\right) \tag{4.2.3}$$

$$\sigma\left(pn \to \Delta^{0}p\right) = \frac{1}{4} \sigma\left(I=1\right) \tag{4.2.4}$$

$$\sigma\left(nn \to \Delta^{0}n\right) = \frac{1}{4} \sigma\left(I=1\right) \tag{4.2.5}$$

$$\sigma\left(nn \to \Delta^{-}p\right) = \frac{3}{4} \sigma\left(I=1\right) \tag{4.2.6}$$

For N = Z systems the average matrix element is:

$$\bar{\sigma} = \frac{1}{4}\left(\sigma' + \frac{1}{2}\sigma' + \frac{1}{2}\sigma' + \sigma'\right) = \frac{3}{4}\sigma' \tag{4.2.7}$$

We therefore define $\sigma' = 4\bar{\sigma}_{av}/3$, where

$$\sigma_{av} = \frac{1}{2}\left(\sigma_{np} + \sigma_{nn}\right) \qquad (4.2.8)$$

in order to recover the results before. the introduction of isospin.

The inverse reactions are obtained by using the reciprocity relation:

$$\tilde{\sigma}\left(N\Delta \rightarrow NN\right) = \frac{1}{4}\left(\frac{P_{N\Delta}}{P_{NN}}\right)^{2}\sigma\left(NN \rightarrow N\Delta\right) \qquad (4.2.9)$$

where the identity and the spin factors are taken into account. The branching ratios are obtained again by the conservation of isospin:

$$\sigma\left(\Delta^{++}n \rightarrow pp\right) = \frac{3}{4}\tilde{\sigma} \qquad (4.2.10)$$

$$\sigma\left(\Delta^{+}p \rightarrow pp\right) = \frac{1}{4}\tilde{\sigma} \qquad (4.2.11)$$

$$\sigma\left(\Delta^+ n \to pn\right) = \frac{1}{2}\tilde{\sigma} \qquad (4.2.12)$$

$$\sigma\left(\Delta^0 p \to pn\right) = \frac{1}{2}\tilde{\sigma} \qquad (4.2.13)$$

$$\sigma\left(\Delta^0 n \to nn\right) = \frac{1}{4}\tilde{\sigma} \qquad (4.2.14)$$

$$\sigma\left(\Delta^- p \to nn\right) = \frac{3}{4}\tilde{\sigma} \qquad (4.2.15)$$

The pairs $\Delta^{++}p$ and $\Delta^- n$ are forbidden by isospin conservation to decay into two nucleons.

4.2.3 N-N cross-section data.

We also introduce into the code more accurate experimental total (elastic and inelastic) nucleon-nucleon cross-sections (Appendix 7.6). The experimental data was evaluated for accuracy and reliability. Old data were discarded. The final selection was then smoothed and interpolated with cubic spline subroutines (IMSL-79). A simplified parametrization is also

- 69 -

used in the preliminary calculations in this chapter and also to test the sensitivity of the results to the cross-section inputs.

4.3 Chemical equilibrium.

4.3.1 Preliminaries.

If we have a reaction $N + N = X + N$ where X is an excited state of N with a definite excitation energy and spin-isospin, then the law of chemical equilibrium dictates that

$$\frac{N_x}{N_N} = \frac{g_x}{g_N} e^{-E_x/T} \qquad (4.3.1)$$

Here g_x and g_N are the degeneracies of X and N respectively. The assumption involved is that there is sufficient time for equilibration. Most chemical reactions will take place in a container where experimentally the reactants can be left for a very long time.

In heavy-ion reactions the situation is quite complicated. There is no wall within which the reactants can be kept for an arbitrarily long time. For medium mass nuclei, collisions fall off after a time of 20 fm/c. For pion production through delta, the deltas have a mass distribution so that the simple formula

written above is not directly applicable. For cascade calculations, the temperature is not given a priori; it has to be deduced following a somewhat arbitrary procedure.

To eliminate the complication of continuous mass distribution we first study the population of a fictitious excitation in the nucleon at an excitation energy of 20 Mev with spin 3/2 and isospin 3/2. We shall inappropriately call it a "delta" for facility of expression. A small excitation energy should increase the numbers of "deltas" required for the equilibration. The only reactions considered in our calculations are: $N + N \rightarrow N + N$, $N + N \rightarrow N + \Delta$, and $\Delta + \Delta \rightarrow \Delta + \Delta$. The cross-sections are assumed to be the same as the average nucleon-nucleon cross-sections, but the inelastic cross-sections are adjusted to be consistent with an excitation of 20 Mev and are also scaled by a factor of 1.75. This factor increases the reaction rates without affecting the conditions of equilibrium. The elastic cross-sections were also adapted by removing the minimum collision energy restriction used to account approximately for the Pauli Principle, because of the low excitation energy of the "deltas". More specifically we modify the simplified parametrization of equations (7.6.2) and (7.6.3) as follows:

$$\sigma_{ND} = \frac{36 \left(\sqrt{s} - 1.896 \right)^2}{0.015 + \left(\sqrt{s} - 1.896 \right)^2} \qquad (4.3.2)$$

$$\sigma_{NN} = \frac{35}{1 + 100(\sqrt{s} - 1.876)} + 20 \qquad (4.3.3)$$

The cross-sections for the inverse reactions are calculated using the reciprocity relation.

We can estimate the temperature of the colliding system in two different methods, which are both based on the assumption of thermal equilibrium while the second one contains in addition the assumption of chemical equilibration:

(a) The first method is used by experimentalists to extract a temperature from the spectra obtained from the data. It consists in fitting an exponential curve to the tail of the spectra, and it depends only on the assumption that the system obeys a Maxwell-Boltzmann distribution (Appendix 7.8.2). We apply this procedure to the results of cascade calculations, where we use the nucleon spectra integrated over all directions to improve the statistics (Figures 9.3 to 9.6).

(b) The temperature can be estimated from the chemical equilibrium constant K calculated as the ratio of "deltas" to nucleons in any stage of the collision in the cascade code (Appendix 7.8.1) according to the equation:

$$K = \frac{n_\Delta}{n_N} \approx 4 e^{-20/T} \qquad (4.3.4)$$

This simple expression applies only if the resonance mass distribution has a single constant value.

We apply these methods to the collisions of identical nuclei at 800 A.Mev with masses varying from A = 20, to A = 80, as shown in table 4.3.1 below. For a system in thermal and chemical equilibrium these two estimates of the temperature should be identical. Their difference indicates the lack of chemical equilibration.

TABLE 4.3.1 The chemical equilibrium constant.

Fireball temperatures from the chemical equilibrium constant and from an exponential fit to the tail of the distribution.

Mass Number	n_Δ/n_N	T_{exp}	T_K
20	0.84 ±0.02	58.3	12.6
40	1.076±0.018	64.2	14.9
60	1.169±0.015	63.5	15.9
80	1.053±0.011	66.3	14.6

The examination of the table above shows that:

(1) the two temperatures calculated by methods (a) and (b) are always surprisingly different from one another. The temperature from the exponential fit to the tail of the momentum distribution is always higher than the one

obtained from the chemical equilibrium constant. This difference seems to indicate a departure from chemical equilibration. The temperature of the system can be determined from a thermodynamic fireball calculation, following the usual procedure including only nucleons and "deltas". For the collision of two A = 40 nuclei the one-fireball model yields a temperature T = 99 Mev, and the two-fireball model gives T = 92 Mev. Both models predict a ratio of about 3.34 in sharp contrast to the value of 1.08 from the intranuclear cascade (Table 4.3.1). The sensitivity of the temperature on changes in the equilibrium constant (ratio of "deltas" to nucleons) can be evaluated from equation 4.3.4. The differential of T with respect to K leads to:

$$\Delta T = \frac{20}{K \cdot \left(\ln \frac{4}{K} \right)^2} \cdot \Delta K \qquad (4.3.5)$$

If K = 1.0, then T = 10·ΔK, and if K = 3.0, then T = 80·ΔK. We see that if the equilibrium constant determination varies by only one unit the temperature can vary between 10 Mev to 80 Mev. Thus even if the number of "deltas" is approximately equal to, but lower than the equilibrium value, the predicted temperature can be very different.

(2) As the masses of the colliding nuclei increase the temperatures from methods (a) and (b) seem to move towards

limiting values suggesting that the size of the system becomes immaterial after a certain value and does not improve the conditions for the achievement of equilibrium.

Could we have ever reached chemical equilibrium in the intranuclear cascade calculations? Is the time scale too short? Is it possible that the feature which prevents the attainment of chemical equilibrium is the quick disassembly of the reactants? We study these questions by artificially confining the system (for A = 40 on A = 40) inside a spherical container wall. As the collision takes place and the two nuclei interpenetrate each other, the container has its radius reduced to the extent that the system allows during the compression stage. When the minimum radius is reached, it is thereafter maintained constant. The particles confined to this volume are reflected whenever they reach the walls, while conserving energy and momentum (Appendix 7.8.3), and are then allowed to continue their interactions over a long period of time. This way a steady state condition is reached in which the numbers of nucleons and "deltas" fluctuate little around their average values. The equilibrium constant ($K = n_\Delta/n_N$) is followed up to 70 fm/c for one single run. At 30 fm/c its value is already over 3.0, from there on it fluctuates between 2.8 and 4.7. These values are more comparable with the predictions of the one or two fireball models strongly suggesting that the conditions for chemical equilibration have been reached here.

It is important to note that small changes in the equilibrium

constant K can lead to large changes in the estimated temperature. Therefore one could say now that if chemical equilibrium is not attained in the collision, at the stage of maximum compression the deviation from equilibrium can be small. The assumption of thermal equilibration is very good, but the assumption of chemical equilibrium is only approximately realized by the system. Our preliminary steps show that the system deviates from chemical equilibration and we can express the conditions for equilibrium in the cascade model by confining the participants to a fixed volume.

4.3.2 Calcium on calcium.

We now study the system calcium on calcium at 977 A.Mev and b = 0 impact parameter. The experimental data (Sandoval-80) for argon on potassium chloride at 977 A.Mev shows 2.35±0.07 negative pions, which we can estimate to be equivalent to 3 x 2.35 = 7.05 deltas. The two fireball model predicts for this case 15.5 deltas, roughly twice as many.

The intranuclear cascade (Figure 9.7) shows that the number of deltas increases steadily during the collision up to the stage of maximum compresion of the system, where it reaches the value of 17.3, and after that it begins to fall slowly during the expansion phase, down to 14.5 deltas at 22 fm/c. In a second cascade calculation we constrain the reacting system to the smallest volume it attains during the compression stage and follow its evolution up to 30 fm/c. Here the number of deltas

increases even more than in the previous case and fluctuates between 20 and 22 after about 16 fm/c. This is approximately the number of deltas that would have existed in equilibrium if the system had not started to dissipate itself too soon. Another run of the cascade code shows that if the system is constrained as before and then allowed to expand freely after 20 fm/c the number of deltas begins to fall again after the attainment of equilibrium down to 17.5 at 40 fm/c.

We can see that the number of deltas in this collision reaches about 80% of the equilibrium value during the stage of maximum compression. After that the number of deltas falls off gradually as a result of the adiabatic expansion until it reaches the point where there are no more interactions and the system dissolves completely. This reduction of the number of deltas is here seen clearly as the result of adiabatic cooling of the fireball.

We have shown clearly above using the intranuclear cascade code that the attainment of chemical equilibrium for the calcium on calcium system at 977 A.Mev and zero impact parameter is only a first order approximation during the stage of maximum compression. Although thermal equilibrium can be realized very fast, it seems that the attainment of chemical equilibration takes substantially longer and the fireball already begins to decay before that can happen.

4.4 Pion cross-sections.

In the case of the central collisions of nuclei of medium masses the cascade and the thermodynamic models produce somewhat similar predictions. When the number of participants is small, as for example in the case of collisions with non-zero impact parameters, chemical equilibration is doubtful. It is therefore very useful to compute the inclusive pion production cross-sections, which involves integrations over all impact parameters, using the cascade code. Here we use the extended version containing the isospin formalism and completely revised nucleon-nucleon cross-section data. We also use a simplified parametrization of the nucleon-nucleon cross-sections for the purpose of testing the sensitivity of the calculated results to changes in the cross-section input data.

Table 4.4.1 shows the predictions of the intranuclear cascade for the pion cross-sections and compares them with the experimental data. In all cases the inclusive pion cross-sections are overestimated by approximately a factor of two. The sensitivity of the results to the input cross-sections is tested with a simpler parametrized version of the N-N cross-sections. Table 4.4.2 shows the comparison for central collisions only. The discrepancy reported for central collisions (Stock-82) remains also in the impact parameter averaged calculations.

TABLE 4.4.1 Total inclusive pion cross-sections.

Comparison of the predictions of the cascade code with
the experimental data for the total inclusive pion
cross-sections. The experimental data are from Nagamiya-81.

Nuclei	Energy A.Mev	σ_{π^-}(barn) experiment	σ_{π^-}(barn) theory	σ_{π^+}(barn) experiment	σ_{π^+}(barn) theory
C+C	800	.16±.05	.30±.06		
C+Pb	800	1.17±.35	2.70±.41		
Ne+NaF	400	.086±.026	.117±.025		
Ne+NaF	800	.41±.12	.72±.11		
Ne+Cu	400			.14±.04	.30±.09
Ne+Cu	800	.89±.27	1.80±.23	.77±.23	1.78±.24
Ne+Pb	400	.39±.12	.78±.19	.21±.06	.59±.20
Ne+Pb	800	2.10±.63	4.79±.53	1.37±.41	2.91±.42
Ar+KCl	800	1.4±.4	2.23±.16		

TABLE 4.4.2 Sensitivity to the cross-section data.

Mean multiplicities in central collisions of Ar + KCl showing
the sensitivity to the N-N cross-section parametrization
(Figure 9.1). The experimental data are from Sandoval-80.

Energy A.Mev	$\langle n_{\pi^-}\rangle$ empirical data	$\langle n_{\pi^-}\rangle$ actual parametr.	$\langle n_{\pi^-}\rangle$ simple parametr.
360	0.20±.01	0.50±.11	0.75±.08
556	0.79±.03	2.00±.16	2.56±.11
772	1.58±.05	3.75±.23	3.88±.17
977	2.35±.07	4.63±.27	5.07±.15

5 - AVERAGE MULTIPLICITIES AND GEOMETRY

5.1 Introduction.

Multiplicity here is defined as the number of charged particles emerging from an event (collision). The primordial charge is defined as the number of protons from both the projectile and the target that become participants during the collision. The measured charges must be distinguished from the primordial charges. As a result of the collision a number of tracks become visible due to protons, deuterons, tritons, He-3, He-4, and heavier fragments, as well as positive and negative pions. The theoretical multiplicity is not only a function of the geometrical assumptions of the model (number of participants), but also of the dynamical assumptions regarding the production of composites and the pions.

The average charge multiplicity involves all impact parameters and is given by (Gosset-77):

$$\langle M \rangle = \frac{\int n_c(b)\, 2\pi b\, db}{\int 2\pi b\, db} \qquad (5.1.1)$$

where $n_c(b) = n_p(b) + n_\Lambda(b) + n_t(b) + n_{He}(b) + \ldots + n_{\pi^+}(b) + n_{\pi^-}(b)$. Gutbrod et al introduced the concept of associated multiplicity (Gutbrod-78): all the charged particles emerging from an event are measured in coincidence with the detection of a charged particle at 90 degrees to the beam direction in the laboratory frame. The trigger particle can be a proton or any other charged light fragment. In central collisions, that is in those collisions with small impact parameters, a larger number of charged particles are produced thus increasing the probability of having one of them reaching the detector at 90 degrees. Therefore the associated multiplicity has a strong bias in favor of the more central collisions, and is given by (Cecil-79):

$$\langle M_a \rangle = \frac{\int [n_c(b) - 1] \frac{dn}{d\Omega}\left(\frac{\pi}{2}, b\right) 2\pi b\, db}{\int \frac{dn}{d\Omega}\left(\frac{\pi}{2}, b\right) 2\pi b\, db} \qquad (5.1.2)$$

It has been found experimentally (Gutbrod-78) that the associated multiplicity is a function of the beam energy for a given projectile and target combination. This result has been advanced as a proof that the straight clean-cut participant-spectator geometry fails for the more central collisions (Gutbrod-79, Sandoval-80). The associated multiplicity, however, tests a combination of geometrical and

dynamical assumptions, since the number of charged particles depends not only upon the primordial charges but also upon the model employed for composite and for pion productions. If the geometrical properties alone are to be tested, we have to compare primordial charge cross-sections, which are given by:

$$\sigma_Q = \int n_Q (b) \, 2\pi b \, db \qquad (5.1.3)$$

where $n_Q(b) = n_p(b) + n_d(b) + n_t(b) + 2(n_{3He}(b) + n_{4He}(b)) + \ldots + n_{\pi^+}(b) - n_{\pi^-}(b)$. The participant-spectator picture may still be valid, but the independence of the number of participants on the collision energy assumed previously may have to be given up.

5.2 Fireball type models.

Both the one-fireball and the two-fireball models overestimate the pion cross-sections by a factor of two or more. The two-fireball/blast-wave model, however, is constrained from the beginning to produce the correct pion cross-sections. This model is also consistent with the results of the Cugnon cascade, as we have seen in chapter 3. Therefore it is an interesting model to use in the investigation of the multiplicities.

In the two-fireball/blast-wave model the critical density and the temperature are adjustable parameters. These parameters are varied so that the ratios of the cross-sections of protons to deuterons, and of protons to pions can be constrained to their experimental values. The translational collective flows account for the anisotropy of the spectra in the center of mass frame of the participants and at the same time reduces the amount of energy that is available for thermalization. As it turns out, the amount of energy in translational motion does not reduce sufficiently the temperature of the fireballs so that the ratios of the cross-sections can coincide with their experimental values. Therefore it is also necessary to introduce radial collective flows of the type considered in the implosion-explosion model. It is argued that the particles near the surface of a dense and hot fireball face an anisotropic environment which induces a reduction in the randomness of their kinetic energies so that they acquire an average outward radial velocity V_r.

One of the basic assumptions of the two-fireball/blast-wave model is that each hadronic species follows a Maxwell-Boltzmann distribution in each one of the infinite number of radial frames moving with the velocity V_r. One can show using the Lorentz invariance of the product Ed^3n_i/dp^3 that in the rest frame of each fireball it leads to the following distribution (Appendix 7.1):

$$\frac{dn_i}{dp^3} = \frac{\gamma_r q_i V e^{\mu_i/T}}{16\pi}\left[(x_2 - x_1 + 1)e^{x_1} - (x_2 + x_1 + 1)e^{-x_1}\right]\frac{e^{-x_2}}{x_1 x_2} \quad (5.2.1)$$

with $\gamma_r = 1/\sqrt{1 - V_r^2}$, $x_1 = \gamma_r V_r p/T$, and $x_2 = \gamma_r E/T$. The thermodynamic calculation in this model consists in solving equations 2.1.5 to 2.1.8 for the conserved quantities (the baryon number B, the charge Q, the energy E), and the critical density ρ_c of the fireballs to determine the parameters of the model (the chemical potentials, the temperature, and the volume of the fireballs). The calculations take their simplest form in the radial frames of the fireballs, where the Maxwell-Boltzmann distribution can be used directly. The parameters of the model are then defined in these frames. The energy of the collision in the center of mass system is connected to the energy available for thermalization in the radially expanding frames by two successive Lorentz transformations:

$$E_r = \frac{1}{\gamma_r} \cdot \frac{1}{\gamma} E \qquad (5.2.2)$$

where γ connects the center of mass and the fireball frames, and γ_r connects the fireball and the radial frames.

Nearly 40% of the energy of the collision goes into the radial expansion making this effect far more important than the translational collective flows. The later become even less

important as the masses of the colliding ions increase and the transparency factor approaches zero. This means that in practice we are essentially working with the implosion/explosion model in the cases where at least one of colliding ions is a medium size nucleus or heavier.

We produce several calculations with this model for different values of the critical density and the fraction f of the energy available for thermalization in the radial frames. This fraction f is identical with the radial gamma factor in equation 5.2.2. We use the data of Nagamiya et al (Nagamiya-81) for the collisions of neon on lead at 400, 800, and 2100 A.Mev. The best fitting values of the energy fraction f and the freeze-out density ρ_c are shown in the Table 5.2.1 below:

TABLE 5.2.1 Energy fraction and critical density.

Radial energy fraction and freeze-out density
determined in the two-fireball/blast-wave model.

E (A.Mev)	f(%)	ρ_c (fm^{-3})
2100	52.5	0.14
800	50.0	0.05
400	33.0	0.03

The value of the freeze-out density for the collision at 2100 A.Mev is found to be only slightly lower than the normal nuclear density. This is the number that best fits the data and it may be an indication of the breakdown of the validity of this model at these energies. An examination of the table shows a clear correlation between the collision energy and both the

radial energy fraction f and the freeze-out density. Qualitatively one could say that as the collision energy increases so does the violence of the explosion with a possible consequence that the chemical equilibrium is frozen at higher densities as the expansion times are reduced.

These results can now be used to calculate the average multiplicities and compare with the data of Gutbrod et al (Gutbrod-78); the results are shown in Table 5.2.2 below:

TABLE 5.2.2 Average associated multiplicities.

Average associated multiplicities in the
two-fireball/blast-wave model.
The experimental data are from Gutbrod-78.

	Theory	Data
Ar + U		
400 A.Mev (f=33%, λ=0.03)	37	25
1.05 A.Gev (f=51%, λ=0.06)	43	55
He + U		
1.05 A.Gev (f=51%, λ=0.06)	8	10
Ne + U		
400 A.Mev (f=33%, λ=0.03)	23	18
1.05 A.Gev (f=51%, λ=0.06)	27	33
2.10 A.Gev (f=52%, λ=0.14)	33	58

We see that the model overestimates the experimental results at the lower energies, but grossly underestimates the figures at the higher energies. Is is obvious that the model fails here.

It is also interesting to know the predictions of the simple one-fireball model. In this model the Maxwell-Boltzmann distribution holds in the rest frame of the fireball. The calculations are identical but simpler than in the previous

case. Here all the energy of the collision is available for thermalization. Surprisingly this model can reproduce the experimental data quite well (Cecil-79) when the freeze out density is chosen equal to 0.12 nucleon/fm^3. The results of our calculations are shown in Table 5.2.3:

TABLE 5.2.3 Average associated multiplicities.

Average associated multiplicities in the
one-fireball model ($\lambda = 0.12$ nucleon/fm^{++}).
The experimental data are from Gutbrod-78.

		Theory	Data
Ar + U	0.40 A.Gev	39	25
	1.05 A.Gev	60	55
He + U	0.40 A.Gev	7	5
	1.05 A.Gev	10	10
Ne + U	0.25 A.Gev	22	12
	0.40 A.Gev	24	19
	1.05 A.Gev	36	34
	2.10 A.Gev	53	59
Ne + Au	0.40 A.Gev	23	20
	2.10 A.Gev	51	59
Ne + Ag	2.10 A.Gev	43	42
Ne + Al	0.40 A.Gev	11	11
	2.10 A.Gev	23	20
Ar + Ca	1.05 A.Gev	27	24
He + Al	0.40 A.Gev	4	4

We are left with the task of explaining this success of the one-fireball model particularly above the 1.0 A.Gev collision energies. It is possible that for collision energies above 1.0 A.Gev compression and expansion may not take place at all, as suggested by Sobel et al (Sobel-75). The validity of the straight cut geometrical assumption at the lower energies has

been questioned by Nagamiya and Gyulassy (Nagamiya-82). We see that the one-fireball model can explain the energy dependence of the associated multiplicities much better than its more elaborate version, the two-fireball/blast-wave model. The former overestimates the number of pions by at least a factor of two, while the latter is constrained from the beginning to the correct pion cross-sections. Also the total amount of energy available for thermalization in the one-fireball model is definitely larger than in the two-fireball/blast-wave model where some 40% of the collision energy is tied up in the collective radial expansion; this implies much higher fireball temperatures in the simpler model. And this combination of higher, fireball temperatures and the overestimation of the number of pions both contribute to produce a much higher prediction of the associated multiplicities in the one-fireball model. This is the most likely explanation of its apparent success.

The number of participants is calculated here using the assumption of a clean-cut straight geometry; but as we mentioned before, the validity of this assumption cannot be rejected or accepted on the basis of these results. The calculations above for both models test a combination of geometrical and dynamical assumptions, and we cannot separate their contributions from one another. That requires the measurement of the primordial charge cross-sections, that depend solely on the geometry of the collision. We could say that it is unfortunate that the numbers of pions (positive and

negative) are not reported separetely from the other particles in Gutbrod-78.

5.3 Primordial charge cross-sections.

We leave temporarily the topic of associated multiplicities and look at the data pertaining to primordial charge cross-sections. This cross-section is defined in equation 5.1.3 and can be obtained from the data of Nagamiya et al (Nagamiya-81). The data are shown in Table 5.3.3. As we mentioned before, in a strict geometrical model the primordial charge cross-section is independent of the beam energy. The experimental data clearly indicate some energy dependence. We therefore look for an improvement to the geometrical overlap model.

A Glauber type model seems worth pursuing here. This model also assumes straight line trajectories, but the number of nucleons participating now depend upon the nucleon-nucleon cross-section. In the relevant energy range considered here the nucleon-nucleon cross-section increases with energy (Table 5.3.1) so that one has some hope of getting the energy dependence seen in Table 5.3.3.

TABLE 5.3.1   Average total N-N cross-sections.

Average total nucleon-nucleon cross-sections
calculated from parametrized experimental data.
The incident kinetic energy per nucleon E_k corresponds
to the nucleon-nucleon center of mass energy E .

E_k(Mev)	E_{CM}(Gev)	σ_{NN}(barn)
250	1.997	33.37
400	2.066	29.93
800	2.241	42.59
1050	2.343	43.07
2100	2.731	42.75

We derive the formula used for this calculation now. Let a nucleon be incident on a target at an impact parameter b. At this impact parameter the nucleon has to go through an amount of matter given by

$$\xi_t(b) = \int \rho_t(b, z)\, dz \qquad (5.3.1)$$

where $\rho_t(b, z)$ is the nuclear density function, and z is the direction of motion of the incident proton. The probability that it will emerge on the other side is

$$e^{-\sigma_{NN}\, \xi_t(b)} \qquad (5.3.2)$$

Therefore the probability that it becomes a participant is then

$$1 - e^{-\sigma_{NN} \xi_t(b)} \qquad (5.3.3)$$

Now suppose that the proton in question belongs to a projectile nucleus. The protons in the projectile are not localized, but can be described in terms of their projected density $\xi_p(\vec{s})$ in the perpendicular plane to the direction of the collision, and $\vec{s}$ is the distance from the center of the projectile in this plane:

$$\xi_p(\vec{s}) = \int \rho(\vec{s}, z) \, dz \qquad (5.3.4)$$

Each proton in the projectile nucleus can be approximated by an average density as $\xi_p(\vec{s})/A_p$. We must have

$$\int \xi_p(\vec{s}) \, d^2s = A_p \qquad (5.3.5)$$

The probability of having Z participant protons from the projectile is

$$P_z(b) = \binom{Z_p}{Z} (1 - P_b)^Z P_b^{Z_p - Z} \qquad (5.3.6)$$

with P_b given by:

$$P_b = \frac{1}{A_p} \int d^2 s \, \xi_p(\vec{s}) \, e^{-\sigma_{NN} \xi_t (\vec{s} + \vec{b})} \qquad (5.3.7)$$

$P_z(b)$ is normalized as can easily be verified by summing over Z and using Newton's binomial theorem. Now the average number of participant protons from the projectile is

$$\sum_z Z P_z(b) = \sum_z \binom{Z_p}{z} z \, (1 - P_b)^z \, P_b^{Z_p - z} \qquad (5.3.8)$$

which is easily summed by noting that

$$x \cdot \frac{\partial}{\partial x} (x + y)^n = x \frac{\partial}{\partial x} \sum_m \binom{n}{m} x^m y^{n-m} \qquad (5.3.9)$$

or

$$n x (x + y)^n = \sum_m \binom{n}{m} m \, x^m y^{n-m} \qquad (5.3.10)$$

where we let x = 1 - P_b, y = P_b, and n = Z_p. Then

$$\sum_z Z P_z(b) = Z_p (1 - P_b) \qquad (5.3.11)$$

Therefore the average primordial charge cross-section for the projectile is

$$\sigma_p(Q) = Z_p \int d^2s \, (1 - P_b) \qquad (5.3.12)$$

Similarly, we obtain the average primordial cross-section for the target:

$$\sigma_t(Q) = Z_t \int d^2s \, (1 - \bar{P}_b) \qquad (5.3.13)$$

where

$$\bar{P}_b = \frac{1}{A_p} \int d^2s \, \xi_t(\vec{s} + \vec{b}) \, e^{-\sigma_{NN} \xi_p(\vec{s})} \qquad (5.3.14)$$

The total average primordial charge cross-section is the sum

$$\sigma_z(Q) = \sigma_p(Q) + \sigma_t(Q) \qquad (5.3.15)$$

The average number of participants from the projectile should not show much change as a function of the collision energy, but those from the target are expected to be much more sensitive. This follows from equation 5.3.2, if the target is much larger than the projectile.

Much work has been done in the past on the parametrization of the projected nuclear density function $\xi(s) = \int \rho(s,z)dz$, where

$\rho(s,z)$ is a realistic nuclear density distribution. A very accurate parametrization is given below (Cecil-80):

$$\xi(s) = \begin{cases} 2\bar{\rho}\left(R_0^2 - s^2\right)^{1/2} , & s < \hat{R} \\ c_1 \bar{\rho} e^{-c_2(s-\hat{R})} , & s \geq \hat{R} \end{cases} \qquad (5.3.16)$$

where

$$c_1 = 2\left(R_0^2 - \hat{R}^2\right)^{1/2} , \qquad c_2 = \left(\frac{2}{c_1}\right)^2 \hat{R} \qquad (5.3.17)$$

and the values of the parameters are presented in Table 5.3.2.

TABLE 5.3.2   Projected nuclear densities.

Parameters for the projected nuclear densities
(from G. Cecil, M.Sc. Thesis, McGill University 1980)

Nucleus	R_0 (fm)	$\hat{R}$ (fm)	$\bar{\rho}$ (fm^{-3})
He-4	1.3823	1.1415	0.22456
Ne-20	2.7417	2.3976	0.17335
Ar-40	3.4147	2.9923	0.18102
Cu-63	4.1704	3.7749	0.17217
Pb-208	6.5918	6.2807	0.15900
U-238	6.7282	6.3108	0.16951

The primordial charge cross-sections for the collisions of neon on lead are calculated using the Glauber type theory described above. The results are presented in Table 5.3.3. The predictions of the fireball models with straight clean-cut geometry are shown at the same time for comparison.

TABLE 5.3.3 Primordial charge cross-sections.

Primodial charge cross-sections (barns) for neon on lead.
The experimental data are from Nagamiya-81. The experimental
value at 2.1 A.Gev was estimated from the data.

Energy (A.Mev)	Fireball models	Glauber type	Exp. data
400	43.3	42.7	31.1
800	43.3	46.3	48.6
2100	43.3	49.0	56.1

Comparing with the data we reach the conclusion that while the
Glauber type theory does show that the primordial charge
cross-sections increases with the collision energy, the
predictions are still too flat.

Now we turn attention again to the associated multiplicities.
The Glauber type theory can also be used to calculate only the
numbers of participants and spectators (Nagamiya-82) thus
replacing the straight cut geometry in the fireball model.
Although the Glauber type theory is based on straight line
geometry, the changes in the nucleon-nucleon total
cross-sections with the collision energies lead to changes in
the numbers of participants and spectators as a function of the
energy. Table 5.3.4 shows the results for the system neon on
uranium at an impact parameter b = 0.36 fm.

TABLE 5.3.4   Numbers of participants.

Number of participants from the Glauber type theory
for the collision of neon on uranium at b = 0.36 fm.

Energy (A.Mev)	Glauber type	Straight Geometry
250	86.7	85.2
400	84.6	85.2
1050	94.6	85.2
2100	94.8	85.2

We note that the number of participants is approximately the same below 1.0 A.Gev and increases by about 10% at higher energies. So we can expect some increase in the multiplicities at the higher energies and practically no change at the lower ones. These changes, however, are not enough to explain the data. Table 5.3.5 shows the one-fireball model results when the calculation of the numbers of participants is based on the Glauber type theory. A comparison with Table 5.2.3 shows very little change.

. TABLE 5.3.5   Average associated multiplicities.

Average associated multiplicities in the one-fireball model (ρ = 0.12 nucleons/fm^3) with the number of participants from the Glauber type theory. The experimental data are from Gutbrod-78.

		Theory	Data
Ar + U	0.40 A.Gev	38	25
	1.05 A.Gev	63	55
He + U	0.40 A.Gev	5	5
	1.05 A.Gev	9	10
Ne + U	0.25 A.Gev	21	12
	0.40 A.Gev	23	19
	1.05 A.Gev	38	34
	2.10 A.Gev	56	59

The associated multiplicities calculated in the two-fireball/blast-wave model is too flat compared with the experimental data. The one-fireball model prediction of the associated multiplicities is good, but this model overestimates the number of pions by a factor of two. For the primordial charge cross-sections the fireball type models predict a constant value independent of the collision energy; this is a consequence of the straight clean-cut geometry. The Glauber type theory produces a much better energy dependence, but it is still too flat compared with the experimental data.

5.4 The cascade model and geometry.

The numbers of the participants and the spectators are perhaps best determined in the cascade model. We use here the same code already described in section 4.2 of Chapter 4. The code follows the collision of two nuclei in the nucleon-nucleon center of mass system. Relativistic mechanics is used throughout. We extended the original version of the code by introducing the isospin formalism to allow for the collisions of charge asymmetric systems, and also used completely revised average total nucleon-nucleon cross-section parametrizations.

Point-like nucleons are assigned random positions inside the spheres of radii $1.12 \, A^{1/3}$, where A is the mass number, representing the colliding nuclei in their rest frames. This

version does not include the initial Fermi motion nor any field effects. These important physical characteristics of nuclei do not affect significantly the results we are interested in this Thesis. Pauli principle effects are mocked approximately by forbidding soft collisions when the total center of mass energy of two colliding nucleons is below 1895 Mev (Cugnon-81).

Single pion production in nucleon-nucleon collisions is introduced via the formation and decay of the delta resonances, that are assumed to have a mass distribution. The elastic $\Delta + \Delta \rightarrow \Delta + \Delta$ and $N + \Delta \rightarrow N + \Delta$ cross-sections are assumed to be the same as for the nucleons in free space. The inelastic $N + \Delta \rightarrow N + N$ cross-sections are obtained by detailed balance from the corresponding $N + N \rightarrow N + \Delta$ cross-sections. The delta lifetime is assumed to be much larger than the collision time: the surviving deltas at the end of the collision determine the number of pions.

The nucleons in each nucleus are assigned initial equal and opposite momenta to Lorentz boost them to the desired collision energy. As the cascade begins their positions and momenta are updated at regular time intervals. When two nucleons pass each other at their closest distance of approach, and this distance is below a minimum value, the pair is allowed to scatter. The different channels available are chosen by Monte Carlo sampling of the ratios of the corresponding cross-sections. We use the isospin formalism to calculate the branching ratios and their corresponding cross-sections. The nucleon has spin $J = 1/2$ and

isospin $I = 1/2$; the delta resonance has $J = 3/2$ and $I = 3/2$. A pair of nucleons can be in the state $I = 1$ or $I = 0$, while the pair delta-nucleon can have $I = 2$ or $I = 1$. Isospin conservation then, allows only the coupling of the $I = 1$ states. The calculations are finished by the time that the number of collisions falls practically to zero. Each cascade run is repeated with different random numbers from thirty to forty times in order to obtain sufficient statistics to calculate the average values of the quantities of interest and their standard deviations.

At the end of the collision those nucleons that did not suffer any interaction at all have a final momentum equal to its initial value. At first it would seem that this fact could provide a suitable criterion to decide if a nucleon was a participant or a spectator. A preliminary calculation shows that this criterion grossly overestimates the number of participants and leads to erroneous results. A less stringent criterion is necessary here. The nucleons can suffer soft or hard collisions and that could provide another criterion to calculate the number of participants. It remains to define what we mean by soft and hard collisions, and we can do this by comparing the initial and the final momenta. But since the nucleons loose their identities in the interactions this cannot be a one to one comparison, and therefore we look only at the nucleons at the end of the cascade calculation.

A nucleon is counted as a spectator if its final momentum does

not differ either from the initial momenta of the projectile nucleons or from the initial momenta of the target nucleons by more than a prescribed amount; otherwise it is a participant. The surviving delta resonances at the end of the cascade are always participants. The decay of the surviving deltas result in the final pion multiplicities and it is recognized that these can only come from the participants.

We choose the momentum change cut off as the Fermi momentum in an undisturbed nucleus. This choice is quite resonable in view of the fact that the nucleons in undisturbed nuclei suffer interactions with a momentum transfer of the order of the Fermi momentum or less. However, the use of the Fermi momemtum as a cut off value may seem a little artificial in view of the absence of Fermi motion in the cascade code used. Nevertheless, it may be the only available choice which will not be entirely arbitrary.

This criterion for defining the participants in the cascade code affects directly the calculated multiplicities because it eliminates from counting all the spectator charges. The absence of field effects implies that the model is incapable of predicting the production of composites. At the end of the simulation runs the only species present are the protons, the neutrons and the deltas that decay into pions. The primordial charge cross-section is then calculated as

$$\sigma_Q = \sigma_p + \sigma_{\pi^+} - \sigma_{\pi^-} \qquad (5.4.1)$$

The four-momentum change between the final four-momentum p and the initial four-momentum p_o is

$$t = (p - p_o)^2 = 2\left(m^2 - E_o E + \vec{p}_o \cdot \vec{p}\right) \qquad (5.4.2)$$

The cut off value t_o is calculated assuming a three-momentum change of $q_o = 270$ Mev/c, which is the Fermi momentum in an undisturbed nucleus:

$$t_o = 2m\left(m - E_{q_o}\right) = -7.15 \times 10^{-2} \; Gev^2 \qquad (5.4.2)$$

A three-momentum change larger than q_o corresponds to a four-momentum change smaller than t_o. Therefore if $t > t_o$ the particle is assumed to have been a spectator. The particles lose their identities during an interaction and that makes it impossible to tell if originally it came from the projectile or the target. Therefore it is necessary to test for changes in their momenta with respect to the initial momenta of the target and the projectile. In the case of inelastic interactions the particles are automatically defined to be participants. The number of participants for the reaction of neon on lead are shown in Table 5.4.1 below.

TABLE 5.4.1 Numbers of participants.

Number of participants for the collision of neon on lead calculated in the cascade model. The straight clean-cut geometrical calculation is shown for comparison.

b(fm)	400 A.Mev	800 A.Mev	Geometry
1.0	65.3±1.1	92.0±1.4	81.2
2.0	63.3±1.1	88.6±1.4	78.9
3.0	61.8±1.0	82.8±1.4	74.8
4.0	54.8±0.9	76.2±1.3	67.9
5.0	45.7±1.2	61.6±1.3	55.3
6.0	34.7±1.0	48.2±1.2	40.6
7.0	24.0±1.1	36.1±1.6	26.2
8.0	13.9±0.8	17.3±1.4	13.9
9.0	4.1±0.6	8.4±0.8	4.9

Examination of these results show that the numbers of participants depend quite clearly on the collision energies. For the collision at 800 A.Mev the numbers of participants in the cascade model are only slightly higher than the corresponding geometrical results and follow them closely. At 400 A.Mev however, the number of participants is much smaller. This is a rather pleasing result. The primordial charge cross-sections are presented in Table 5.4.2. Another cascade calculation using a cut off momentum of 300 Mev/c is presented at the same time to illustrate the sensitivity of the primordial charge cross-sections to changes in the value of the cut off momentum.

TABLE 5.4.2 Primordial charge cross-sections.

Primordial charge cross-sections (barns) in the
cascade model for the system neon on lead.
The experimental data are from Nagamiya-81.

E (A.Mev)	Cascade $(q_{\bullet} = .27 \text{Gev/c})$	Cascade $(q_{\bullet} = .30 \text{Gev/c})$	Experiment
400	36.7±1.8	29.1±1.6	31.1±20%
800	50.1±2.2	41.5±2.1	48.6±20%

These results are in close agreement with the experimental data
within their margins of errors, and show the correct dependence
on the collision energy. The primordial charge cross-sections
depend only on the geometry of the collision in the sense that
they reflect exactly the numbers of participants. If the number
of participants were independent of the collision energy then
the primordial charge cross-sections would be a constant
function. Both the fireball type models with their . straight
clean-cut geometry, and the Glauber type theory do not produce
the correct collision energy dependence.

The success of the cascade code in this regard still leaves
some questions unanswered. What would be the effect of the
initial Fermi motion and the field effects?   The   total
inclusive pion cross-sections are overestimated in the cascade
model by about a factor of 2 as in the simple one-fireball
model. This is another point of weakness of these results.

6 – SUMMARY AND CONCLUSIONS

We began the presentation of this work with a general overview of the field of heavy-ion physics. There we saw that it is a new branch of nuclear science that evolved in the past ten years into a major field of research. Despite its recent origins one can distinguish different areas characterized by a range of collision energies where different physical phenomena become predominant.

The so-called participant-spectator region, also known as the Bevalac physics region, extends roughly from 200 A.Mev to 4.0 A.Gev; this Thesis is solely concerned with this region. It is characterized by two stages: a fast energy deposition stage associated with the participants, and a slow stage associated with the spectators. In a somewhat simplistic way one could say that the participants are formed by the overlapping portions of the projectile and the target nucleons that are mutually swept during the collision.

A great amount of data and theoretical models are available in the participant-spectator region. There are thermal models, intranuclear cascades, hydrodynamic models and many others.

This proliferation of different models is obviously due to the great difficulty in approaching the problem in fundamental terms and the limitations of each model. Most models have been formulated within a semi-classical framework around which one can attempt to introduce quantum effects. The support for a semi-classical description comes mainly from the relative high momenta of the colliding ions and small wavelengths compared with the characteristic distances of the system. The thermodynamic model and the intranuclear cascades are among the most successful approaches in explaining the data collected so far in this region.

Thermodynamics was first applied to sub-atomic phenomena by Enrico Fermi in the early fifties, and more recently with the addition of geometrical concepts it forms the basis of the thermodynamic fireball model of heavy-ion collisions. Geometry leads to the participant-spectator picture; these are evaluated numerically assuming straight geometrical clean cuts or using Glauber theory, which gives almost identical results. The participants are assumed to fuse completely to form a fireball where both thermal and chemical equilibrium are achieved, thus allowing the calculation of cross-sections or multiplicities that can be compared with the experimental data. The fireball expands and when all interactions freeze, the ideal gas thermodynamics is applied. Extentions and elaborations of this model have been introduced. One can consider two fireballs to represent the residual collective motions in the longitudinal direction. One can also introduce collective outward radial

flows to represent the fireball explosions resulting from the anisotropic environment faced by hot and dense fireballs.

The intranuclear cascade may be neither a model nor a theory but a simulation. It is a microscopic "model" without any adjustable parameters using only the total elastic and inelastic nucleon-nucleon cross-sections as inputs, and has been used in the range from 200 A.Mev to 2.0 A.Gev: The main advantages of this "model" are the possibility of calculating non-observable quantities such as the maximum densities reached during the collision, off-equilibrium situations, fluctuations, and finite particle number effects.

The first part of this Thesis is concerned with the question of thermal equilibration in heavy-ion collisions. This problem is addressed by comparing the results of two models: the thermodynamic fireball model including longitudinal and radial collective flows, and the intranuclear cascade of Cugnon et al. Cugnon et al calculated the final rapidity and perpendicular momentum distributions for the collisions of two calcium-like nuclei at zero impact parameter. These distributions were fit with appropriate Maxwell-Boltzmann curves leading to different transverse and longitudinal temperatures, thus conflicting with the results of the one-fireball model. We show in this Thesis that the two-fireball model reproduces the basic features of their calculations, and the agreement is greatly improved when collective radial flows are added to the fireball model. There is however, a discrepancy in the asymmetry ratios. This we

believe is probably due to the deviations of the results of the intranuclear cascade from a perfect Maxwell-Boltzmann distribution. We may say in conclusion that the results of the cascade calculation of Cugnon et al are in good agreement with the predictions of the thermodynamic two-fireball/blast-wave model. The latter contains the implicit assumption of thermal equilibration. Therefore we can say that thermal equilibrium is reached during the collision of the two calcium-like nuclei in the Cugnon cascade.

The related question of chemical equilibration has been investigated before by other authors under varying assumptions. The thermodynamic fireball models assume that chemical equilibrium along with thermal equilibrium is achieved by the participants during the collision. In the cascade model the final number of deltas (and therefore also of pions) depends on its rates of production and absorption. There is chemical equilibrium if the two rates are equal. There has been much debate on the question of chemical equilibration in heavy-ion collisions and some disagreement still exists on this matter.

We study this problem using the intranuclear cascade. The basic code is extended by the introduction of the isospin formalism. This is necessary because much of the experimental data available is for non-symmetric systems $N \neq Z$. At the same time the total elastic and inelastic nucleon-nucleon experimental cross-section data is reviewed to produce a new parametrization for the cascade code. The sensitivity of the end results in

the cascade calculations to changes in the cross-section parametrizations is evaluated by comparing calculations using the actual cross-section parametrization with calculations using a simplified parametrization.

We do a preliminary calculation of central collisions of equal nuclei using the cascade code. In a further investigation we artificially confine the participants into a spherical cavity at the stage of maximum compression. That situation defines a condition of chemical equilibrium. It shows that during the stage of maximum compression in the normal cascade calculation the system closely approaches chemical equilibrium. It could attain the condition of chemical equilibration if it did not dissipate much too soon.

In view of the positive results from this preliminary simplified calculation, we can study an actual collision. We define the situation of chemical equilibration for the case of an actual system by placing it inside a container wall that allows it to evolve continuously in a constant volume. At later times, beyond the point where chemical equilibration is attained, the container wall is removed to allow the system to expand freely. The comparison with the normal cascade calculations show clearly that the system approaches chemical equilibrium within 20% at the stage of maximum compression.

The cascade model and the thermodynamic fireball model are consistent with one another from the point of view of thermal

and chemical equilibration. But chemical equilibrium is a rougher approximation. Particularly in the case of peripheral collisions, where the numbers of participants are very small compared with collisions at zero impact parameter, the attainment of chemical equilibrium is very questionable. The calculation of the total inclusive pion cross-sections involves an integration over all the impact parameters; therefore the comparison with the results for zero impact parameter alone is an indication of the extent to which the participants in peripheral collisions deviate from equilibrium. In all cases we find that the predicted number of pions is always overestimated by about a factor of two. The introduction of the isospin formalism in the cascade code was very instrumental in this calculation because the available data contains mostly charge asymmetric systems ($N \neq Z$). A new parametrization of the total (elastic and inelastic) nucleon-nucleon cross-section is used in this calculation, and at the same time we test the sensitivity of the end results by using a simplified parametrization for these cross-sections.

The two-fireball/blast-wave model is successful in reproducing the results of the intranuclear cascade. It is now interesting to calculate its predictions for the average associated multiplicities. The thermal models usually overestimate the number of pions by at least a factor of two, but this model constrains from the beginning the pion cross-sections to their correct experimental values. This is done by varying two parameters of the model: the fireball temperature and the

- 109 -

freeze out density. The temperature of the fireball can be reduced by the introduction of collective degrees of freedom represented in the model by two fireballs moving in opposite directions and by radial explosions in each fireball. About 40% of the collision energy is consumed by the radial explosions. These two parameters are determined by fitting the ratios of protons to deuterons and the ratio of protons to negative pions to the experimental data of Nagamiya et al for the collisions of neon on lead at 400, 800 and 2100 A.Mev. The model overestimates the associated multiplicities at the lower energies, but as the energy of the collision increases the calculated results fall progressively much shorter of the experimental results. The one-fireball model predicts the experimental results correctly in general. The experimental data on associated multiplicities does not report the cross-section for pions separately so that we cannot test for the primordial charge cross-sections. The associated multiplicity tests a combination of geometrical and dynamical assumptions which cannot be disentangled, whereas the primordial charge cross-sections depend on the geometry alone.

We observed that the average total nucleon-nucleon cross-sections increases by more than 40% when the collision energy increases from 400 A.Mev to 1.05 A.Gev. Assuming a straight line trajectory for the nucleons, a Glauber type theory predicts that the numbers of participants depend on the energy of the collision through the total nucleon-nucleon cross-sections. Our calculations based on the Glauber type

theory produced some energy dependence of the primordial charge cross-sections, but not enough to explain the experimental data.

The intranuclear cascade provides an alternative model to study the primordial charge cross-sections. We define a criterion to determine the number of participants based on the change between the final and the initial momenta of the particles. Because the particles lose their identities during the interactions it is necessary to consider both the projectile and the target momenta. The change in momentum is taken to be equal to the Fermi momentum of an undisturbed nucleus. At 800 A.Mev the numbers of participants obtained in this way are higher than the corresponding numbers calculated in the clean geometry; at 400 A.Mev on the other hand, the figures are substantially smaller. The primordial charge cross-sections for the collisions of neon on lead reproduce the right energy dependence and also agree with the experimental data within the error limits.

The intranuclear cascade code overestimates by a factor of two the total inclusive pion cross-sections. These results are not affected by the criterion for defining the number of participants in terms of the Fermi momentum because all deltas in the freeze-out stage are regarded as participants. Some authors (Stock-82, Harris-84) have attempted to interpret the overestimation of the number of pions as the result of the absence of compressional effects in the intranuclear cascade

and develop from that an estimate of the equation of state for nuclear matter.

This very interesting result was obtained with a cascade code that did not include in the calculation the initial Fermi motion of the nucleons, nor did it include any field effects; the Pauli principle is only approximately taken into account by forbidding soft collisions. The formation of composites is also excluded from the model. It would be highly desirable to complete this study by doing a calculation with a more complete cascade code.

7 - APPENDICES

7.1 Thermodynamic calculations.

The thermodynamic calculations consist in finding the solutions of the equations for the conserved quantities (equations 2.1.5 to 2.1.8) analytically if possible, or numerically in most cases.

7.1.1 The one-fireball model.

A relativistic Maxwell-Boltzmann distribution (equation 2.1.2) is assumed valid in the frame of the fireball for each one of the hadronic species present. The number of particles $n_i(b)$ in the fireball is obtained immediately as a function of parameters to be determined later:

$$n_i(b) = \frac{g_i V}{(2\pi)^2} e^{\mu_i/T} \int_0^{4\pi} d\Omega \int_0^{\infty} e^{-\frac{1}{T}\sqrt{m_i^2 + p^2}} \, p^2 dp \qquad (7.1.1)$$

The first integration is done immediately, and for the second one we use the change of variables:

$$p = m_i \sinh t \qquad (7.1.2)$$

and integrate by parts once:

$$n_i(b) = \frac{q_i V}{2\pi^2} e^{\mu_i/T} \frac{m_i^3}{3} \int_0^\infty e^{-\frac{m_i}{T} \cosh t} \sinh^4 t \, dt \qquad (7.1.3)$$

The integral above is proportional to the MacDonald function $K_2(m_i/T)$ (Abramowitz-68):

$$\int_0^\infty e^{-z \cosh t} \sinh^{2\nu} t \, dt = \frac{\Gamma\left(\nu + \frac{1}{2}\right) K_\nu(z)}{\pi^{1/2} (z/2)^\nu} \qquad (7.1.4)$$

for $\nu = 2$ and $z = m_i/T$. Direct substitution now leads to equation 2.1.3:

$$n_i(b) = \frac{q_i V}{2\pi^2} e^{\mu_i/T} m_i^2 T \, K_2(m_i/T) \qquad (7.1.5)$$

The total energy $E_i(b)$ for each kind of particle in the fireball is obtained by evaluating the integral:

$$E_i(b) = \int_0^{4\pi} d\Omega \int_0^\infty E(p) \frac{d^3 n_i}{dp^3} p^2 dp =$$

$$= \frac{g_i \cdot V e^{\mu_i/T}}{2\pi^2} \int_0^\infty \sqrt{m_i^2 + p^2} \; e^{-\frac{1}{T}\sqrt{m_i^2 + p^2}} \; p^2 dp \qquad (7.1.6)$$

Using again the same change of variable (7.1.2) we get:

$$E_i(b) = \frac{g_i V m_i^4 e^{\mu_i/T}}{2\pi^2} \int_0^\infty e^{-\frac{m_i}{T} \cosh t} (1 + \sinh^2 t)\, \sinh^2 t \; dt \qquad (7.1.7)$$

The first integral is proportional to $K_1(m_i/T)$ and the second one to $K_2(m_i/T)$; substitution leads to equation 2.1.4:

$$E_i(b) = \frac{g_i V}{2\pi^2} e^{\mu_i/T} m_i^3 T \left[K_1 \left(\frac{m_i}{T} \right) + \frac{3T}{m_i} K_2 \left(\frac{m_i}{T} \right) \right] \qquad (7.1.8)$$

7.1.2 The two-fireball model.

All that has been said above in section 7.1.1 is directly applicable in this case, but now in each of the fireballs' rest frames. The temperature and the chemical potentials are now defined in these two frames. Equations 2.1.5 to 2.1.8 for the conserved quantities are written in the center of mass frame of the two fireballs. The number of each hadronic species is an invariant, but the energies in the center of mass frame are connected to the energies in each fireball rest frame by a Lorentz transformation:

$$E_i^*(b) = \frac{E_i(b)}{\sqrt{1 - [\mathcal{P}_f(b)/E_0(b)]^2}} \qquad (7.1.9)$$

where $E_i(b)$ is given by equation 7.1.8.

If $(\mathcal{E}_i, \vec{\mathcal{P}}_i)$ and $(\mathcal{E}_f, \vec{\mathcal{P}}_f)$ are the target (projectile) participant four-momenta respectively before and after the collision (Das Gupta-78), then:

$$\mathcal{P}_f(b) = e(b) \cdot \mathcal{P}_i \qquad (7.1.10)$$

The one-fireball model is recovered as the masses of the ions increase and the transparency factor e approaches zero. In general it can be calculated (Das Gupta-79) as:

$$e(b) = 0.55^{0.47 + 0.61 \bar{\nu}(b)} \qquad (7.1.11)$$

where $\bar{\nu}(b)$ is the average number of collisions that a projectile (target) nucleon suffers with the target (projectile) nucleus; it is calculated as the ratio of the average length traversed by a nucleon in the other nucleus $\bar{l}(b)$, and the nucleon mean free path in the collision (Das Gupta-79). For normal nuclear matter we have $\lambda = 1.8$ fm (Das Gupta-79). Two colliding spherical nuclei with constant density and sharp surfaces of radii R_1 and R_2 have the nucleon mean

free path (Das Gupta-79), at the impact parameter b given by:

$$\bar{\ell}(b) = \frac{2\int_0^{Y_m} dy \int_{x_1}^{x_2} [R_1^2(y) - x^2]^{1/2} [R_2^2(y) - (b-x)^2]^{1/2} dx}{\int_0^{Y_m} dy \int_{x_1}^{x_2} [R_1^2(y) - x^2]^{1/2} dx}$$

(7.1.12)

At the impact parameter b = 0:

$$\bar{\ell}(0) = \frac{2\int_0^{R} dy \int_0^{R} (R^2 - x^2 - y^2) dx}{\int_0^{R} dy \int_0^{R} (R^2 - x^2 - y^2)^{1/2} dx}$$

(7.1.13)

we obtain after an elementary integration the value $\bar{\ell}(0) = 3R/2$, for two equal nuclei of radius R.

7.1.3 The implosion-explosion model.

Consider a reference frame moving radially outwards with respect to the rest frame of the fireball. There is an infinite number of such radial frames. The basic assumption is that in a neighborhood of each one of them the constituents of the fireball obey a local relativistic Maxwell-Boltzmann distribution. The objective is to determine the resulting distributions in the fireball rest frame.

We make use again of the Lorentz invariance of the product Ed^3n/dp^3 and take the average over all the radial directions:

$$E \frac{d^3 n_i'}{dp^3} = \frac{1}{4\pi} \int_0^{4\pi} d\Omega \; E_r \frac{d^3 m_i'}{dp_r^3} = .$$

$$= \frac{g_i V}{16\pi^3} e^{\mu'/T} \int_0^{\pi} \sin\theta \, d\theta \; E_r \, e^{-E_r/T} \qquad (7.1.14)$$

But $E_r = \gamma_r (E - V_r p \cos\theta)$; then

$$E \frac{d^3 u_i}{dp^3} = \frac{g_i V \gamma_r e^{\mu'/T}}{16\pi^3} \int_0^{\pi} (E - V_r p \cos\theta) e^{-\frac{\gamma_r}{T}(E - V_r p \cos\theta)} d(\cos\theta) \qquad (7.1.15)$$

The integration can be carried out by elementary means and we finally arrive at Eq. (2.1.16):

$$\frac{d^3 n_i'}{dp^3} = \frac{A \gamma_r e^{-x_2}}{2 x_1 x_2} \left[(x_2 - x_1 + 1) e^{x_1} - (x_2 + x_1 + 1) e^{-x_1} \right] \qquad (7.1.16)$$

where $A = g_i V(b) e^{\mu'/T}/8\pi$, $x_1 = \gamma_r V_r p/T$, $x_2 = \gamma_v E/T$.

The limiting value of equation 7.1.16 when $V_r \to 0$ is obtained by noting that $\gamma_r \to 1$, $x_1 \to 0$, and $x_2 \to E/T$:

$$\lim_{V_r \to 0} \frac{d^3 n_i}{dp^3} = A \, e^{-E/T} \qquad (7.1.17)$$

which is the Maxwell-Boltzmann distribution in the rest frame

of the fireball.

7.1.4 The two-fireball/blast-wave model.

The thermodynamic calculations take their simplest form if
equations 2.1.5 to 2.1.8 for the conserved quantities are
written in the expanding frames of each fireball, where the
Maxwell-Boltzmann distributions are assume to be valid; in this
case the equations developped above for the one-fireball model
are applicable, but now the temperature and the chemical
potentials are defined in the expanding radial frames. If the
calculations are done in the rest frames of the fireballs, then
the distribution of equation 2.1.16 must be used and it is
necessary to resort to numerical methods much sooner.

The critical density ρ_c and the temperature are adjustable
parameters to fit the experimental ratios of the cross-sections
σ_p/σ_k and σ_p/σ_π. The temperature is a function of the amount
of energy that is available for thermalization, so that the
velocity of radial expansion V_r is ultimately the adjustable
parameter in this case. The energy available for thermalization
in the radially expanding frames is related by a Lorentz
transformation to the fireball rest frames:

$$E_r = \frac{1}{\gamma_r} E \qquad (7.1.18)$$

where γ_r is the gamma factor between these two frames.

7.2 Decay of the deltas.

In the two-body decay of a delta resonance the distribution of one daughter particle in the rest frame of the fireball arises from its distribution in the rest frame of the delta and the distribution of the delta in the rest frame of the fireball:

$$E\frac{d^3 n_i}{dp^3} = \int E' \frac{d^3 n_i'}{dp'^3} \cdot \frac{d^3 n_\Delta}{dp_\Delta^3} d^3 p_\Delta \qquad (7.2.1)$$

In the rest frame of the delta each daughter particle is distributed as (Kapusta-77, Das Gupta-81):

$$E' \frac{d^3 n_i'}{dp^3} = \frac{1}{4\pi p_0} \delta(E' - E_{oi}) \qquad (7.2.2)$$

where $E_{oi}^2 = m_i^2 + p_0^2$. We integrate over all the momentum space to check the normalization constant:

$$n_i = \frac{1}{4\pi} \int_0^{4\pi} d\Omega \int_0^\infty \frac{\delta(E' - E_{oi})}{E' p_0} p'^2 dp' =$$

$$= \int_0^\infty \frac{\delta(E' - E_{oi})}{E' \sqrt{E_{oi}^2 - m_i^2}} \cdot \sqrt{E'^2 - m_i^2} \, E' dE' = 1 \qquad (7.2.3)$$

as expected. In the fireball frame the delta has a velocity $\vec{V}_\Delta = \vec{p}_\Delta / E_\Delta$, energy $E_\Delta^2 = m_\Delta^2 + p^2$, and $\gamma_\Delta = E_\Delta / m_\Delta$. The energy E'

of the daughter particle in the delta frame is related to its energy E in the fireball frame by a Lorentz transformation:

$$E' = \gamma_\Delta \left(E - \vec{V}_\Delta \cdot \vec{p} \right) = \left(E_\Delta E - \vec{p}_\Delta \cdot \vec{p} \right) / m_\Delta \qquad (7.2.4)$$

Choose a coordinate system with the z-axis along the direction of motion of the daughter particle; then equation 7.2.1 becomes:

$$E \frac{d^3 n_i'}{dp^3} = \frac{1}{4\pi p_0} \int \delta\left(E' - E_{0i} \right) \frac{d^3 n_\Delta}{dp_\Delta^3} \, d\phi \, d(\cos\theta) \, p_\Delta^2 \, dp_\Delta \qquad (7.2.5)$$

First we integrate over the angular variables, noting that

$$\delta\left(E' - E_{0i} \right) = \frac{\delta\left(\cos\theta - \cos\theta_0 \right)}{\left| \partial E' / \partial(\cos\theta) \right|} = \frac{m_\Delta}{p_\Delta p} \delta\left(\cos\theta - \cos\theta_0 \right) \qquad (7.2.6)$$

where $\cos\theta_0 = \left(E_\Delta E - m_\Delta E_{0i} \right) / p_\Delta p$:

$$E \frac{d^3 n_i'}{dp^3} = \frac{m_\Delta}{2 p_0 p} \int_{p_\Delta^-}^{p_\Delta^+} \frac{d^3 n_\Delta}{dp_\Delta^3} p_\Delta \, dp_\Delta = \frac{m_\Delta}{2 p_0 p} \int_{E_\Delta^-}^{E_\Delta^+} \frac{d^3 n_\Delta}{dp_\Delta^3} E_\Delta \, dE_\Delta \qquad (7.2.7)$$

The limits of integration $E_\Delta^\pm$ are obtained from the condition that $E'' = E_{0i}$, as required by the angular integration over the δ-function. Then, from equation 7.2.4:

$$E_{oi} = \frac{1}{m_\Delta} \left(E_\Delta E - p_\Delta p \cos\theta \right) \qquad (7.2.8)$$

which leads to a second degree equation in E_Δ:

$$\left(E^2 - p^2 \cos\theta \right) E_\Delta^2 - 2\left(m_\Delta E_{oi} E \right) E_\Delta + m_\Delta^2 \left(E_{oi}^2 + p^2 \cos^2\theta \right) = 0 \qquad (7.2.9)$$

with a discriminant

$$\Delta = 4 m_\Delta^2 \left(E_{oi}^2 - E^2 + p^2 \cos^2\theta \right) p^2 \cos^2\theta \qquad (7.2.10)$$

which for $\cos\theta = \pm 1$ gives the result

$$E_\Delta^\pm = \frac{m_\Delta}{m_i^2} \left(E E_{oi} \pm p_o p \right) \qquad (7.2.11)$$

7.2.1 The one-fireball model.

In the one-fireball model the delta resonances are assumed to obey a relativistic Maxwell-Boltzmann distribution; we can thus proceed to complete the integration of equation 7.2.7:

$$E\frac{d^3 n_i}{dp^3} = \frac{m_\Delta}{2 p_0 p} \cdot \frac{g_\Delta V e^{\mu_\Delta/T}}{(2\pi)^3} \int_{E_\Delta^-}^{E_\Delta^+} e^{-E_\Delta/T} E_\Delta \, dE_\Delta \qquad (7.2.12)$$

and arrive after some elementary algebra at the result:

$$E\frac{d^3 n_i}{dp^3} = \frac{g_\Delta V}{8\pi^3} e^{\frac{1}{T}\left(\mu_\Delta - \frac{m_\Delta E_m E}{m_i^2}\right)}$$

$$\left[\frac{m_\Delta T}{p_0 p}\left(\frac{m_\Delta E_m E}{m_i^2} + T\right)\sinh\frac{m_\Delta p_0 p}{m_i^2 T} - \frac{m_\Delta^2 T}{m_i}\cosh\frac{m_\Delta p_0 p}{m_i^2 T}\right] \qquad (7.2.13)$$

7.2.2 The two-fireball model.

Equation 7.2.13 above holds in the frame of each fireball. The left hand side, which is Lorentz invariant, can be written in their center of mass frame. The energy and momentum in the right hand side are expressed in terms of center of mass quantities by a Lorentz transformation. Then the results are added together:

$$E^*\frac{d^3 n_i}{dp^{*3}} = E_1^*\frac{d^3 n_i}{dp_1^{*3}} + E_2^*\frac{d^3 n_i}{dp_2^{*3}} \qquad (7.2.14)$$

7.2.3 The two-fireball/blast-wave model.

We start again from equation 7.2.7 now written in the rest frames of each fireball, but the distribution of the deltas is given by equation 7.1.16. We get for each fireball:

$$E\frac{d^3 n_i}{dp^3} = \frac{g_i V m_\Delta \gamma_r e^{\mu_i/T}}{32\pi R p} \int_{E_\Delta^-}^{E_\Delta^+} \left[(x_2 - x_1 + 1)e^{x_1} - (x_2 + x_1 + 1)e^{-x_1}\right] \frac{e^{-x_2} E_\Delta dE_\Delta}{x_1 x_2} \quad (7.2.15.)$$

with $x_1 = \gamma_r V_r \sqrt{E_\Delta^2 - m_\Delta^2}/T$, and $x_2 = \gamma_r E_\Delta/T$. The integration has to be done numerically here (IMSL-79). The rest of the calculations are identical to the case of the two-fireball model.

7.3 The rapidity distributions.

The rapidity y is defined along an axis as

$$y = \frac{1}{2} \log \frac{E + p_{\shortparallel}}{E - p_{\shortparallel}} \quad\quad (7.3.1)$$

for a particle of energy E and momentum p with projection $p_{\shortparallel}$ along the axis and $p_\perp$ in the perpendicular plane. The variables $(p_\perp, p_{\shortparallel})$ and (E, y) are connected by the transformation

$$E^2 = m_i^2 + p_\perp^2 + p_\parallel^2 \quad , \qquad y = \frac{1}{2} \log \frac{\sqrt{m_i^2 + p_\perp^2 + p_\parallel^2} + p_\parallel}{\sqrt{m_i^2 + p_\perp^2 + p_\parallel^2} - p_\parallel} \qquad (7.3.2)$$

and its inverse

$$p_\perp = \frac{(E^2 - m_i^2 \cosh^2 y)^{1/2}}{\cosh y} \quad , \qquad p_\parallel = E \tanh y \qquad (7.3.3)$$

with a Jacobian

$$\frac{\partial(p_\perp, p_\parallel)}{\partial(E, y)} = \frac{E^2}{\cosh y \, (E^2 - m_i^2 \cosh^2 y)^{1/2}} \qquad (7.3.4)$$

The following relation holds:

$$p_\perp \, dp_\perp \, dp_\parallel = \frac{E^2}{\cosh^2 y} \, dE \, dy \qquad (7.3.5)$$

7.3.1 The one-fireball model.

Using cylindrical coordinates $(p_\perp, \phi, p_\parallel)$ we integrate the relativistic Maxwell-Boltzmann distribution with respect to the angular variable, transform to the new variables (E, y) and integrate over the energy; we obtain the rapidity distribution dn_i/dy:

$$\frac{dn_i}{dy} = 2\pi \int_{m_i \cosh y}^{\infty} \frac{d^3 n_i}{dp^3} \frac{E^2}{\cosh^2 y} \, dE = \qquad (7.3.6)$$

$$= \frac{g_i V e^{\mu_i/T}}{4\pi^2 \cosh^2 y} \int_{m_i \cosh y}^{\infty} e^{-E/T} E^2 \, dE \qquad (7.3.7)$$

The lower limit of integration corresponds to $p_{\perp} = 0$, which implies $E^2 = m_i^2 + p^2 = m_i^2 + E^2 \tanh^2 y$, or $E = m_i \cosh y$. After integrating we get:

$$\frac{dn_i}{dy} = \frac{g_i V T^3}{4\pi^2 \cosh^2 y} \left[1 + \left(\frac{m_i}{T} \cosh y + 1 \right)^2 \right] e^{-\frac{1}{T}(\mu_i - m_i \cosh y)} \qquad (7.3.8)$$

This equation can be expressed in terms of the number of particles $\dot{n}_i(b)$ using equation 7.1.5. We get:

$$\frac{dn_i}{dy} = \frac{n_i(b) \cdot T^2}{2 m_i^2 \cosh^2 y \, K_2\left(\frac{m_i}{T} \right)} \left[1 + \left(\frac{m_i}{T} \cosh y + 1 \right)^2 \right] e^{-\frac{1}{T}(\mu_i - m_i \cosh y)} \qquad (7.3.9)$$

7.3.2 The two-fireball model.

In the center of mass frame of the two fireballs we can write:

$$\frac{d^3 n_i}{dp^{*3}} dp^{*3} = \frac{E}{E^*} \frac{d^3 n_i'}{dp^3} d^3 p^*$$

(7.3.10)

and using equation 7.3.5 we get

$$2\pi \frac{d^3 n_i}{dp^{*3}} \cdot \frac{E^* dE^* dy^*}{\cosh^2 y^*} = 2\pi E \frac{d^3 n_i'}{dp^3} \frac{E^* dE\, dy^*}{\cosh^2 y^*}$$

(7.3.11)

Therefore

$$\frac{dn_i'}{dy^*} = \frac{2\pi}{\cosh^2 y^*} \int_{m_i \cosh y^*}^{\infty} E\, E^* dE^* \frac{d^3 n_i'}{dp^3}$$

(7.3.12)

Now assume that the particles in the fireball frame follow a Maxwell-Boltzmann distribution and use the Lorentz transformation:

$$E = \gamma_F \left(E^* \pm V_F\, p_\shortparallel^* \right) = \gamma_F E^* \left(1 \pm V_F \tanh y^* \right)$$

(7.3.13)

$$\therefore \frac{dn_i}{dy^*} = \frac{g_i V e^{\mu_i/T} \gamma_F (1 \pm V_F \tanh y^*)}{(2\pi)^3 \cosh^2 y^*} \int_{m_i \cosh y^*}^{\infty} e^{-\gamma_F E^*(1 \pm V_F \tanh y^*)} E^{*2} dE^*$$

(7.3.14)

Here V denotes the volume associated with each fireball. Introduce the notation

$$\phi^{\pm} = \cosh y^* \pm V_F \sinh y^* \qquad (7.3.15)$$

to simplify the equation. Integrating and adding the distributions for each fireball together we get finally:

$$\frac{dn_i}{dy^*} = \frac{g_i V e^{\mu_i/T} T^3}{(2\pi\gamma_F)^2}\left[\left\{\left(\frac{m_i\gamma_F\phi^+}{T}+1\right)^2+1\right\}\frac{e^{-\frac{\gamma_F}{T}m_i\phi^+}}{\phi^+} + \right.$$

$$\left. + \left(\frac{m_i\gamma_F\phi^-}{T}+1\right)^2\frac{e^{-\frac{\gamma_F}{T}m_i\phi^-}}{\phi^-}\right] \qquad (7.3.16)$$

The same result may be obtained more simply by noting that

$$y^* = \frac{1}{2}\log\frac{E^*+p_u^*}{E^*-p_u^*} = y + \frac{1}{2}\log\frac{1+V_F}{1-V_F} \qquad (7.3.17)$$

so that $dy^* = dy$, and we can write:

$$\frac{dn_i}{dy^*} = \frac{dn_i}{dy}\left(y=y^*-\frac{1}{2}\log\frac{1+V_F}{1-V_F}\right) + \frac{dn_i}{dy}\left(y=y^*-\frac{1}{2}\log\frac{1+V_F}{1-V_F}\right) \quad (7.3.18)$$

where each term on the right-hand-side is obtained from equation 7.3.8 by substituting the indicated value of the argument. The end result is again equation 7.3.16 above.

When the surviving deltas at the freeze-out point decay into nucleons and pions their distributions are obtained from equation 7.3.12, where now the integrand contains the distribution $E d^3 n_i / dp^3$ from equation 7.2.13 for the decay products:

$$\frac{dn_i^{\pm}}{dy^*} = \frac{g_i V e^{\mu_\Delta/T}}{4\pi^2 \cosh^2 y^*} \int_{m_i \cosh y^*}^{\infty} \left[\left(\frac{m_\Delta E_{0i}}{m_i^2} \phi^{\pm} E^* + T \right) \frac{m_\Delta T}{p_0 \chi^{\pm}} \right.$$

$$\left. \cdot (\alpha^{\pm} - \omega^{\pm}) + \frac{m_\Delta^2 T}{m_i^2} (\alpha^{\pm} + \omega^{\pm}) \right] E^* dE^* \qquad (7.3.19)$$

where we use the notation

$$\chi^{\pm} = \left[(\phi^{\pm} E^*)^2 - m_i^2 \right]^{1/2} \qquad (7.3.20)$$

$$\alpha^{\pm} = \exp \left[\frac{m_\Delta p_0 \chi^{\pm}}{m_i^2 T} - \frac{m_\Delta E_{0i}}{m_i^2 T} \phi^{\pm} E^* \right] \qquad (7.3.21)$$

$$\omega^{\pm} = \exp \left[- \frac{m_\Delta p_0 \chi^{\pm}}{m_i^2 T} - \frac{m_\Delta E_{0i}}{m_i^2 T} \phi^{\pm} E^* \right] \qquad (7.3.22)$$

Equation 7.3.19 is evaluated numerically using the integration subroutine DCADRE (IMSL-79). The results for the two fireball

are added together:

$$\frac{dn_i}{dy^*} = \frac{dn_i}{dy_1^*} + \frac{dn_i}{dy_2^*}$$

(7.3.23)

7.3.3 The two-fireball/blast-wave model.

We write equation 7.3.6 in the rest frames of each fireball where now the distribution 7.1.16 is used in the integrand:

$$\frac{dn_i}{dy} = \frac{f_i \sqrt{\gamma_r} \, e^{\mu_i/T}}{16 \cosh^2 y} \int_{m_i \cosh y}^{\infty} \left[(x_2 - x_1 + 1) e^{x_1} - (x_2 + x_1 + 1) e^{-x_1} \right] \frac{e^{-x_2} E^2 \, dE}{x_1 \, x_2}$$

(7.3.24)

with $x_1 = \gamma_r V_r \sqrt{E^2 - m_i^2}/T$, and $x_2 = \gamma_r E/T$. The distribution in the center of mass frame is obtained from equation 7.3.18:

$$\frac{dn_i}{dy^*} = \frac{dn_i}{dy} \left(y = y^* + \frac{1}{2} \log \frac{1 + V_F}{1 - V_F} \right) + \frac{dn_i}{dy} \left(y = y^* - \frac{1}{2} \log \frac{1 + V_F}{1 - V_F} \right)$$

(7.3.25)

For each species from the decay of the deltas in the rest frame of each fireball we get from equations 7.2.7 and 7.3.6:

$$\frac{dn_i}{dy} = \frac{\pi m_\Delta}{P_0 \cosh^2 y} \int_{m_i \cosh y}^{\infty} \frac{E \, dE}{\sqrt{E^2 - m_i^2}} \int_{E_\Delta^-}^{E_\Delta^+} \frac{d^3 n_\Delta}{dp_\Delta^3} E_\Delta \, dE_\Delta$$

(7.3.26)

where the distribution of the deltas is given again by equation 7.1.16. The evaluation of the double integral is done

numerically (IMSL-79). Equation 7.3.25 is used to get the final distribution in the center of mass frame.

7.4 The perpendicular momentum distributions.

7.4.1 The one-fireball model.

Take again cylindrical coordinates and integrate over ϕ and $p_{\parallel}$:

$$\frac{dn_i}{dp_{\perp}} = 2\pi\, p_{\perp} \int_{-\infty}^{\infty} \frac{d^3 n_i}{dp^3}\, dp_{\parallel} =$$

$$= \frac{g_i V e^{\mu_i/T}}{4\pi^2}\, p_{\perp} \int_{-\infty}^{\infty} e^{-\frac{1}{T}\sqrt{m_i^2 + p_{\perp}^2 + p_{\parallel}^2}}\, dp_{\parallel} \qquad (7.4.1)$$

Change variables to $p_{\parallel} = \left(m_i^2 + p^2\right)^{1/2}\cdot\sinh t$. The integrand is an even function; then

$$\frac{dn_i}{dp_{\perp}} = \frac{g_i V e^{\mu_i/T}}{2\pi^2}\, p_{\perp}\sqrt{m_i^2 + p_{\perp}^2} \int_{0}^{\infty} e^{-\frac{1}{T}\sqrt{m_i^2 + p_{\perp}^2}\,\cosh t}\cdot\cosh t\cdot dt \qquad (7.4.2)$$

Integrating once by parts we find that the resulting integral is also expressible in terms of the MacDonald function $K_1(\sqrt{m_i^2 + p_{\perp}^2}/T)$. Finally:

$$\frac{dn_i}{dp_\perp} = \frac{g_i V e^{\mu_i/T}}{2\pi^2} p_\perp \sqrt{m_i^2 + p_\perp^2} \; K_1\left(\frac{1}{T}\sqrt{m_i^2 + p_\perp^2}\right) \qquad (7.4.3)$$

This equation can be expressed in yterms of the number of particles $n_i(b)$ using equation 7.1.5. We get:

$$\frac{dn_i}{dp_\perp} = \frac{n_i(b)}{m_i^2 \, T \, K_2\left(\frac{m_i}{T}\right)} \, p_\perp \sqrt{m_i^2 + p_\perp^2} \; K_1\left(\frac{1}{T}\sqrt{m_i^2 + p_\perp^2}\right) \qquad (7.4.4)$$

7.4.2 The two-fireball model.

We start again with equation 7.3.10 and integrate over the parallel momentum $p_\parallel$:

$$\frac{dn_i}{dp_\perp^*} = 2\pi \, p_\perp^* \int_{-\infty}^{\infty} \frac{E}{E^*} \, \frac{d^3 n_i}{dp^3} \, dp_\parallel^* \qquad (7.4.5)$$

Change the variable of integration from the center of mass system to the fireball frame:

$$p_\parallel^* = \gamma_F \left(p_\parallel \pm V_F E\right) \quad , \quad dp_\parallel^* = \frac{E^*}{E} \, dp_\parallel \qquad (7.4.6)$$

Then:

$$\frac{dn_i}{dp_\perp^*} = 2\pi p_\perp^* \int_{-\infty}^{\infty} \frac{d^3 n_i}{dp^3} \, dp_\shortparallel \qquad (7.4.7)$$

This integration is the same as in equation 7.4.1 for the Maxwell-Boltzmann case, and we get equation 7.4.3 for each fireball. Finally for both:

$$\frac{dn_i'}{dp_\perp^*} = \frac{g_i V e^{\mu_i/T}}{\pi^2} p_\perp^* \sqrt{m_i^2 + p_\perp^{*2}} \cdot K_1\left(\frac{1}{T}\sqrt{m_i^2 + p_\perp^{*2}}\right) \qquad (7.4.8)$$

For the products of the decay of the deltas we use equation 7.2.13 in equation 7.4.5:

$$\frac{dn_i'}{dp_\perp^*} = \frac{g_\Delta V e^{\mu_\Delta/T}}{\pi^2} p_\perp^* \int_0^{\infty} \frac{dp_x}{E} e^{-\frac{m_\Delta E_{ni} E}{m_i^2 T}} \cdot$$

$$\cdot \left[\frac{m_\Delta T}{p_0 p}\left(\frac{m_\Delta E_{ni} E}{m_i^2} + T\right) \sinh\frac{m_\Delta p_0 p}{m_i^2 T} - \frac{m_\Delta^2 T}{m_i^2} \cosh\frac{m_\Delta p_0 p}{m_i^2 T}\right] \qquad (7.4.9)$$

where we substitute $p = (p_\perp^2 + p_\shortparallel^2)^{1/2}$ and $E^2 = m_i^2 + p^2$. The integration must be done numerically and we use again the subroutine DCADRE (IMSL-79).

7.4.3 The two-fireball/blast-wave model.

The calculations here are entirely analogous, except that one has to use the appropriate distributions for this model in the integrands. Using equation 7.1.16 into equation 7.4.7 we get:

$$\frac{dn_i}{dp_\perp^*} = \frac{\lambda_i V \gamma_r e^{\mu_i/T}}{4} p_\perp^* \int_0^\infty \left[(x_2 - x_1 + 1)e^{x_1} - (x_2 + x_1 + 1)e^{-x_1}\right] \frac{e^{-x_2}}{x_1 x_2} d\varphi_\parallel \qquad (7.4.10)$$

with $\quad x_1 = \gamma_r V_r \sqrt{p_\perp^{*2} + p_\parallel^2}\,/T, \qquad x_2 = \gamma_\gamma \sqrt{m_i^2 + p_\perp^{*2} + p_\parallel^2}\,/T.$ The integral is evaluated numerically using DCADRE (IMSL-79).

The distribution for each species from the decay of the deltas is obtained by plugging 7.2.7 into 7.4.7 and using 7.1.16:

$$\frac{dn_i}{dp_\perp^*} = \frac{g_0 m_\Delta p_\perp^* e^{\mu_\Delta/T}}{16 p_0} \int_{-\infty}^\infty \frac{d\varphi_\parallel}{\sqrt{p_\perp^{*2} + p_\parallel^2}\,\sqrt{u_i^2 + p_\perp^{*2} + p_\parallel^2}} \cdot$$

$$\cdot \int_{E_\Delta^-}^{E_\Delta^+} \left[(x_2 - x_1 + 1)e^{x_1} - (x_2 + x_1 + 1)e^{-x_1}\right] \frac{e^{-x_2}}{x_1 x_2} E_\Delta\, dE_\Delta \qquad (7.4.11)$$

The double integral is evaluated using the subroutine DBLIN (IMSL-79).

We are also interested in the evaluation of $\langle p_\perp^{*2} \rangle$. It is obvious that $\langle p_\perp^{*2} \rangle = \langle p_\perp^2 \rangle$ so we can do the evaluation in the rest frame of the fireball:

$$\langle P_\perp^{*2} \rangle = \frac{1}{n_i} \int_0^\infty P_\perp^2 \frac{dn_i}{dp_\perp} dp_\perp \qquad (7.4.12)$$

Using equation 7.4.1:

$$\langle P_\perp^{*2} \rangle = \frac{2\pi}{n_i} \int_0^\infty P_\perp^2 \cdot P_\perp dp_\perp \int_{-\infty}^\infty \frac{d^3 n_i}{dp^3} dp_\parallel \qquad (7.4.13)$$

and plugging equation 7.1.16:

$$\langle P_\perp^{*2} \rangle = \frac{g_i V e^{\mu_i/T}}{8 n_i} \int_0^\infty P_\perp^3 dp_\perp \int_{-\infty}^\infty \left[(x_2 - x_1 + 1) e^{x_1} - (x_2 + x_1 + 1) e^{-x_1} \right] \frac{e^{-x_2} dp_\parallel}{x_1 x_2} \qquad (7.4.14)$$

with $x_1 = \gamma_r V_r \sqrt{P_\perp^2 + P_\parallel^2} / T$, $x_2 = \gamma_r \sqrt{m_i^2 + P_\perp^2 + P_\parallel^2} / T$.

For the decay products from the deltas we get from equation 7.4.13 using equation 7.2.7:

$$\langle P_\perp^{*2} \rangle = \frac{g_\Delta m_\Delta V e^{\mu_\Delta/T}}{16 P_0 n_i} \int_0^\infty P_\perp^3 dp_\perp \int_{-\infty}^{+\infty} \frac{dp_\parallel}{\sqrt{P_\perp^2 + P_\parallel^2} \sqrt{m_i^2 + P_\perp^2 + P_\parallel^2}} \cdot$$

$$\cdot \int_{E_\Delta^-}^{E_\Delta^+} \left[(x_2 - x_1 + 1) e^{x_1} - (x_2 + x_1 + 1) e^{-x_1} \right] \frac{e^{-x_2}}{x_1 x_2} E_\Delta dE_\Delta \qquad (7.4.15)$$

with $x_1 = \gamma_r V_r P_\Delta / T$, $x_2 = \gamma_r E_\Delta / T$.

7.5 The parallell momentum distributions.

7.5.1 The one-fireball model.

We obtain the $dn_i/dp_{||}$ distribution by taking cylindrical coordinates $(p_\perp, \phi, p_{||})$ and integrating over ϕ and $p_\perp$:

$$\frac{dn_i}{dp_{||}} = 2\pi \int_0^\infty \frac{d^3 n_i}{dp^3} \, p_\perp \, dp_\perp =$$

$$= \frac{g_i V e^{\mu_i/T}}{4\pi^2} \int_0^\infty e^{-\frac{1}{T}\sqrt{m_i^2 + p_\perp^2 + p_{||}^2}} \, p_\perp \, dp_\perp \qquad (7.5.1)$$

Change variables to $p_\perp = \sqrt{m_i^2 + p_{||}^2} \cdot \sinh t$; then:

$$\frac{dn_i}{dp_{||}} = \frac{g_i V e^{\mu_i/T}}{4\pi^2} (m_i^2 + p_{||}^2) \int_1^\infty e^{-\frac{1}{T}\sqrt{m_i^2 + p_{||}^2} \cosh t} \cosh t \cdot d(\cosh t) \qquad (7.5.2)$$

and finally

$$\frac{dn_i}{dp_{||}} = \frac{g_i V e^{\mu_i/T}}{4\pi^2} T \left(T + \sqrt{m_i^2 + p_{||}^2} \right) e^{-\frac{1}{T}\sqrt{m_i^2 + p_{||}^2}} \qquad (7.5.3)$$

7.5.2 The two-fireball model.

In the center of mass frame of the two fireballs we can write equation 7.3.9 and integrate over the perpendicular momentum $p_\perp$:

$$\frac{dn_i'}{dp_{\parallel}^*} = 2\pi \int_0^\infty \frac{E}{E^*} \frac{d^3 n_i'}{dp^3} \, p_\perp^* \, dp_\perp^* = 2\pi \int_0^\infty \frac{E}{E^*} \frac{d^3 n_i'}{dp^3} \, p_\perp \, dp_\perp \tag{7.5.4}$$

Convert all quantities to the center of mass frame:

$$E = \gamma_F \left(E^* \pm V_F \, p_{\parallel}^* \right) \tag{7.5.5}$$

and then

$$\frac{dn_i^\pm}{dp_{\parallel}} = \frac{g_i V e^{\mu_i/T}}{(2\pi)^2} \int_0^\infty \gamma_F \left(E^* \pm V_F p_{\parallel}^* \right) e^{-\frac{\gamma_F}{T} \left(E^* \pm V_F p_{\parallel}^* \right)} \cdot \frac{p_\perp^* \, dp_\perp^*}{E^*} \tag{7.5.6}$$

Change the variable of integration

$$p_\perp^* = \sqrt{m_i^2 + p_{\parallel}^2} \, \sinh t = \alpha \sinh t \tag{7.5.7}$$

then:

$$\frac{dn_i^{\pm}}{dp_{\shortparallel}^{*}} = \frac{g_i V}{4\pi^2} e^{\mp(\mu_i \pm \gamma_F V_F p_{\shortparallel}^{*})} \int_1^{\infty} \gamma_F (\alpha \cosh t \pm V_F p_{\shortparallel}^{*}) e^{-\frac{\gamma_F \alpha}{T} \cosh t} \alpha \, d(\cosh t) \quad (7.5.8)$$

and now after an elementary integration we get:

$$\frac{dn_i^{\pm}}{dp_{\shortparallel}^{*}} = \frac{g_i V T}{4\pi^2} e^{\mp(\mu_i \pm \gamma_F V_F p_{\shortparallel}^{*})} \left[\sqrt{m_i^2 + p_{\shortparallel}^{*2}} + \frac{T}{\gamma_F} \pm V_F p_{\shortparallel}^{*} \right] e^{\mp \gamma_F p_{\shortparallel}^{*}/T} \quad (7.5.9)$$

Finally for the two fireballs:

$$\frac{dn_i}{dp_{\shortparallel}^{*}} = \frac{g_i V T^2}{2\pi^2 \gamma_F} e^{\frac{1}{T}\left(\mu_i - \gamma_F \sqrt{m_i^2 + p_{\shortparallel}^{*2}}\right)}$$

$$\cdot \left[\left(1 + \frac{\gamma_F}{T} \sqrt{m_i^2 + p_{\shortparallel}^{*2}}\right) \cosh \frac{\gamma_F p_{\shortparallel}^{*}}{T} - \frac{\gamma_F V_F p_{\shortparallel}^{*}}{T} \sinh \frac{\gamma_F V_F p_{\shortparallel}^{*}}{T} \right] \quad (7.5.10)$$

where V is the volume of each fireball.

7.5.3 The two-fireball/blast-wave model.

The calculations here are entirely analogous. Using the distribution from equation 7.1.16 into equation 7.5.4:

$$\frac{dn_i}{dp_{\parallel}^*} = \frac{\gamma \gamma_r q_i V}{8} e^{\mu_i/T} \int_0^\infty \left(1 \pm \frac{V_F p_{\parallel}^*}{E^*}\right)\left[(x_2 - x_1 + 1)e^{x_1} - (x_2 + x_1 + 1)e^{-x_1}\right]\frac{e^{-x_2} p_\perp dp_\perp}{x_1 x_2} \quad (7.5.11)$$

with $\quad x_1 = \gamma \gamma_r V_r (p_{\parallel}^* \pm V_F E^*)/T, \quad x_2 = \gamma \gamma_r (E^* \pm V_F p_{\parallel}^*)/T, \quad$ and
$E^* = (m_i^2 + p_\perp^2 + p_{\parallel}^{*2})^{1/2}$. The integration is done numerically.

The distribution from the decay of the deltas is obtained by plugging equation 7.2.7 into equation 7.5.4 and using equation 7.1.16:

$$\frac{dn_i}{dp_{\parallel}^*} = \frac{q_i m_\Delta V e^{\mu_\Delta/T}}{8 p_0} \int_0^\infty \left(1 \pm \frac{V_F p_{\parallel}^*}{E^*}\right)\frac{p_\perp dp_\perp}{\sqrt{p_\perp^2 + p_{\parallel}^{*2}}} \int_{E_\Delta^-}^{E_\Delta^+}\left[(x_2 - x_1 + 1)e^{x_1} - (x_2 + x_1 + 1)e^{-x_1}\right]\frac{e^{-x_2} E_\Delta dE_\Delta}{x_1 x_2} \quad (7.5.12)$$

with $\quad x_1 = \gamma_r V_r \sqrt{E_\Delta^2 - m_\Delta^2}/T, \quad x_2 = \gamma_r E_\Delta /T, \quad$ and
$E^* = (m_i^2 + p_{\parallel}^{*2} + p_\perp^2)^{1/2}$. The double integral is done numerically using DBLIN (IMSL-79).

We also want to evaluate $\langle p_{\parallel}^{*2}\rangle$ in order to calculate the asymmetry ratio Y. We have:

$$\langle p_{\parallel}^{*2}\rangle = \frac{1}{n_i}\int_{-\infty}^\infty p_{\parallel}^{*2}\frac{dn_i}{dp_{\parallel}^*}\, dp_{\parallel}^* = \frac{1}{n_i}\int_{-\infty}^{+\infty} p_{\parallel}^{*2}\, dn_i \quad (7.5.13)$$

Using a Lorentz transformation to the fireball rest frame $p_{\parallel}^* = \gamma (p_{\parallel} \pm V_F E)$ we get:

$$\langle p_{\parallel}^{*2} \rangle = \gamma^2 \left[\langle p_\parallel^2 \rangle + v_F \langle E^2 \rangle \right] \qquad (7.5.14)$$

since $\langle p_\parallel E \rangle = 0$ when summed over both fireballs. Noting that $E^2 = m_i^2 + p_\perp^2 + p_\parallel^2$, we obtain finally:

$$\langle p_\parallel^{*2} \rangle = \gamma^2 \left[(1 + v_F) \langle p_\parallel^2 \rangle + v_F^2 (m_i^2 + \langle p_\perp^2 \rangle) \right] \qquad (7.5.15)$$

The asymmetry ratio is then:

$$\gamma = \frac{\langle p_\perp^{*2} \rangle}{\langle p_\parallel^{*2} \rangle} = \frac{\langle p_\perp^2 \rangle}{\gamma^2 \left[(1 + v_F) \langle p_\parallel^2 \rangle + v_F^2 (m_i^2 + \langle p_\perp^2 \rangle) \right]} \qquad (7.5.16)$$

The value of $\langle p_\perp^2 \rangle$ is calculated in Appendix 7.4.3.

7.6 Nucleon-nucleon scattering cross-sections.

7.6.1 Elastic and inelastic cross-sections.

Neutron-proton cross-sections in the energy region 200 Mev - 1.0 Gev have been measured since the early 1950's. Total cross-sections suffered from large systematic errors, and it is

only in the 1970's with the availability of better machines and detector systems that we have more accurate measurements (Dieterle-77). Traditionally n-p cross-sections were obtained indirectly from p-p and p-d measurements. Now good quality secondary neutron beams have become available at the new facilities. Saclay, for example, produces a monoenergetic neutron beam by stripping deuterons with protons. Accordingly we reject all the data that was measured prior to 1970. We use the CERN-HERA compilation (Flaminio-79) and the measurements done by Devlin et al (Devlin-73), which they claim:

> "...has high statistical precision and good momentum resolution. The statistical accuracy of the data is between 0.2% and 0.7% and the total systematic uncertainty is believed to be even less".

Proton-proton cross-sections have always been much more easily measured than the corresponding neutron-proton cross-sections. As it would be expected the data contains fewer systematic errors. Most of the data is clustered along a well defined curve. The Landolt-Börnstein (Hellwege-73) compilations are used. It presents a narrower selection from which more uncertain data has been eliminated.

More specifically the sources of the data and their energy ranges are summarized below. Here √s̄ denotes the center of mass energies.

TABLE 7.6.1 Sources of cross-section data.

The sources of data for each type and energy range.

p-p total: $1.995 < \sqrt{s} < 2.997$ Gev   (Hellwege-73, page 9)

p-p elastic: $1.955 < \sqrt{s} < 2.061$ Gev   (Hellwege-73, page 9)
                $2.075 < \sqrt{s} < 2.981$ Gev   (Hellwege-73, page 15)

n-p total: $1.998 < \sqrt{s} < 2.858$ Gev   (Devlin-73, Table iv)

n-p elastic: $1.998 < \sqrt{s} < 2.043$ Gev   (Devlin-73, Table iv)
                $2.323 < \sqrt{s} < 4.111$ Gev   (Flaminio-79, page 83)

The n-p and p-p cross-sections are treated with the cubic spline interpolation IMSL subroutine ICSVKU. Average nucleon-nucleon cross-sections are calculated as the arithmetic average between the p-p and n-p cross-sections. The inelastic cross-sections are obtained by difference between the total and the elastic. The average curves are parametrized again using the same subroutine. The value of the cubic spline aproximation for the cross-sections at the center of mass energy $\sqrt{s}$ is given by an expression of the type:

$$\sigma(\sqrt{s}) = \left\{ [c(i,3)\, \omega_i(\sqrt{s}) + c(i,2)]\, \omega_i(\sqrt{s}) + c(i,1) \right\} \omega_i(\sqrt{s}) + y(i) \qquad (7.6.1)$$

where $w_i(\sqrt{s}) = \sqrt{s} - z(i)$, and we must have $z(i) < \sqrt{s} < z(i+1)$.

The parameters for equation 7.6.1 are listed in the tables below:

TABLE 7.6.2   N-N inelastic cross-sections.

Cubic spline parametrization of the inelastic cross-sections.

c(i,1)	c(i,2)	c(i,3)	y(i)	z(i)
-338.07763	1582.2971	-1653.8394	20.812821	1.8800
96.614842	589.00714	-3334.7371	3.2776453	2.0802
67.298960	-800.13229	4109.8799	19.121772	2.2191
17.397228	157.92819	-1429.7512	21.448271	2.2968
22.613541	-50.667749	42.191495	22.503403	2.3454
-			-	-
				2.8400

TABLE 7.6.3   N-N elastic cross-sections.

Cubic spline parametrization of the elastic cross-sections.

c(i,1)	c(i,2)	c(i,3)	y(i)	z(i)
-500.84952	2695.6847	-5603.0369	62.729973	1.8900
-73.930420	300.97468	-619.75450	29.887576	2.0325
-39.198997	161.27893	-430.52425	25.769023	2.1076
-19.212680	14.039639	9.0099979	22.758478	2.2216
-14.378134	18.104950	-15.804888	20.217122	2.3720
-	-	-	-	2.8300

R. L. Hatch (Hatch-79) presents a another parametrization of the average nucleon-nucleon cross-sections that produces curves very similar to our own. We also use a simplified parametrization to test the sensitivity of the results to a change in cross-section. This simplified parametrization, for the inelastic cross-setion is

$$\sigma_{in}(\sqrt{s}) = \frac{20\left(\sqrt{s}-2.015\right)^2}{0.015 + \left(\sqrt{s}-2.015\right)^2} \qquad (7.6.2)$$

and for the elastic is

$$\sigma_{el}(\sqrt{s}) = \frac{35}{1 + 100(\sqrt{s} - 1.8993)} + 20 \tag{7.6.3}$$

The elastic, inelastic and total cross-sections, both in the simplified parametrization and the actual one appear in Figure 9.1.

7.6.2 Elastic differential cross-sections.

The elastic differential cross-sections are assumed to be the same as for diffraction scattering, with an exponential form (Perl-74):

$$\frac{d\sigma}{dt} = a\, e^{b(\sqrt{s})\cdot t} \tag{7.6.4}$$

where $t = -2p^2(1 - \cos\theta)$ is the four-momentum transfer ($0 > t > -2p^2 = t_0$), and

$$b(\sqrt{s}) = \frac{6[3.65(\sqrt{s} - 1.866)]^6}{1 + [3.65(\sqrt{s} - 1.866)]^6} \tag{7.6.5}$$

7.7 The intranuclear cascade code.

7.7.1 The basic code.

In this appendix we give a detailed description of the cascade code that we have used. It is a simple version of the Bertsch-Cugnon code; it assumes the complete isospin degeneracy of all species in the model, and more sophisticated features such as Fermi motion, Pauli blocking and field effects are not included. We modified this code to allow for the collisions of unequal nuclei and introduced the isospin formalism.

(a) Preliminaries.

Initially each nucleus is represented by a sphere centered on the coordinates $(x_0, 0, z_p)$ and $(-x_0, 0, -z_t)$, where $b = 2 x_0$ is the impact parameter, $z_t = 1.12 A_t^{1/3}$ and $z_p = 1.12 A_p^{1/3}$ are the target and projectile radii respectively. The nucleons are assigned random positions inside each sphere according to a uniform distribution:

$$r_i = \left\{ \begin{array}{c} z_p \\ z_t \end{array} \right\} \left[GGUBFS(w) \right]^{1/3} \qquad (7.7.1)$$

$$\cos\theta_i = 1 - 2.0 \; GGUBFS(w) \qquad (7.7.2)$$

$$\phi_i = 2\pi \ \text{GGUBFS}(W) \tag{7.7.3}$$

GGUBFS(W) is subroutine that generates a random number uniformily distributed in the interval (0,1) where W is a 'seed'. Every time this function is invoked it returns a new seed which is automatically used in each subsequent call.

Each nucleon is then assigned its position in cartesian coodinates:

$$x_i = r_i \sin\theta_i \cos\phi_i \pm x_0 \tag{7.7.4}$$

$$y_i = r_i \sin\theta_i \sin\phi_i \tag{7.7.5}$$

$$z_i = \frac{1}{\gamma}\left(r_i \cos\theta_i + \begin{Bmatrix} z_p \\ -z_t \end{Bmatrix}\right) \tag{7.7.6}$$

Here γ is the Lorentz factor. Each nucleus receives a Lorentz boost along the z-axis with a momentum p_0 or $-p_0$ in the nucleon-nucleon center of mass corresponding to the projectile kinetic energy:

$$p_o^2 = \frac{1}{2} m_N t_1 \qquad (7.7.7)$$

where m_N is the nucleon mass, t_1 is the projectile kinetic energy per nucleon.

(b) Start the simulation of the collision.

At the beginnig of each time interval Δt the program calculates the distances R_{ij} and the center of mass energies s_{ij} between all pairs (i,j) of baryons:

$$R_{ij} = \left[(x_i - x_j)^2 + (y_i - y_j)^2 + (z_i - z_j)^2 \right]^{1/2} \qquad (7.7.8)$$

$$s_{ij} = (E_i + E_j)^2 - (\vec{p}_i + \vec{p}_j)^2 \qquad (7.7.9)$$

If the distance for a pair is below 1.7 fm and their center of mass energy s_{ij} is above 3.61 Gev, then the pair is a good candidate for scattering. By forbidding N-N scattering below 3.61 Gev, which corresponds to about 50 Mev kinetic energy, the Pauli principle is upheld approximately in the early stages of the collision.

The distance between the pair (i,j) in their center of mass frame at any time t between two collisions is obtained by a Lorentz transformation:

$$R_{ij}(t) = \gamma_{ij}\left[\vec{\beta}_{ij}\cdot(\vec{r}_i - \vec{r}_j)\frac{\vec{\beta}_{ij}}{\beta_{ij}} - \vec{\beta}_{ij}t\right] + \left[(\vec{r}_i - \vec{r}_j) - \vec{\beta}_{ij}\cdot(\vec{r}_i - \vec{r}_j)\frac{\vec{\beta}_{ij}}{\beta_{ij}}\right] \quad (7.7.10)$$

At the start of the time interval $\triangle t$, we get:

$$R_{ij}(0) = (\gamma_{ij}-1)\vec{\beta}_{ij}\cdot(\vec{r}_i - \vec{r}_j)\frac{\vec{\beta}_{ij}}{\beta_{ij}} + (\vec{r}_i - \vec{r}_j) \quad (7.7.11)$$

The individual momenta of the pair is again obtained by a Lorentz transformation:

$$\vec{P}_{ij} = \gamma_{ij}\left[\vec{P}_i\cdot\frac{\vec{\beta}_{ij}}{\beta_{ij}} - \beta_{ij}E_i\right]\frac{\vec{\beta}_{ij}}{\beta_{ij}} + \left[\vec{P}_i - \vec{P}_i\cdot\vec{\beta}_{ij}\frac{\vec{\beta}_{ij}}{\beta_{ij}}\right] \quad (7.7.12)$$

which reduces to:

$$\vec{P}_{ij} = \left[(\gamma_{ij}-1)\vec{P}_i\cdot\frac{\vec{\beta}_{ij}}{\beta_{ij}} - \gamma_{ij}E_i\right]\vec{\beta}_{ij} + \vec{P}_i \quad (7.7.13)$$

If the component of $\vec{R}_{ij}(0)$ in the direction of the momenta,

$$b_{ij} = \left| \vec{R}_{ij}(0) \wedge \frac{\vec{P}_{ij}}{P_{ij}} \right| \quad (7.7.14)$$

is larger than 1.32 fm the pair will not approach each other close enough for scattering to occur. This distance corresponds to the maximum total N-N cross-section σ_{NN} = 55 mb.

The distance of approach at one half the time interval Δt:

$$d_{ij} = P_{ij} \left(\frac{1}{E_i} + \frac{1}{E_j} \right) \cdot \frac{\Delta t}{2} \qquad (7.7.15)$$

is also required to be smaller than b_{ij}.

(c) A scattering occurs.

The average elastic and inelastic cross-sections σ_{el} and σ_{in} are determined as a function of the center of mass energy s of the pair. The choice of one particular channel is now determined by drawing a random number x_1 uniformily distributed in the interval $(0,1)$. The interval $(0,1)$ is divided into 3 subintervals $(0, \sigma_{el}/\sigma_{pN})$, $(\sigma_{el}/\sigma_{pN}, (\sigma_{el}+\sigma_{in})/\sigma_{pN})$, $((\sigma_{el}+\sigma_{in})/\sigma_{NN},1)$. If x_1 falls in the last bin no scattering takes place at all.

If x_1 falls in the first bin the elastic channel is chosen. The four-momentum transfer t is obtained integrating equation 7.6.4 in the intervals $(t_1, t_0 = -2p^2)$ and $(0, t_1)$ and taking the ratio. This ratio is is chosen by drawing another random number x:

$$t_1 = \frac{1}{b(s)} \log \left[(1-x) e^{b(s)t_0} + x \right] \qquad (7.7.16)$$

The elastic scattering angle is:

$$\cos \theta_s = 1 - t_1/t_0 \qquad (7.7.17)$$

When the random number x falls in the second bin there are three possibilities:

(i) If the center of mass energy s is below the threshold for the production of deltas, or if the pair is made up of two deltas there is no possibility of inelastic scattering.

(ii) If both members of the pair are nucleons one delta is produced with a mass (Baldoni-62):

$$m_\Delta = \frac{3}{4}(s - 2.015) + 1.077 \leq 1.231 \qquad (7.7.18)$$

and linear momentum:

$$P_{j\Delta} = \frac{1}{2s}\left[(s^2 - m_\Delta^2 - m_j^2)^2 - 4(m_\Delta \cdot m_j)^2\right]^{1/2} \qquad (7.7.19)$$

(iii) If there is one delta and one nucleon, the delta is de-excited into a nucleon, with a cross-section calculated from detailed balance:

$$\sigma_\Delta = \frac{1}{8}\left(\frac{P}{P_{ij}}\right)^2 \sigma_i \qquad (7.7.20)$$

where

$$P = \sqrt{\frac{s^2}{4} - m_N^2} \qquad (7.7.21)$$

The scattering angle θ_s is chosen so that $\cos\theta_s$ is distributed at random and uniformily between -1 and 1. The azimuthal angle ϕ_s is chosen at random for all the cases above, thus violating the consevation of angular momentum here.

The new momentum coordinates are calculated as a function of the old and the new angles (Section 7.7.3):

$$P_x = P\left[-\sin\theta_s \sin\phi \sin\phi_s + \cos\phi\left(\cos\theta \sin\phi_s \cos\phi_s + \cos\phi_s \sin\theta\right)\right] \qquad (7.7.22)$$

$$P_y = P\left[\sin\theta_s \cos\phi \sin\phi_s + \sin\phi\left(\cos\theta \sin\phi_s \cos\phi_s + \cos\phi_s \sin\theta\right)\right] \qquad (7.7.23)$$

$$P_z = P \left[\cos\theta \cos\theta_s - \sin\theta \sin\theta_s \cos\phi_s \right] \qquad (7.7.24)$$

(d) Update momenta and coordinates.

The new momenta for each particle, that scattered according to the scheme of item (c), are converted back to the original frame using the same equation (7.7.13) with $\vec{\beta}_{ij}$ replaced by $-\vec{\beta}_{ij}$. The new updated coordinates then become:

$$\vec{r}_i(t+\Delta t) = \vec{r}_i(t) + \frac{\vec{P}_i}{E_i}\Delta t \qquad (7.7.25)$$

(e) Statistics.

The procedure described above is is repeated for each time interval until the number of collisions falls below a specified value or until a total preset time limit is reached. This simulation of one nucleus-nucleus collision is repeated a number of times so that the average values of the physical quantities of interest can be calculated along with their standard deviations.

7.7.2 The kinematics of scattering angles.

Assume that a unit vector $\hat{r}$ is defined by the angles (θ, ϕ) in a given coordinate system (x, y, z). The vector $\hat{r}$ represents the direction of motion of a particle before scattering takes place. After scattering the vector $\hat{r}$ is transformed into a unit vector $\hat{r}'$ defined by a change in direction by the scattering angle θ_s, which determines the momentum transfer, and also by an arbitrary angle ϕ_s around the direction of $\hat{r}$. We have:

$$\hat{r} = e^{-i\theta J_y} e^{-i\phi J_z} \hat{z} \tag{7.7.26}$$

and $\hat{r}'$ is given by:

$$\hat{r}' = e^{-i\phi J_z} e^{-i\theta J_y} e^{-i\phi_s J_z} e^{-\theta_s J_y} \hat{z} \tag{7.7.27}$$

Expressing the vectors and the operators in the spherical basis:

$$x = \frac{1}{\sqrt{2}} \begin{pmatrix} 1 \\ 0 \\ -1 \end{pmatrix} \quad , \quad y = \frac{1}{i\sqrt{2}} \begin{pmatrix} 1 \\ 0 \\ 1 \end{pmatrix} \quad , \quad z = \begin{pmatrix} 0 \\ 1 \\ 0 \end{pmatrix} \tag{7.7.28}$$

and carrying out some algebra, we finally arrive at the equations 7.7.22 to 7.7.24.

7.8 Chemical equilibrium calculations.

7.8.1 The equilibrium constant.

The number of particles in a system in thermal equilibrium can be calculated from the Maxwell-Boltzmann distribution. In the non-relativistic limit equation (2.1.2) gives:

$$n_i = \frac{g_i V e^{\mu_i/T}}{(2\pi)^3} e^{-m_i/T} \cdot \int_0^{4\pi} d\Omega \int_0^\infty e^{-p^2/2mT} p^2 dp = \qquad (7.8.1)$$

$$= \frac{g_i V}{2\pi^2} e^{\mu_i/T} (2m_i T)^{3/2} \int_0^\infty e^{-x^2} x^2 dx \qquad (7.8.2)$$

The integral above is tabulated and equals $\sqrt{\pi}/4$. Therefore,

$$n_i = \frac{g_i V}{8\sqrt{\pi^3}} (2m_i T)^{3/2} e^{-\frac{1}{T}(\mu_i - m_i)} \qquad (7.8.3)$$

Now when the reaction $N + N \rightleftharpoons N + \Delta$ in the system achieves chemical equilibrium, the equilibrium constant K is calculated by applying equation (7.8.3) to each of the species present, and we get:

$$K = \frac{n_\Delta}{n_N} = \frac{g_\Delta}{g_N}\left(\frac{m_\Delta}{m_N}\right)^{3/2} e^{-(m_D - m_N)/T} \tag{7.8.4}$$

Entering the numerical values into the above expression ($g_D = 16$, $g_N = 4$, $m_D = 958$ Mev, and $m_N = 938$ Mev), we get:

$$K = \frac{n_\Delta}{n_N} \approx 4\, e^{-20/T} \tag{7.8.5}$$

The corresponding relativistic result is obtained similarly from equation (2.1.3), and we get:

$$K = \frac{n_\Delta}{n_N} \approx 4.2\, \frac{K_2(958/T)}{K_2(938/T)} \tag{7.8.6}$$

7.8.2 The exponential fit to the spectra.

For a system in thermal equilibrium we can write equation (2.1.2) for the momentum distribution:

$$dn_i = \frac{g_i V}{(2\pi)^3} e^{-E/T} d\Omega\, p^2 dp \tag{7.8.7}$$

But

$$p^2 dp = p E dE = E \sqrt{E^2 - m_i^2} \, dE \qquad (7.8.8)$$

and we can write it as:

$$\frac{1}{E \sqrt{E^2 - m_i^2}} \frac{dn_i'}{dE} = \frac{g_i V}{2\pi^2} e^{\mu_i/T} e^{-E/T} \qquad (7.8.9)$$

Plotting the left hand side of the above expression against the energy E we obtain an exponential curve, from which an estimate of the temperature of the system is extracted.

In the non-relativistic limit equation (7.8.9) is reduced to the form:

$$\frac{1}{E} \frac{dn_i}{dE} = \frac{g_i V}{\pi^2} \left(\frac{m_i^3}{2}\right)^{\frac{1}{2}} e^{\frac{1}{T}(\mu_i - m_i)} e^{-E/T} \qquad (7.8.10)$$

which is again an exponential curve as a function of the energy E.

7.8.3 Kinematics in a spherical container.

Assume that a particle of momentum $\vec{P} = (P_1, P_2, P_3)$ hits the internal surface of a sphere at the point $\vec{r} = (x_1, x_2, x_3)$. Determine its momentum $\vec{Q} = (Q_1, Q_2, Q_3)$ after the collision takes place.

We write the momentum $\vec{P}$ in terms of its components parallel and perpendicular to the position vector $\vec{r}$:

$$\vec{P} = (\vec{P}.\vec{r})\frac{\vec{r}}{r^2} + \left[\vec{P} - (\vec{P}.\vec{r})\frac{\vec{r}}{r^2}\right] \qquad (7.8.11)$$

This is transformed after the collision by reversing the component of the momentum perpendicular to the surface:

$$\vec{Q} = -(\vec{P}.\vec{r})\frac{\vec{r}}{r^2} + \left[\vec{P} - (\vec{P}.\vec{r})\frac{\vec{r}}{r^2}\right] \qquad (7.8.12)$$

$$\vec{Q} = \vec{P} - 2(\vec{P}.\vec{r})\frac{\vec{r}}{r^2} \qquad (7.8.13)$$

so that we finally get in term of the components:

$$Q_i = P_i - \frac{2x_i \sum_{j=1}^{3} x_j P_j}{\sum_{i=1}^{3} x_i^2} \qquad (7.8.14)$$

This result is incorporated into the cascade code in order to confine the participants into a spherical volume over a period of time to establish the conditions for chemical equilibrium.

8 - REFERENCES

(Abramowitz-68)   M. Abramowitz and I. A. Stegun, Handbook of Mathematical Functions, Dover Publications, Inc. (1968) 376.

(Backe-83)   H. Backe, Nucl. Phys. A400 (1983) 451c.

(Baldoni-62)   Baldoni, Nuovo Cim. 26 (1962) 1376.

(Bertsch-84)   G. F. Bertsch, H. Kruse and S. Das Gupta, Phys. Rev. C29 (1984) 673.

(Bodmer-81)   A. R. Bodmer and C. N. Panos, Nucl. Phys. A356 (1981) 517.

(Boguta-82)   J. Boguta, Phys. Lett. 109B (1982) 251.

(Bondorf-82)   J. P. Bondorf, Nucl. Phys. A387 (1982) 25c.

(Cahay-83)   M. Cahay, J. Cugnon, and J. Vandermeulen, Nucl. Phys. A411 (1983) 524.

(Cecil-79)   G. Cecil, S. Das Gupta and A. Mekjian, Phys. Rev. C20 (1979) 1021.

(Cecil-80)   G. Cecil, S. Das Gupta, and W. D. Meyers, Phys. Rev. C22 (1980) 2018.

(Cugnon-80)   J. Cugnon, Phys. Rev. C22 (1980) 1885.

(Cugnon-80a)   J. Cugnon and S. E. Koonin, Nucl. PHys. A355 (1980) 477.

(Cugnon-81)   J. Cugnon, T. Mizutani, and J. Vandermeulen,

Nucl. Phys. A352 (1981) 505.

(Cugnon-81a)   J. Cugnon, J. Knoll and J. Randrup, Nucl. Phys. A350 (1981) 444.

(Cugnon-81b)   J. Cugnon, Phys. Rev. C23 (1981) 2094.

(Cugnon-82)   J. Cugnon, Nucl. Phys. A387 (1982) 191c.

(Cugnon-83)   J. Cugnon and M. Jaminon, Phys. Lett. 123B (1983) 155.

(Das Gupta-78) S. Das Gupta, Phys. Rev. C18 (1978) 2773.

(Das Gupta-78a) S. Das Gupta, Phys. Rev. Lett. 41 (1978) 1450.

(Das Gupta-79) S. Das Gupta and C. S. Lam, Phys. Rev. C20 (1979) 1192.

(Das Gupta-81) S. Das Gupta and A. Z. Mekjian, Phys. Rep. 72 (1981) 131.

(Devlin-73)   T. J. Devlin, W. Johnson, J. Norem, K. Vosburgh, R. E. Mischke, and W. Schimmerling, Phys. Rev. D8 (1979) 136.

(Dieterle-77)   B. D. Dieterle, A.I.P. Conference Proceedings 41: Nucleon-nucleon Interactions (1977) 35. (D. F. Measday, H. W. Fearing and A. Strathdee, editors).

(Faessler-83)   A. Faessler, Nucl. Phys. A400 (1983) 565c.

(Fermi-50)   E. Fermi, Prog. Theor. Phys. 5 (1950) 570.

(Flaminio-79)   V. Flaminio, I. F. Graf, J. D. Hansen, W. G. Moorhead, and D. R. O. Morrison, CERN-HERA 79-03 (1979).

(Forest-80)   E. Forest, S. Das Gupta, and C. S. Lam, Phys. Rev. C21 (1980) 1989.

(Fraenkel-82)   Z. Fraenkel, Nucl. Phys. A374 (1982) 475c.

(Gale-83)   C. Gale, A. C. Maso, S. Das Gupta, and B. K. Jennings, Phys. Rev. C28 (1983) 164.

(Gelbke-83)   C. K. Gelbke, Nucl. Phys. A400 (1983) 473c.

(Glauber-70)   R. J. Glauber and G. Mathiae, Nucl. Phys. B21 (1970) 135.

(Gosset-77)   J. Gosset, H. H. Gutbrod, W. G. Meyer, A. M. Poskanzer, A. Sandoval, R. Stock, and G. D. Westfall, Phys. Rev. C16 (1977) 629.

(Gosset-78)   J. Gosset, J. I. Kapusta, and G. D. Westfall, Phys. Rev. C18 (1978) 844.

(Gosset-82)   J. Gosset, Nucl. Phys. A374 (1982) 447c.

(Gutbrod-78)   H. H. Gutbrod, in Proceedings of the Fourth High Energy Heavy Ion Summer Study, Lawrence Berkeley Laboratory Report LBL-7766, Berkeley (1978) 1.

(Gutbrod-82)   H. H. Gutbrod, A. I. Warwick and H. Wieman, Nucl. Phys. A387 (1982) 177c.

(Gyulassy-83) M. Gyulassy, Nucl. Phys. A400 (1983) 31c.

(Harris-84)   J. W. Harris and R. Stock, LBL Preprint 17054 (1984).

(Hatch-80)   R. L. Hatch, Ph. D. Thesis, California Institute of Technology (1980) Appendix B.

(Hellwege-73) K. H. Hellwege (ed-in-chief), Landolt-Bornstein, vol. I/7 (1973).

(Henning-83)   W. Henning, Nucl. Phys. A400 (1983) 259c.

(Hufner-75)   H. Hufner, K. Schafer, and B. Schurmann, Phys. Rev. C12 (1975) 1888.

(Hufner-77)   J. Hufner and J. Knoll, Nucl. Phys. A290 (1977)

460.

(Hufner-78)   J. Hufner, in Proceedings of the Fourth High
                   Energy Heavy Ion Summer Study, Lawrence
                   Berkeley Laboratory Report LBL-7766, Berkeley
                   (1978) 135.

(Jakobsson-83)   B. Jakobsson, Physica Scripta 15 (1983) 207.

(Jennings-81)   B. K. Jennings, L. Satpathy, and S. Das Gupta,
                   Phys. Rev. C24 (1981) 440.

(Jennings-82)   B. K. Jennings, S. Das Gupta, and N. Mobed,
                   Phys. Rev. C25 (1982) 278.

(Kapusta-77)   J. I. Kapusta, Phys. Rev. C16 (1977) 1493.

(Libbrecht-79)   K. G. Libbrecht and S. E. Koonin, Phys. Rev.
                   Lett. 43 (1979) 1581.

(Lipschutz-68)   S. Lipschutz, Theory and Problems of
                   Probability, McGraw Hill, New York (1968)
                   Chapter 4.

(Manko-82)   V. I. Manko and S. Nagamiya, Nucl. Phys. A384
                   (1982) 475.

(Mekjian-77)   A. Mekjian, Phys. Rev. Lett. 38 (1977) 640.

(Mekjian-78)   A. Z. Mekjian, Phys. Rev. C17 (1978) 1051.

(Mekjian-82a)   A. Z. Mekjian, Nucl. Phys. A384 (1982) 492.

(Migdal-78)   A. B. Migdal, Rev. Mod. Phys. 50 (1978) 107.

(Mobed-81)   N. Mobed, B. K. Jennings, and S. Das Gupta,
                   Phys. Lett., 106B (1981) 371.

(Montvay-79)   I. Montvay and J. Zimanyi, Nucl. Phys. A316
                   (1979) 490.

(Myers-78)   W. D. Myers, Nucl. Phys. A296 (1978) 177.

(Nagamiya-81)   S. Nagamiya, M. C. Lemaire, E. Moeller, S.

Schnetzer, G. Shapiro, H. Steiner, and I. Tanihata, Phys. Rev. C24 (1981) 971.

(Nagamiya-82)   S. Nagamiya and M. Gyukassy, LBL Preprint - 14035 (1982).

(Ngo-83)   C. Ngo, C. Gregoire, B Remaud, and E. Tomasi, Nucl. Phys. A400 (1983) 259c.

(Noremberg-83)   W. Noeremberg, Nucl. Phys. A400 (1983) 275c.

(Perl-74)   M. L. Perl, High Energy Hadron Physics, J. Wiley & Sons, New York (1974) Chapter 1.

(Pirner-79)   H. J. Pirner and B. Schurmann, Nucl. Phys. A316 (1979) 461.

(Plasil-83)   F. Plasil, Nucl. Phys. A400 (1983) 417c.

(Reif-65)   F. Reif, Fundamentals of Statistical and Thermal Physics, McGraw Hill, New York (1965) 312.

(Roeckl-83)   E. Roeckl, Nucl. Phys. A400 (1983) 131c.

(Sandoval-80)   A. Sandoval, H. H. Gutbrod, W. G. Meyer, R. Stock, Ch. Lukner, A. M. Poskanzer, J. Gosset, J. C. Jourdain, C. H. King, G. King, Nguyen Van Sen, G. D. Westfall, and K. L. Wolf, Phys. Rev. C21 (1980) 1321.

(Sandoval-80a)   A. Sandoval, R. Stock, H. E. Stelzer, R. E. Renfordt, J. W. Harris, J. P. Branniggan, J. V. Geaga, L. J. Rosenberg, L. S. Schroder, and K. L. Wolf, Phys. Rev. Lett. 45 (1980) 874.

(Sarantites-83)   D. G. Sarantites, M. Jaaskelainen, F. A. Dilmanian, H. Puchta, R. Woodward, J. R. Beene, D. C. Hensley, M. L. Halbert, J. Hattula, J. H.

Barker, R. Novotny, L. Adler, R. K. Choudhury, M. N. Namboodiri, R. P. Schmitt, and J. B. Natowitz, Nucl. Phys. A400 (1983) 435c.

(Schurmann-79)   B. Schurmann, Phys. Rev. C20 (1979) 1607.

(Shuryak-80)   E. V. Shuryak, Phys. Rep. 61 (1980) 71.

(Siemens-79)   P. J. Siemens and J. Rasmussen, Phys. Rev. Lett. 42 (1979) 880.

(Sobel-75)   M. Sobel, P. J. Siemens, J. P. Bondorf, and H. Bethe, Nucl. Phys. A251 (1975) 502.

(Specht-83)   H. J. Specht, Nucl. Phys. A400 (1983) 43c.

(Stock-82)   R. Stock, R. Bock, R. Brockman, J. W. Harris, A. Sandoval, H. Stroebele, K. L. Wolf, H. G. Pugh, L. S. Schroeder, M. Maier, R. E. Renfordt, A. Dacal, and M. E. Ortiz, Phys. Rev. Lett. 49 (1982) 1236.

(Stocker-83)   H. Stocker, G. Buchwald, G. Graebner, P. Subramanian, J. A. Maruhn, W. Greiner, B. V. Jacak, and G. D. Westfall, Nucl. Phys. A400 (1983) 63c.

(Warwick-82)   A. I. Warwick, H. H. Wieman, H. H. Gutbrod, M. R. Maier, J. Peter, H. G. Ritter, H. Stelzer, F. Weik, M. Freedman, D. J. Henderson, S. B. Kaufman, E. P. Steinberg, and B. D. Wilkins, LBL Preprint 14015 (1982).

(Westfall-76)   G. D. Westphal, J. Gosset, P. J. Johansen, A. M. Poskanzer, W. G. Myer, H. H. Gutbrod, A. Sandoval and R. Stock, Phys.Rev. Lett. 37 (1976) 1202.

9 - FIGURES

Figure 9.1   Nucleon-nucleon average cross-sections.

Curves A, B and C represent the average N-N cross-sections. A
is the total cross-section; B the inelastic cross-section and C
the elastic cross-section. These were obtained from the nn and
np experimental cross-section data by a process of least square
smoothing and interpolation. The dotted curves A', B' and C'
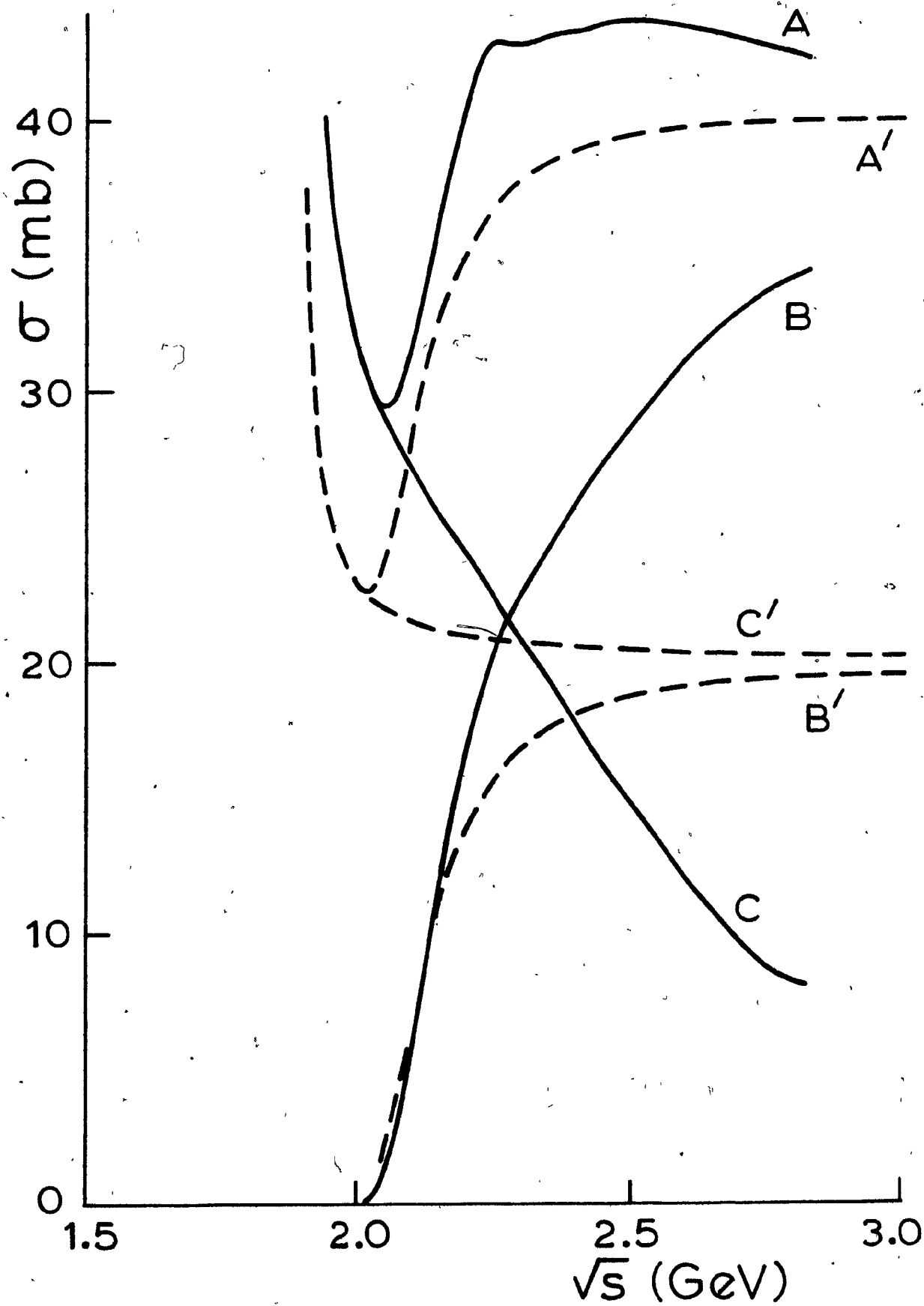are simplified parametrizations used to test the sensitivity of
the end results.

Figure 9.2 Rapidity and perpendicular momentum.

Rapidity and perpendicular momentum distribution curve fits to
relativistic Maxwell-Boltzmann distributions for the case of
Ca-40 on Ca-40 collisions at 1.0 A.Gev and zero impact
parameter. The points were calculated with the
two-fireball/blast-wave model and the solid lines represent the
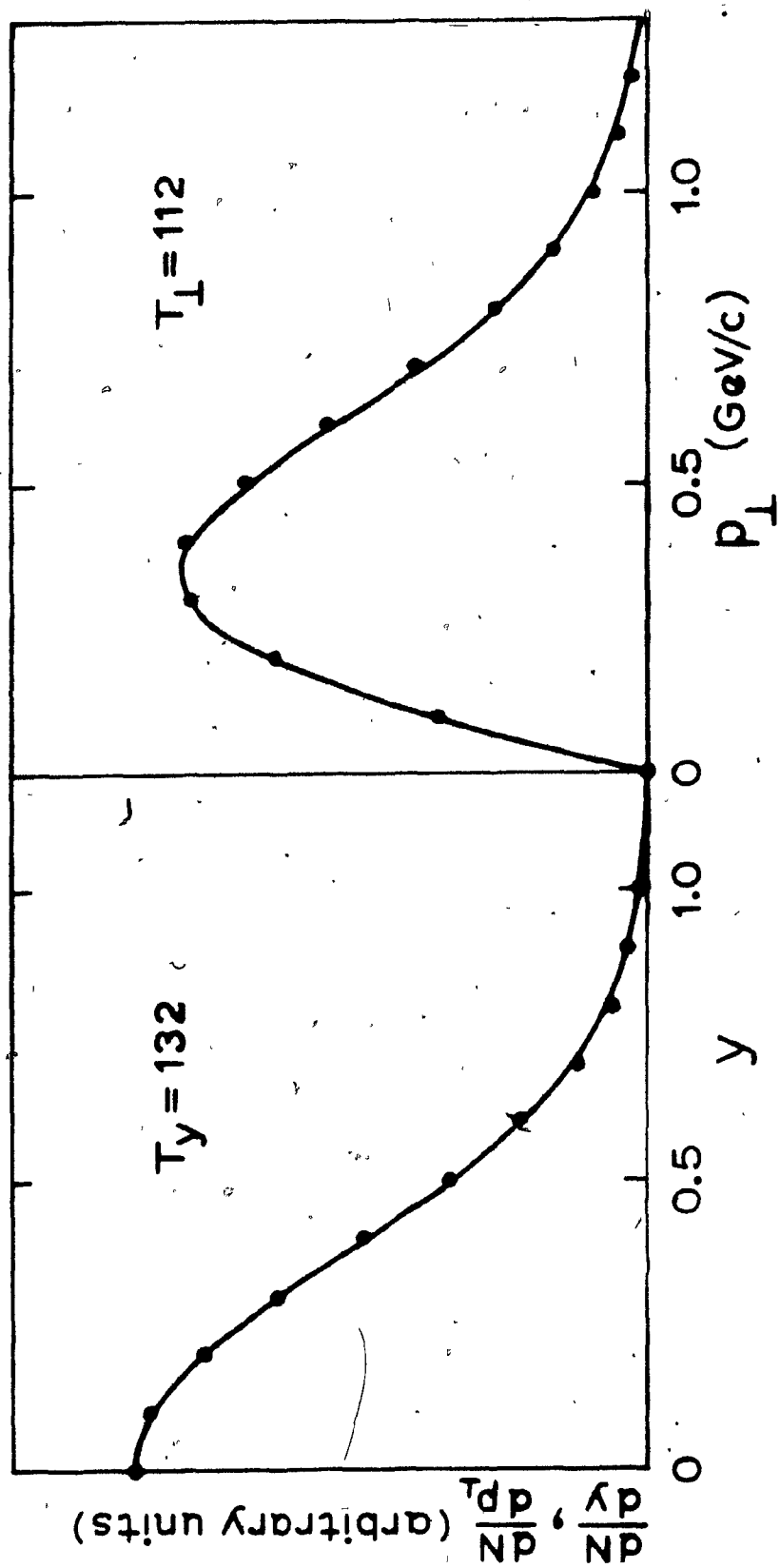best curve fits.

$T_\perp = 112$

$p_\perp$ (GeV/c)

$T_y = 132$

y

$\frac{dN}{dy}$, $\frac{dN}{dp_\perp}$ (arbitrary units)

Figure 9.3   Temperature in the cascade (A=20).

Temperature determination by fitting an exponential· curve to the tail of the energy distribution obtained from the cascade calculation of the collisions at 800 A.Mev of nuclei with mass equal to 20.
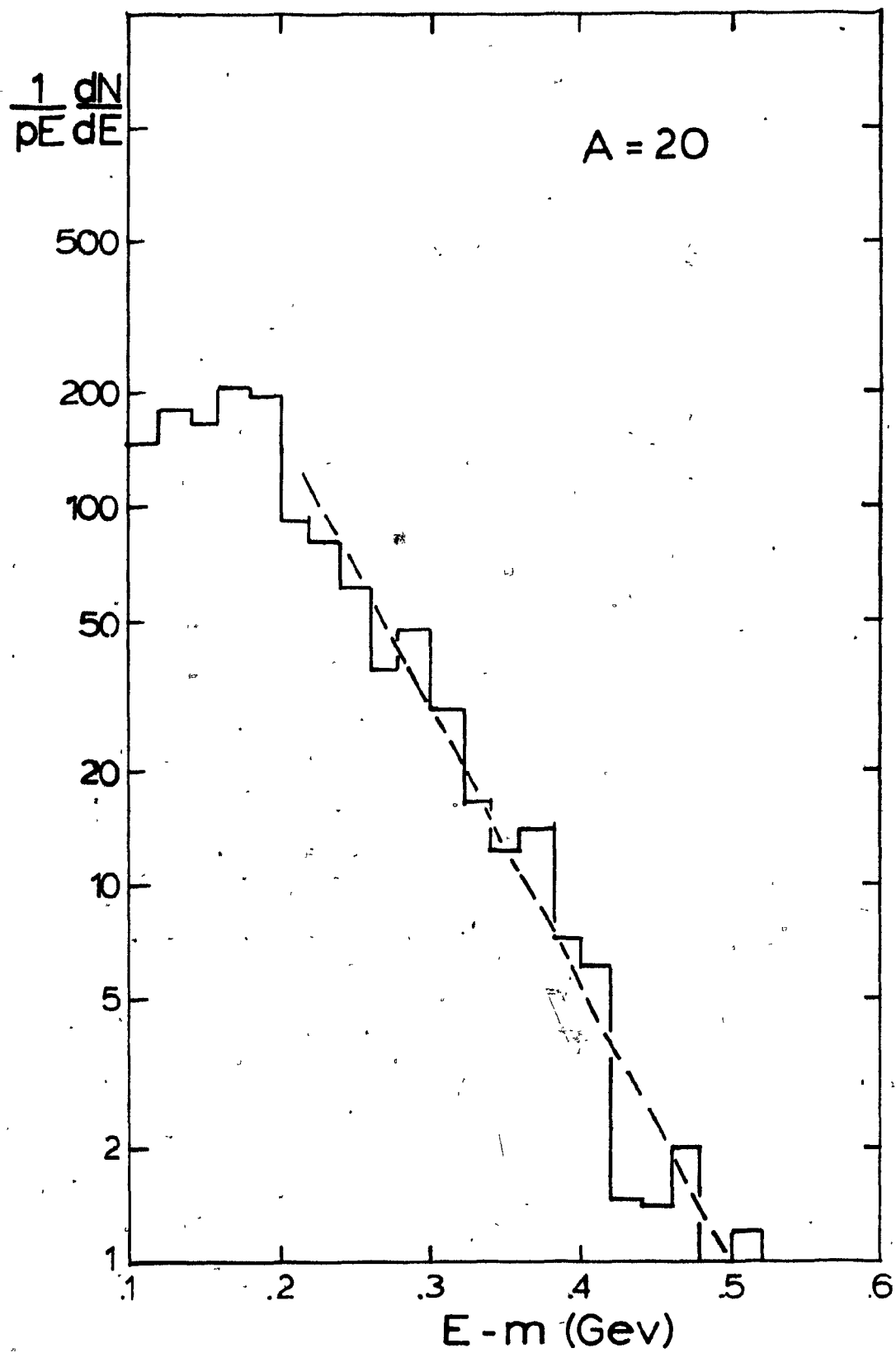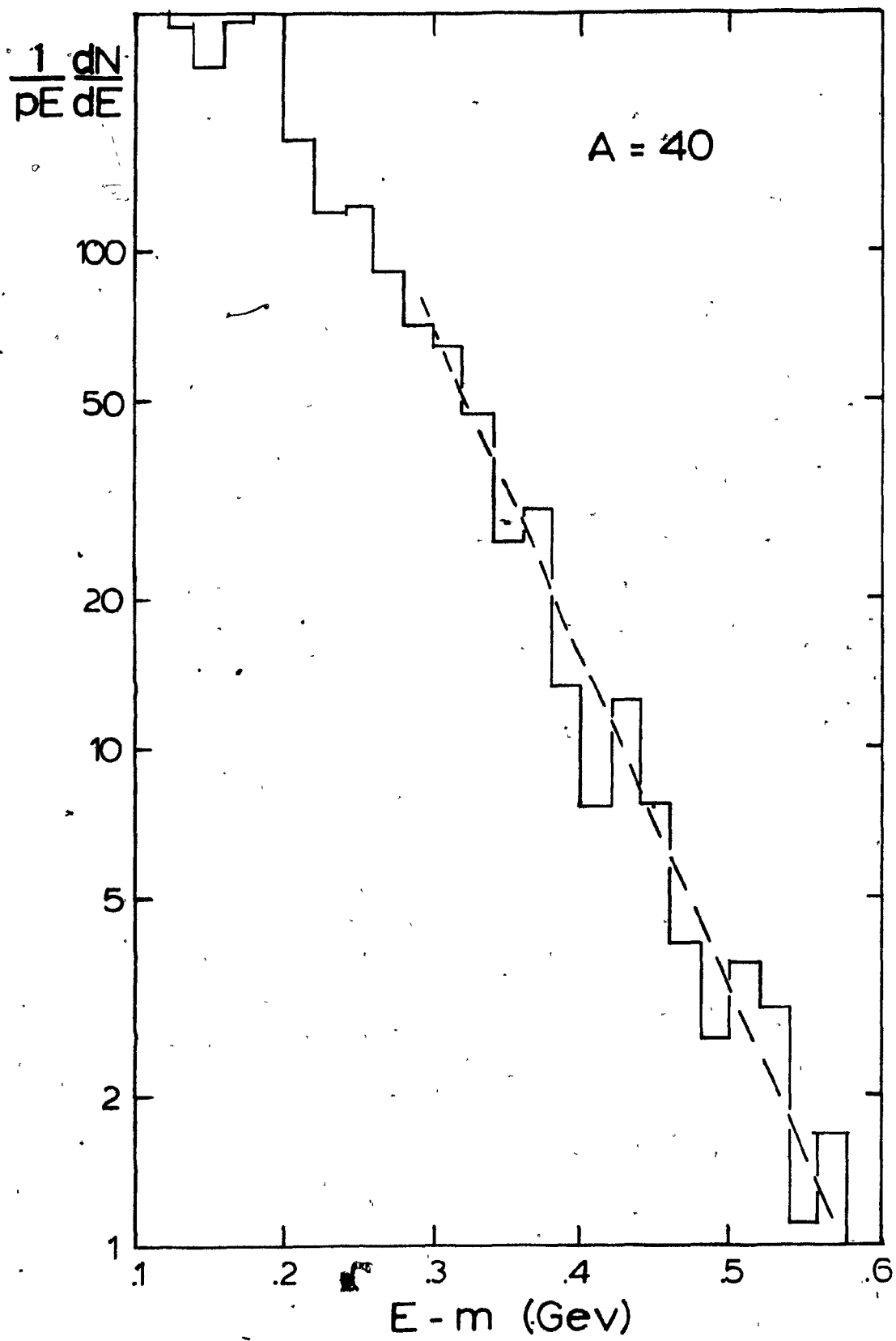
Figure 9.4   Temperature in the cascade (A=40).

Temperature determination   by fitting   an exponential   curve to
the tail of   the energy distribution obtained   from the cascade
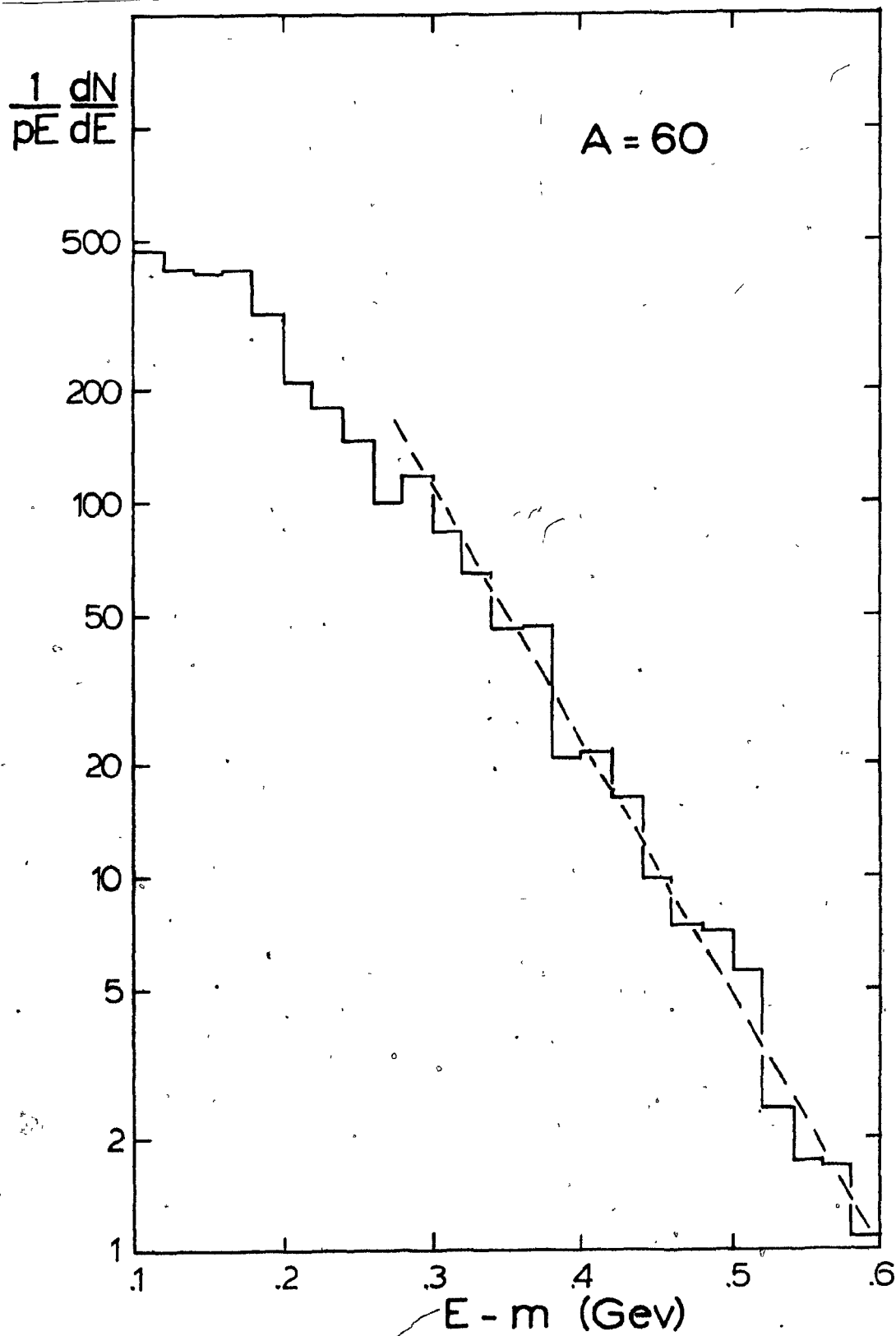calculation of the collisions at 800 A.Mev of nuclei with mass
equal to 40.

Figure 9.5   Temperature in the cascade (A=60).

Temperature determination by fitting an exponential curve to
the tail of the energy distribution obtained from the cascade
calculation of the collisions at 800 A.Mev of nuclei with mass
equal to 60.

$\dfrac{1}{pE}\dfrac{dN}{dE}$

A = 60

E − m (Gev)

Figure 9.6 Temperature in the cascade (A=80).

Temperature determination by fitting an exponential curve to
the tail of the energy distribution obtained from the cascade
calculation of the collisions at 800 A.Mev of nuclei with mass
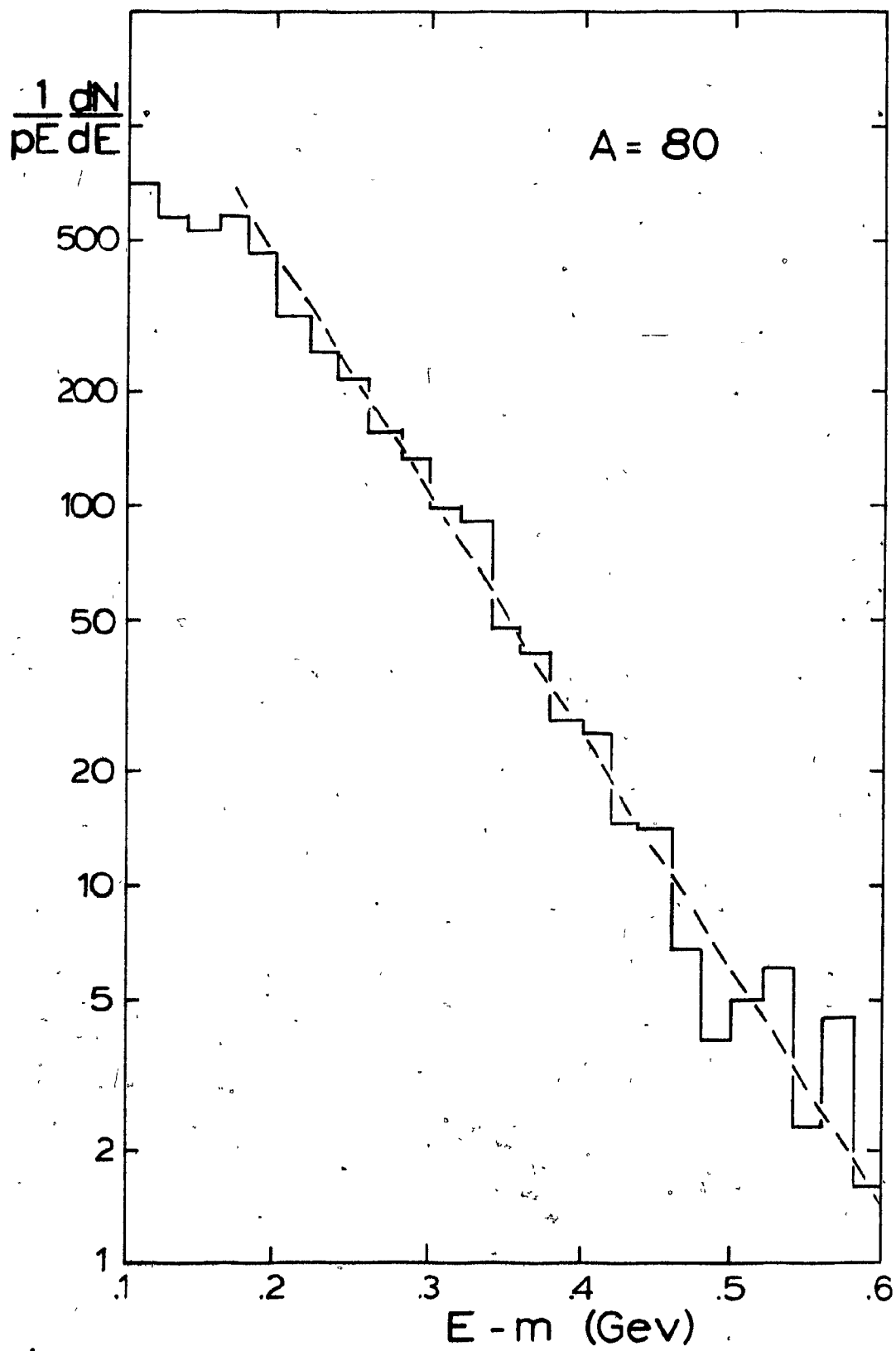equal to 80.

Figure 9.7 Number of deltas in the cascade.

The time evolution of the number of deltas for the system calcium on calcium at 977 A.Mev and zero impact parameter. Curve A represents a normal cascade run. Curve B shows the number of deltas a function of time when the participants are confined in a fixed volume at the point of maximum compression. Curve C is the same as curve B, but at the time 20 fm/c the constraining wall is removed and the participants are allowed to expand freely.
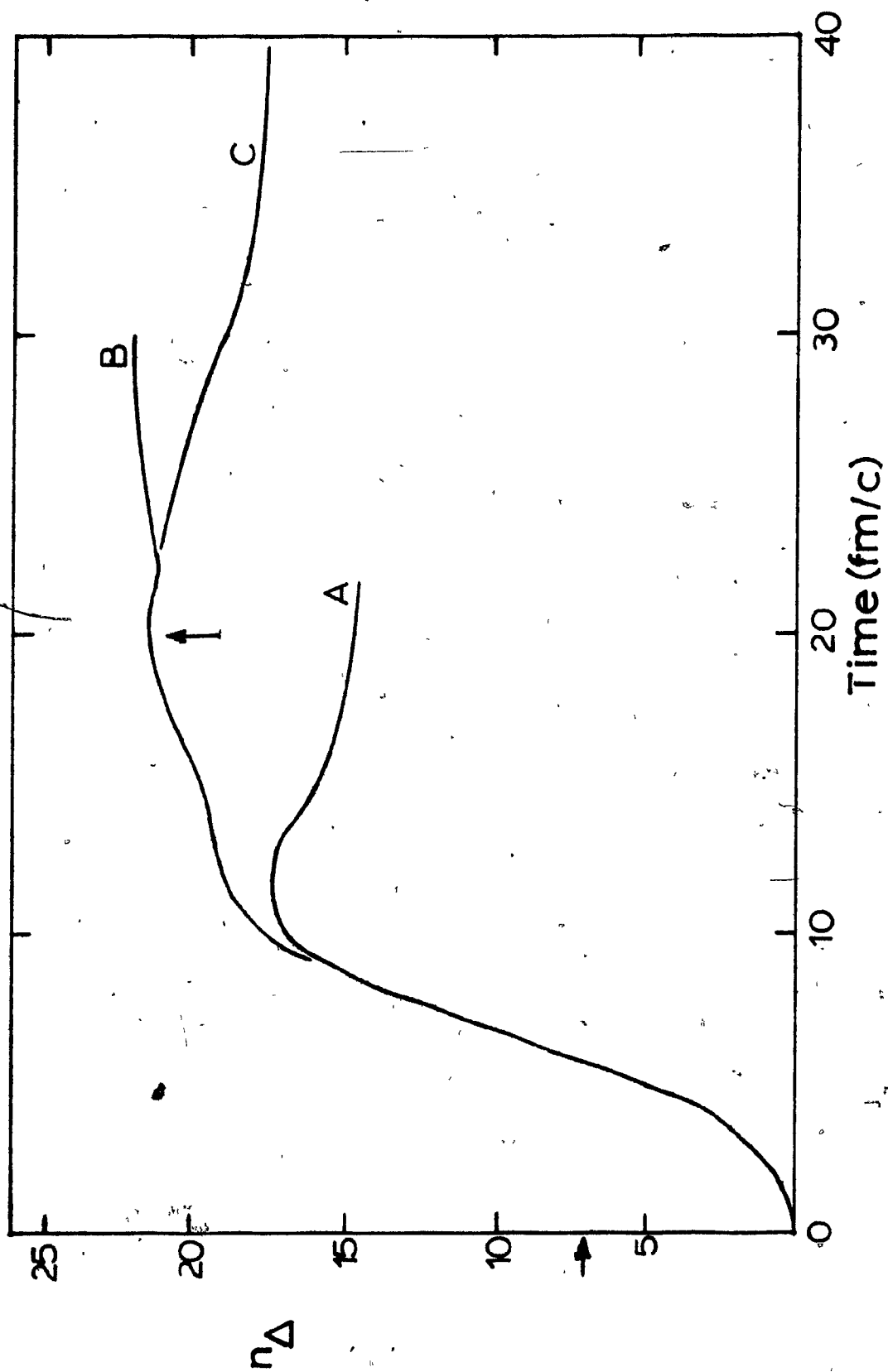
Figure 9.8   Participants: Geometry x Glauber type.

Curves   A and   B   represent the   number   of   participants as   a
function of the impact parameter b for the system neon on lead.
Curve A was   calculated using the straight   clean-cut geometry.
Curve B   was calculated   using the   Glauber type   theory for   a
collision energy of 2.1 A.Gev.